

Cover Page



Universiteit Leiden



The handle <http://hdl.handle.net/1887/31477> holds various files of this Leiden University dissertation.

Author: Buning, Ruth

Title: spFRET studies of nucleosome dynamics modulated by histone modifications, histone variants and neighboring nucleosomes

Issue Date: 2015-01-15

spFRET studies of nucleosome dynamics

modulated by

histone modifications,
histone variants
and
neighboring nucleosomes

Ruth Buning

spFRET studies of nucleosome dynamics modulated by histone modifications, histone variants and neighboring nucleosomes

PROEFSCHRIFT

ter verkrijging van
de graad van Doctor aan de Universiteit Leiden,
op gezag van Rector Magnificus prof. mr. C. J. J. M. Stolker,
volgens besluit van het College voor Promoties
te verdedigen op 15 januari 2015
klokke 11:15 uur

door

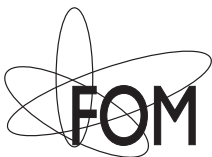
Ruth Buning

geboren te Amsterdam

in 1981

Promotiecommissie

Promotor:	Prof. dr. T. Schmidt	(Universiteit Leiden)
Co-promotor:	Dr. ir. S. J. T. van Noort	(Universiteit Leiden)
Overige leden:	Prof. dr. E. R. Eliel	(Universiteit Leiden)
	Dr. D. M. Heinrich	(Universiteit Leiden)
	Dr. H. van Ingen	(Universiteit Leiden)
	Prof. dr. H. Schiessel	(Universiteit Leiden)
	Prof. dr. C. A. M. Seidel	(Heinrich-Heine Universität Düsseldorf)



Universiteit
Leiden

Casimir PhD Series, Delft-Leiden, 2014-34

ISBN: 978-90-8593-206-2

An electronic version of this thesis can be found at <https://openaccess.leidenuniv.nl>

Dit werk maakt deel uit van het onderzoekprogramma van de Stichting voor Fundamenteel Onderzoek der Materie (FOM), die financieel wordt ondersteund door de Nederlandse Organisatie voor Wetenschappelijk Onderzoek (NWO).

Aan Oma Fien

Contents

Aim and outline of this thesis	1
1 spFRET on nucleosomes	3
1.1 Introduction	6
1.2 The nucleosome	6
1.2.1 Nucleosome dynamics	8
1.3 FRET	10
1.4 Reconstitution of nucleosomes	11
1.4.1 Relation between FRET efficiency and length of unwrapped DNA	14
1.5 spFRET techniques	14
1.5.1 Confocal microscopy	14
1.5.2 Widefield TIRF	15
1.5.3 Alternating Laser Excitation	16
1.6 DNA breathing studied with spFRET	18
1.7 DNA sequence effects	23
1.8 Histone modifications	23
1.9 Nucleosome remodeling	24
1.10 DNA accessibility in nucleosome arrays	27
1.11 Conclusions	29
2 Making spFRET experiments with nucleosomes succeed	31
2.1 Introduction	32
2.2 Reconstitution of nucleosomes with FRET pairs	32
2.2.1 DNA substrate	32
2.2.2 Nucleosome reconstitution	35
2.3 Nucleosomes in a polyacrylamide gel	36
2.4 Sample preparation for spFRET	37
2.4.1 Dilution to single-molecule concentrations	37
2.4.2 Buffer conditions	39

2.4.3	Surface effects	40
2.5	Single-molecule fluorescence spectroscopy	40
2.5.1	Confocal setup	40
2.5.2	Single-molecule burst selection	42
2.5.3	Caveats in spFRET	42
2.6	Quantitative comparison of multiple FRET techniques	44
2.6.1	Bulk fluorescence spectroscopy	44
2.6.2	PAGE and spFRET	46
2.7	Conclusions	50
3	Genetic acetylation defines H3 K56Ac effects	53
3.1	Introduction	56
3.2	Results	57
3.2.1	Production of site-specifically acetylated histones	57
3.2.2	H3 K56Ac does not affect salt-dependent nucleosome stability	59
3.2.3	H3 K56Ac increases DNA breathing in mononucleosomes	60
3.2.4	Formation of higher-order chromatin structure in nucleosome arrays is unaffected by H3 K56Ac	64
3.2.5	The effect of H3 K56Ac on chromatin remodeling	66
3.3	Discussion	68
3.4	Experimental procedures	70
3.4.1	Expression and purification of acetylated histones	70
3.4.2	Single-molecule FRET	71
4	H2A.Z containing nucleosomes with spFRET	73
4.1	Introduction	76
4.2	Materials and Methods	78
4.2.1	Preparation of DNA constructs	78
4.2.2	Preparation of histone octamers	78
4.2.3	Nucleosome reconstitution	80
4.2.4	Polyacrylamide gel electrophoresis	80
4.2.5	spFRET sample preparation	80
4.2.6	Single-molecule fluorescence microscopy	81
4.2.7	Single-molecule data analysis	81
4.3	Results	82
4.3.1	Gel electrophoresis reveals near 100 % reconstitution yield	82
4.3.2	spFRET in gel shows H2A.Z-nucleosomes are more stable	84
4.3.3	FRET distributions are temperature independent	84
4.3.4	spFRET measurements on nucleosomes depend critically on slide passivation	86

4.3.5	H2A.Z nucleosomes are more stable during extended periods of storage	88
4.3.6	Xenopus H2A.Z nucleosomes also more stable	89
4.4	Discussion	89
4.5	Conclusions	95
5	Breathing in dinucleosomes	97
5.1	Introduction	100
5.2	Materials and Methods	102
5.2.1	Preparation of DNA constructs	102
5.2.2	Nucleosome reconstitution	102
5.2.3	Polyacrylamide gel electrophoresis	102
5.2.4	Sample preparation	104
5.2.5	Single-molecule fluorescence microscopy	104
5.2.6	Single-molecule data analysis	106
5.3	Results	108
5.3.1	Gel electrophoresis of (di)nucleosome reconstitutions	108
5.3.2	FRET distributions of mononucleosomes	110
5.3.3	Linker DNA increases DNA breathing	110
5.3.4	DNA breathing is affected by neighboring nucleosomes	112
5.4	Discussion	115
5.4.1	Sample handling	115
5.4.2	Sample heterogeneity	115
5.4.3	Linker DNA increases breathing in mononucleosomes	117
5.4.4	Dinucleosomes	117
5.5	Conclusions	119
	References	121
	Summary	131
	Samenvatting	135
	List of publications	143
	Curriculum Vitae	145
	Dankwoord	147

Aim and outline of this thesis

The principle of encoding genetic information in DNA is common in all living organisms and is very elegant in its simplicity. Yet the translation from genetic code to a functioning living organism that reacts to its environmental conditions is tremendously complex and far from understood. At the basis of the regulation of the genetic code (DNA) in eukaryotes¹, is its organization into nucleosomes: 10 nm wide structures, in which ~ 150 basepairs (bp) of DNA are wrapped around a disk of proteins, the histone octamer. Arrays of nucleosomes are organized in fiber-like structures called chromatin, ultimately forming the well-known chromosome, that, in its most compact state during cell division, can easily be visualized with a normal light microscope. This thesis focusses on the smallest units in chromatin, the nucleosomes, and how the physical nature of these nucleosomes allows for dynamic accessibility of DNA for cellular processes.

Nucleosomes realize a huge compaction of the DNA. In humans, the 2 m of DNA (6 billion bp) present in every cell, forming a coil of $\sim 100 \mu\text{m}$ in diameter if not condensed [1], fits in the cell nucleus of only $\sim 5 \mu\text{m}$ in diameter. The compaction in the form of nucleosomes provides the essential 'tool' to regulate accessibility of DNA. By thermal fluctuations, part of the nucleosomal DNA transiently unwraps from the histone protein core (DNA breathing), making it accessible for the cellular machinery. Changes in the binding energy between DNA and histones alter the breathing probability, which is realized in the cell by modifications to the histones or by incorporating histone variants. The linking of nucleosomes to their neighbors poses constraints on DNA breathing as well. It is therefore not trivial to understand the regulation of DNA accessibility in a physical manner.

To distinguish open nucleosomes (where part of the nucleosomal DNA is unwrapped) from closed nucleosomes (where the nucleosomal DNA is fully wrapped), the use of Fluorescence (or Förster) Resonance Energy Transfer (FRET) is a logical choice. FRET has been used intensively for nucleosome research. Ensemble measurements record the average FRET efficiency of large nucleosome populations. Infor-

¹to which all animals, plants and fungi belong

mation about the conformational heterogeneity or kinetic processes that occur in the sample can only be revealed with single-pair FRET (spFRET), in which FRET is measured in individual nucleosomes.

In this thesis, **Chapter 1** is a review of experiments that have used spFRET to elucidate single nucleosome dynamics. Such experiments show that nucleosomes are in general open for tens of milliseconds and for 10 % of the time. We investigated the influence of modulations of the histone proteins and the presence of linker DNA and neighboring nucleosomes on DNA breathing with spFRET. Several challenges we experienced in spFRET with nucleosomes are described in **Chapter 2**, along with suggestions how to deal with them. In **Chapter 3** we show that specific acetylation of the histone octamers at H3K56 enhances unwrapping of nucleosomal DNA. In **Chapter 4**, nucleosomes containing either the canonical histone H2A or the variant H2A.Z are investigated. We reveal that nucleosomes containing H2A.Z are more stable than their H2A-containing counterparts and thus can act as an accessibility switch for nucleosomal DNA. Finally, in **Chapter 5** we show that electrostatic interactions between linker DNAs and nucleosomes, and interactions between neighboring nucleosomes, enhance DNA breathing.

CHAPTER 1

Single-pair FRET experiments on nucleosome conformational dynamics

Ruth Buning and John van Noort

Based on: Biochimie, vol. 92, no.12, pp. 1729-1740, 2010

Abstract

Nucleosomes, the basic units of DNA compaction in eukaryotes, play a crucial role in regulating all processes involving DNA, including transcription, replication and repair. Nucleosomes modulate DNA accessibility through conformational dynamics like DNA breathing - the transient unwrapping of DNA from the nucleosome, repositioning of nucleosomes along the DNA, or partial dissociation. Single-molecule techniques, in particular single-pair Fluorescence Resonance Energy Transfer (spFRET), have resolved such conformational dynamics in individual nucleosomes. Here, we review the results of FRET experiments on single nucleosomes, including fluorescence correlation spectroscopy (FCS), confocal single-molecule microscopy on freely diffusing nucleosomes and widefield total internal reflection fluorescence (TIRF) microscopy on immobilized nucleosomes. The combined spFRET studies on single nucleosomes reveal a very dynamic organization of the nucleosome, that has been shown to be modulated by post-translational modifications of the histones and by DNA sequence.

1.1 Introduction

DNA in eukaryotes is condensed inside the cell nucleus by roughly an equal mass of histone proteins into a structure called chromatin. While the term chromatin was already proposed in 1882 (“the substance in the nucleus that is readily stained” [2, 3]), even before DNA was identified as the carrier of genetic information, the nucleosome was first discovered in the 1970’s by electron microscopy on chromatin spilling out of ruptured nuclei [4, 5].

The nucleosome is the basic unit of chromatin: a disk of eight histone proteins with 147 bp of DNA wrapped around it. Arrays of nucleosomes are packed into higher-order structures, the details of which are still under debate. Figure 1.1 shows the hierarchical organization of chromatin at different length scales. DNA and histones are localized in the cell nucleus, and regions of higher and lower compaction can be distinguished (figure 1.1a: recent visualization of chromatin compactness using FRET). One of the first detailed images of native chromatin, spilling from ruptured nuclei (figure 1.1b), shows that it consists of fibers of ~ 30 nm in diameter. When these are disrupted, a ‘beads on a string’ structure appears: arrays of nucleosomes connected by short stretches of DNA. The crystal structure of the nucleosome was resolved at 7.0 Å by Richmond et al. in 1984 [6], and in 1997 at 2.8 Å resolution [7] (figure 1.1c).

All processes involving DNA, like transcription, replication and repair, take place in the chromatin environment. Besides compacting DNA, chromatin plays a major role in regulating these processes. By changing chromatin compaction, DNA-accessibility can be modulated. The control of DNA activity by the dynamics of chromatin structure has been investigated at many different levels of chromatin organization. In this review, we will zoom in on the lowest level and mainly focus on DNA dynamics within individual nucleosomes. In particular we will discuss single-molecule experiments using FRET, that have the unique capacity to directly reveal conformational dynamics of DNA inside a single nucleosome. Related to conformational dynamics of DNA inside a single nucleosome, we will also discuss DNA dynamics in assemblies of a few nucleosomes. Though regulation processes are likely to involve modulation of higher order structures as much as the modulation of nucleosome integrity and dynamics, the recent reports on single nucleosomes have laid down a framework that provides a foundation for structural understanding of the much more controversial higher-order chromatin structure.

1.2 The nucleosome

The nucleosome core particle (NCP) consists of 147 bp DNA, corresponding to ~ 50 nm, wrapped in 1.65 superhelical turns around a core of eight histone proteins

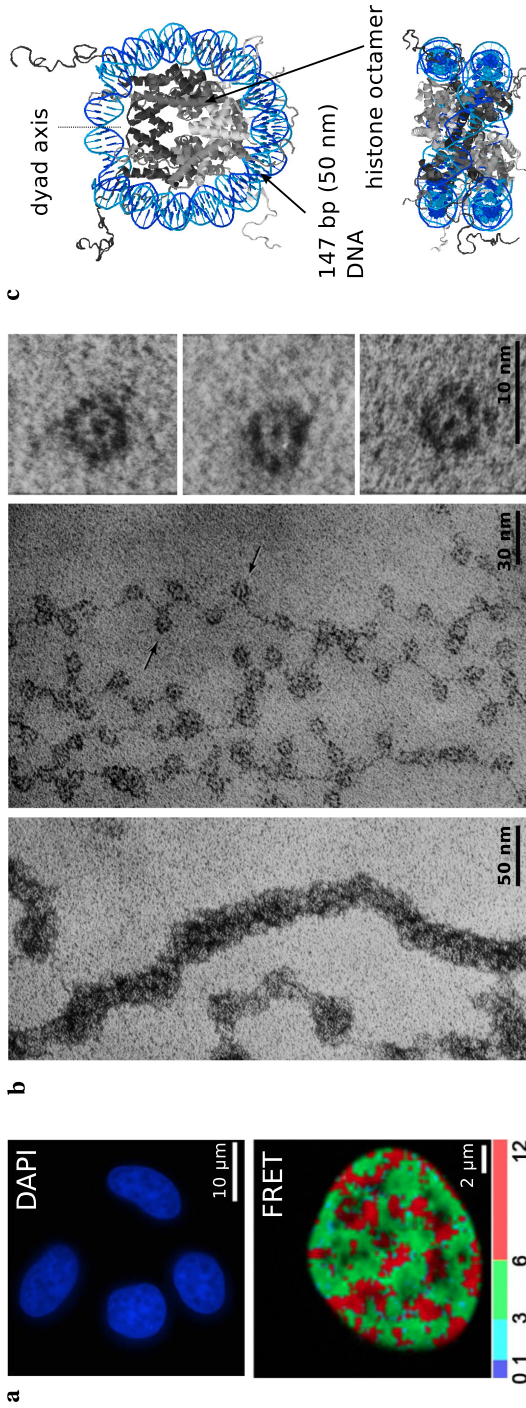


Figure 1.1 – Chromatin at different length scales. **a:** Fluorescence image of HeLa cell nuclei with DAPI stained DNA (top). All DNA of a single cell, 2 m in total, is contained in the cell nucleus of $\sim 10 \mu\text{m}$. FRET map of a HeLa cell nucleus with GFP/mCherry-tagged histones (bottom). High-FRET regions (red) indicate regions where the chromatin is more compacted than in low-FRET regions (green) (adapted from [8]). **b:** Electron micrograph images of native chromatin; left: chromatin spread at low ionic strength, showing a 30 nm thick fiber; middle: chromatin spread at high ionic strength, showing ‘beads on a string’, nucleosomes connected by stretches of DNA; right: isolated mononucleosomes (adapted by permission from Macmillan Publishers Ltd: Nature Reviews Molecular Cell Biology [3], copyright 2003. Originally published in [9–11]). **c:** Crystal structure of the nucleosome core particle (NCP) 1KX5 top- and side- view [12]. 147 bp of DNA is wrapped around an octamer of histone proteins.

[7, 13]. Two copies each of the histones H2A, H2B, H3 and H4 form the histone octamer core. Electrostatic interactions and hydrogen bonds between histones and the DNA backbone occur approximately every ten bp, at the minor groove. These 14 contact points between the histones and the DNA keep the nucleosome together. The persistence length of DNA is about 50 nm, which means that, if unconstrained, DNA is approximately straight on this length scale. Yet in the nucleosome, one persistence length of DNA is wrapped in nearly 2 full turns, rendering the nucleosome a loaded spring. A detailed discussion of the energy balance between binding and bending is given by Prinsen and Schiessel, who show that the average net binding energy per attachment point slightly exceeds one $k_B T$ ([14], [15]), allowing for extensive dynamics. *In vivo*, linker histone H1 or H5 can bind the two exiting DNA strands, stabilizing the nucleosome. Flexible N-terminal tails of the histone proteins protrude to the outside of the nucleosome and may further stabilize DNA-histone interactions. In native chromatin, 10-90 bp linker DNA connects neighboring nucleosomes.

1.2.1 Nucleosome dynamics

By letting nucleosomal DNA temporarily unwrap from the nucleosome, or by regulating the position and density of nucleosomes along genomic DNA, nucleosomes play an essential role in regulating DNA accessibility, and with this transcription. Spontaneous (thermal) fluctuations can lift steric occlusion, providing access to DNA target sites for DNA-processing enzymes that are buried inside nucleosomes. Such fluctuations include (see figure 1.2) [16, 17]: DNA breathing, the transient unwrapping of nucleosomal DNA; H2A-H2B dimer release; and thermal repositioning of the histone octamer with respect to the DNA (sliding). Access to nucleosomal sites can also be catalyzed by remodeling enzymes that use ATP hydrolysis to change the position, structure or composition of nucleosomes.

The N-terminal histone tails may play an important role in regulating nucleosome dynamics. They interact with the nucleosomal DNA by binding or constraining it. The histone tails can also mediate interactions between nucleosomes, thereby organizing higher-order chromatin structure [18, 19].

Post-translational modifications of the histones, like acetylation, methylation, ubiquitylation and phosphorylation of amino acid residues, influence transcription activity. Although nucleosomes were only discovered in the 1970's, that chromatin consisted of nucleic acids and histones was known almost a century before. Already in 1964, it was shown that histone modifications and chromatin transcription are associated [20]. Histone modifications can change the charge of amino acid residues, and thereby alter electrostatic interactions. It is therefore likely that these modifications modulate DNA accessibility at the nucleosome level. Many post-translational modifications on both the histone tails and the globular domain have been mapped [21].

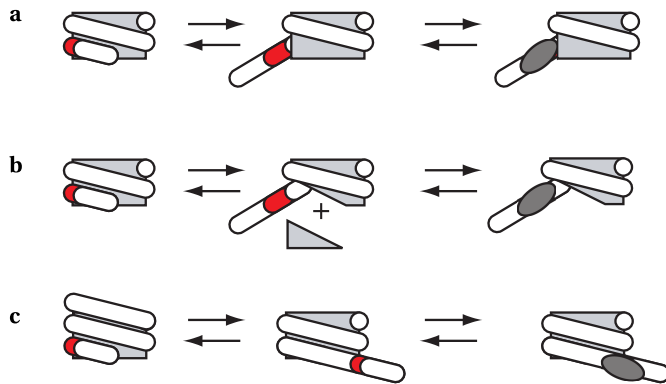


Figure 1.2 – Possible mechanisms for spontaneous site exposure of nucleosomal DNA, providing access to recognition sites (red) for DNA-binding proteins (dark grey). **a:** DNA breathing, **b:** H2A/H2B dimer release, **c:** thermal repositioning.

Nonspecific acetylation of lysine residues on histones is expected to weaken electrostatic interactions between mainly the histone tails and DNA by neutralizing a positive charge. Also, several specific modifications have been associated to the regulation of chromatin dynamics. Especially acetylation of H4 K16, a lysine on the tail of H4 that presumably interacts with the neighboring nucleosome, has been implicated to inhibit the formation of higher-order chromatin structure [22, 23]. The ensemble of post-translational modifications on the histone tails have been proposed to provide a ‘histone code’, that may recruit specific protein factors involved in active remodeling of nucleosomes [24].

In the globular domain, acetylation of H3 K56 is most extensively studied in relation to transcription activity. Numerous reports show that it plays a role in the regulation of DNA repair and replication, transcription and chromatin assembly [21]. This amino acid is located close to the nucleosome exit, where the histone contacts the nucleosomal DNA. It is therefore expected to modulate access to the nucleosomal DNA via DNA breathing.

The first study of DNA dynamics within nucleosomes was reported by Polach and Widom in 1995 [25]. They probed the accessibility of nucleosomal DNA by measuring digestion rates of restriction enzymes as a function of the position of the restriction site inside the nucleosome. Even sites buried far inside the nucleosome are digested, albeit with a lower occurrence. The equilibrium constants for DNA breathing can be determined indirectly from the digestion rates, though correct interpretation of such data is non-trivial [15].

In the last decade, single-molecule biophysics techniques have been applied to study nucleosome and chromatin dynamics. single-molecule experiments reveal co-

existing subpopulations that would otherwise remain obscured by the ensemble average, and allow to probe kinetic processes directly. single-molecule force spectroscopy has been used to probe DNA unwrapping induced by force (for a review, see [26]). Here we will discuss FRET, that has the sensitivity to probe spontaneous unwrapping, even in individual nucleosomes. In that case it is referred to as single pair-FRET (spFRET).

1.3 FRET

Förster/Fluorescence Resonance Energy Transfer is a process in which energy is transferred non-radiatively from a donor molecule (D) to an acceptor molecule (A) [27]. The transferred energy can be emitted as acceptor fluorescence, with a wavelength that is longer than the donor fluorescence. The efficiency of energy transfer is defined as the amount of energy that is transferred from the donor to the acceptor, divided by the total amount of energy absorbed by the donor. The FRET efficiency E depends strongly on the distance between the fluorophores (see also figure 1.3a):

$$E = \frac{1}{1 + \left(\frac{R}{R_0}\right)^6}, \quad (1.1)$$

where R is the distance between the donor and the acceptor, and R_0 the Förster radius, or the distance at which the FRET efficiency is reduced to 0.5. R_0 is typically around 5 nm. This makes FRET an ideal tool to study conformational dynamics of the nucleosome, which has a radius of ~ 5 nm. A detailed discussion of FRET and its biological applications can be found in [28–30].

E can be experimentally determined from the donor and acceptor fluorescence intensities upon excitation of the donor:

$$E = \frac{I_A}{I_A + \gamma I_D}, \quad (1.2)$$

where I_A and I_D are the measured acceptor and donor fluorescence intensities, respectively, and γ is a correction factor containing the donor and acceptor quantum yield and detector efficiencies. When FRET is used for absolute distance measurements, I_A and I_D need to be corrected for direct acceptor excitation and crosstalk between the donor and acceptor channels. A detailed description of how to apply these corrections, as well as how to determine γ , is given by [31]. To translate the corrected E into an absolute distance via equation 1.1, the Förster radius R_0 needs to be known:

$$R_0^6 = \frac{9 \ln 10 \Phi^D \kappa^2 J(\nu)}{128 \pi^5 N_A n^4} = (8.785 \times 10^{-25}) \Phi^D \kappa^2 n^{-4} J(\nu), \quad (1.3)$$

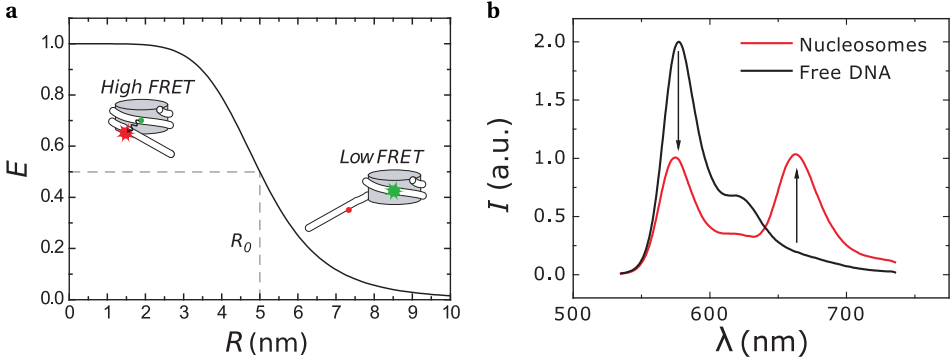


Figure 1.3 – a: FRET efficiency E as a function of the distance between the dyes with a Förster radius R_0 of 5 nm. Since the radius of the nucleosome is ~ 5 nm, the FRET efficiency for labels attached to the DNA will decrease from one to zero for DNA breathing events; **b:** Bulk fluorescence spectrum upon donor excitation for free DNA (black) and for reconstituted nucleosomes (red).

where Φ^D is the donor emission quantum yield in absence of the acceptor, $J(\nu)$ the spectral overlap integral, n the refractive index of the medium, and κ the orientation factor for dipole-dipole coupling. The relative orientation of the dyes with respect to each other determines κ^2 , the value of which can vary between 0 and 4. It is often assumed that the D and A dipole moments are free to rotate in all directions on a timescale much faster than their radiative lifetimes. In this case, the geometric average of the angles can be used and $\kappa^2 = 2/3$. However, in many cases fluorophores are restricted in their movement by the presence of the molecule to which they are attached. When FRET is only used to probe dynamics between different conformational states, changes in E , instead of absolute values of R , are of interest. In this case, γ in equation 1.2 can be assumed to be 1, and the uncorrected E is called the *proximity ratio*.

Deliberately detuning the proximity ratio can be applied to optimally separate two states close in FRET efficiency [32]. Here, the factor γ is manipulated by changing the donor and acceptor detection efficiencies.

Note that the limited fluorescence intensity from single fluorophores results in a relatively large contribution of shot noise in typical spFRET experiments, resulting in a relatively poor signal-to-noise ratio of E , making accurate determination of E challenging.

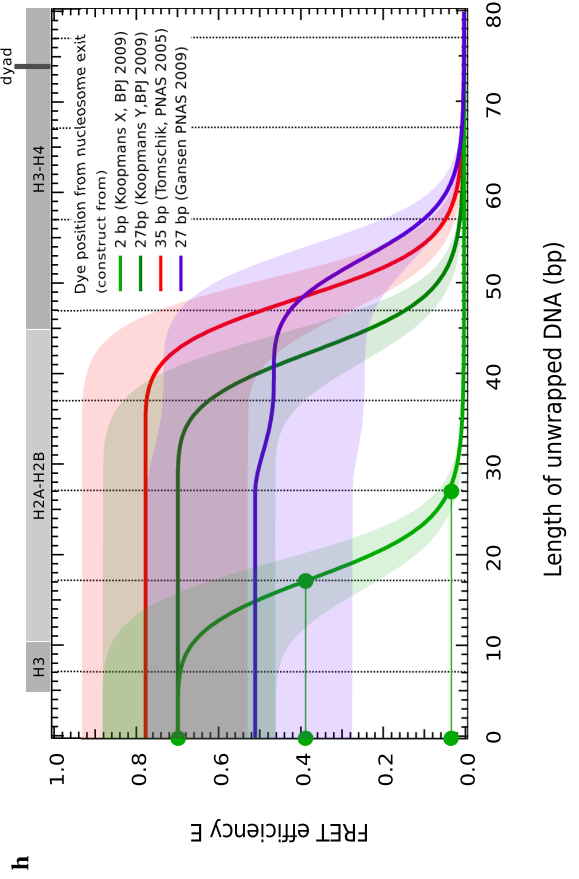
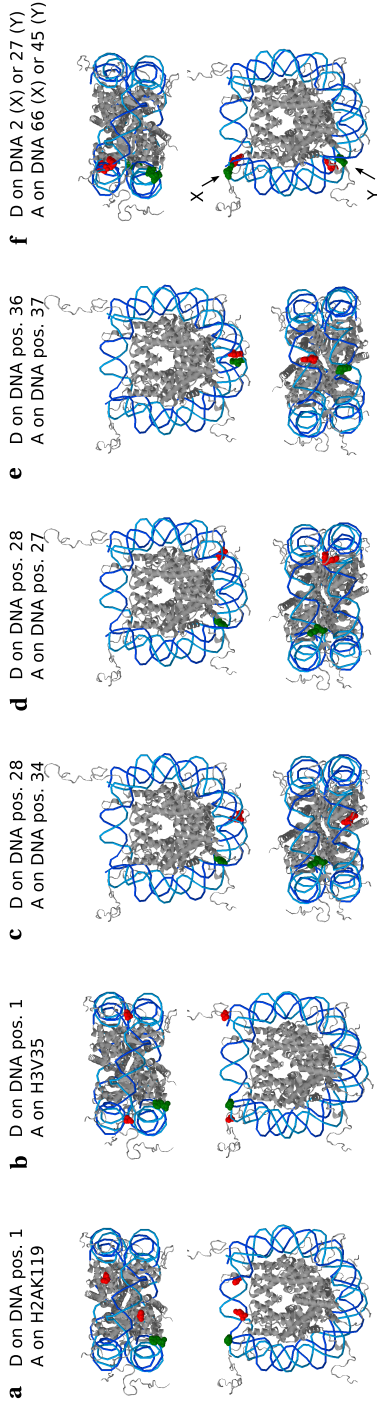
1.4 Reconstitution of nucleosomes

Nucleosomes can be assembled from DNA and purified histones. Simply mixing these two together at physiological salt conditions however results in the formation of non-

specific aggregates. *In vivo*, nucleosome assembly is therefore assisted by histone chaperones. *In vitro*, aggregation is prevented by reconstituting nucleosomes via salt-gradient dialysis. At high salt (typically 2 M monovalent salt), the histone octamers dissociate from the DNA. At 1.2-1.0 M salt, the (H3-H4)₂ tetramer binds to the DNA. Subsequently, at ~700 mM salt, the two H2A-H2B dimers dock onto the tetramer and constrain the ends of the DNA.

Typically, small fluorophores like Cy3 or Cy5 are attached to a DNA base via a 1-2 nm flexible carbon linker, ensuring rotational freedom of the dyes. Alternatively, a donor or acceptor fluorophore can be attached to one of the histones. Since there are two copies of each histone in the nucleosome, histone-labeled nucleosomes can contain no, one, or two copies of the same fluorophore, depending on the labeling stoichiometry, which may complicate quantitative interpretation of the FRET value. For accurate interpretation of the observed FRET efficiencies, a well defined positioning of the dyes is crucial. Therefore, the DNA template usually contains a strong nucleosome positioning element, for example 5S rDNA or the 601-positioning sequence [33]. Fluorescent labels can be incorporated in the nucleosomal DNA through a PCR with fluorescently labeled primers. A detailed protocol for designing and reconstituting mononucleosomes can be found in [34]. Figure 1.3b shows the fluorescence spectrum upon donor excitation for Cy3B- and ATTO647N- labeled unreconstituted DNA and nucleosomes after reconstitution. The spectrum shows that, in the reconstituted nucleosomes, the donor and the acceptor are positioned close enough to each other to show efficient FRET. However, the bulk spectrum hides all conformational dynamics, non-stoichiometric labeling and incomplete reconstitution, which can be prominent under typical experimental conditions.

Figure 1.4 (facing page) – a-f: Selection of nucleosome constructs used for FRET experiments. The NCP is shown, with the bases or amino acids to which the dyes are attached indicated in green (D) or red (A); **a** and **b**: constructs used by Li et al. [35, 36]; **c** and **d**: constructs used by Gansen et al. [32, 37, 38]; **e**: construct used by Tomschik et al. [39]; **f**: construct used by Koopmans et al. [40–42]; **g**: Schematic drawing of the nucleosome. The distance between the bases is calculated via $R_{\text{bases}} = \sqrt{R_{2D}^2 + H^2}$. The distance between the dyes is approximated by taking $R = R_{\text{bases}} + \Delta R$; **h**: Calculated FRET efficiency as a function of the length of unwrapped DNA based on the geometry depicted in g), for four of the constructs shown in a). Input values are: $R_{\text{nuc}} = 4.18$ nm, $H = 2.8$ nm [7], Förster radius for the specific FRET pair used = 5.5-6.5 nm, nm/bp = 0.34. The thick lines represent calculations with ΔR corresponding to the reported FRET efficiencies for fully wrapped nucleosomes. The shaded areas indicate the extremes for excursions of the dyes corresponding to $\Delta R \pm 1$ nm. Vertical dotted lines indicate contact points between the DNA and the histones [7].



1.4.1 Relation between FRET efficiency and length of unwrapped DNA

A variety of different label positions have been reported. In order to compare the results and to deduce generic dynamic properties of nucleosomes, we need to carefully consider the geometries of the FRET-labeled nucleosomes. Figures 1.4a-f show a selection of reported nucleosome constructs. We can estimate how the FRET efficiency evolves when the nucleosomal DNA unwraps via a simple geometric model, schematically drawn in figure 1.4g. The dyes are attached to the DNA by a 1-2 nm flexible linker. Their separation is roughly estimated by calculating the distance between the DNA bases to which they are attached, plus an additional distance ΔR that represents the length of the flexible linker. ΔR is estimated from the reported FRET efficiencies for fully wrapped nucleosomes. Figure 1.4h shows the resulting FRET efficiency as a function of the length of unwrapped DNA for four different nucleosome constructs. DNA has to unwrap as far as ~ 30 bp beyond the label positions to lose FRET completely. If we assume that DNA unwraps from the nucleosomes in discrete steps that correspond to the contact points between the DNA backbone and the histone octamers, it follows that one or two intermediate states could exist as well. Whether the intermediate FRET efficiencies of these states can be distinguished from the high and low FRET states depends on the label positions. However, in many cases it is sufficient to describe DNA breathing with a two-state model where the nucleosome is either in a closed conformation (high E) or an open conformation (low E).

1.5 *spFRET* techniques

single-molecule techniques have allowed to measure a wealth of information that would remain obscured in the ensemble average: rates and lifetimes of dynamic processes and conformational heterogeneity. Specific sub-populations can be selected, to investigate them independently, or for example to exclude inefficient labelled species or not-reconstituted DNA. To detect the fluorescence of single molecules, it is crucial to reduce the background fluorescence originating from other molecules. Common single-molecule fluorescence techniques applied to nucleosomes include confocal microscopy to measure nucleosomes diffusing freely in solution, and widefield total internal reflection (TIRF) microscopy on nucleosomes immobilized to a surface. A schematic layout of both setups is shown in figure 1.5.

1.5.1 Confocal microscopy

With confocal microscopy, the excitation laser is focused to a femtoliter-sized excitation volume. Opposed to scanning confocal microscopy, where an image is created

by scanning the excitation volume through the sample, here time traces of the fluorescence intensity in the stationary laser focus are collected. Each nucleosome that enters the excitation volume gives a burst of fluorescence. The emitted fluorescence is collected by the objective and background fluorescence is rejected by a pinhole. Photons emitted by the donor and by the acceptor are separated and detected by single-photon counting devices like avalanche photodiodes (APDs). The time resolution can be as good as ps- μ s.

When the concentration is low enough, typically 10 – 100 pM, only a single nucleosome at a time will be in the excitation volume. In this case, burst analysis can resolve single-nucleosome FRET efficiencies, yielding the distribution of nucleosome conformations in the sample. The observation time per nucleosome is limited to the diffusion time through the excitation volume, typically a few ms.

The temporal fluctuations in fluorescence intensity can also be analyzed in terms of correlation times. Time traces of photon intensities are generally measured at low concentrations, but not necessarily at the level of single molecules. The normalized correlation function is defined as:

$$G_{1,2}(\tau) = \frac{\langle I_1(t) I_2(t + \tau) \rangle}{\langle I_1(t) \rangle \langle I_2(t) \rangle} - 1, \quad (1.4)$$

where $I_1(t)$ and $I_2(t)$ are the photon intensities of the channels of interest (D or A or a combination), and τ is the lag time. If $I_1 = I_2$, $G(\tau)$ is an autocorrelation, and if $I_1 \neq I_2$, $G(\tau)$ is a cross-correlation.

The fluorescence fluctuations can arise from processes like diffusion and fluorophore photophysics, but also from FRET fluctuations caused by conformational dynamics. The measured correlation function $G(\tau)$ is the product of contributions from these independent processes: $G(\tau) = G_{\text{diff}}(\tau) \times G_{\text{kin}}(\tau)$. When the timescale of conformational dynamics is much longer than the residence time, diffusion dominates the correlation curve, masking the dynamics almost completely.

1.5.2 Widefield TIRF

When nucleosomes are immobilized to the surface of a microscope slide, the observation time per single nucleosome is only limited by bleaching of the fluorophores. Though confocal microscopy can still be used, more often widefield excitation is chosen. A reduction of the background fluorescence is obtained by Total Internal Reflection Fluorescence (TIRF) microscopy, using the evanescent field created by directing the excitation laser to the sample under an angle greater than the critical angle via a prism or the objective. The evanescent field excites only those fluorophores within ~ 100 nm from the surface. Fluorescence is collected by the objective, separated into a donor and acceptor channel using dichroic mirrors, and detected on a CCD cam-

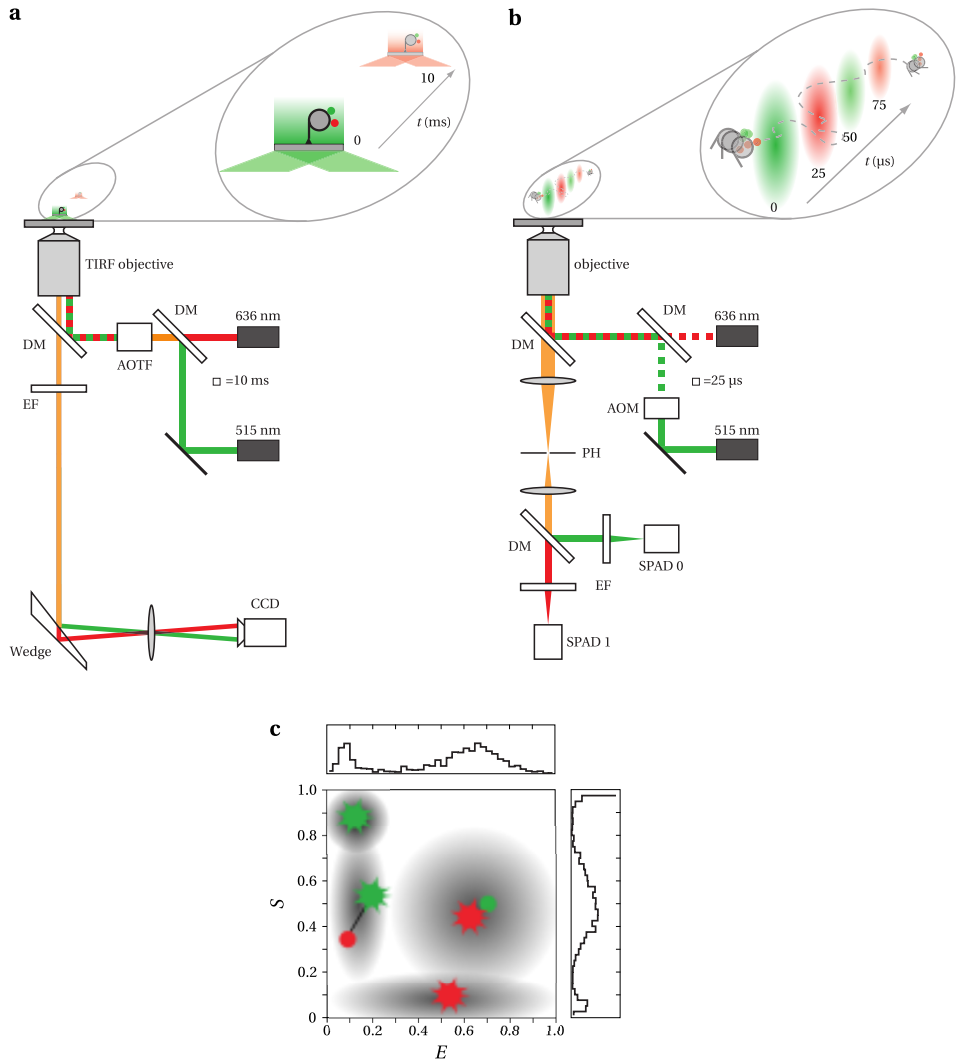
era. The time resolution, given by the readout-time of the CCD camera, is typically ~ 10 ms, limited by the number of photons per frame that is necessary for a reasonable signal-to-noise ratio. Multiple nucleosomes immobilized to the surface can thus be measured in parallel. The observation time for individual nucleosomes can be minutes long, depending on the photostability of the fluorophores. Because of the long observation time, it is even possible to perform multiple experiments on an individual nucleosome, e.g. by varying the buffer conditions during the observation.

The presence of the surface can however form a major obstacle in these studies. As nucleosomes tend to stick nonspecifically, special measures have to be taken to prevent nucleosome-surface interactions. Koopmans et al. showed that polymer-coating the surface with 6-arm polyethylene glycol (starPEG) reduces surface artifacts effectively [41].

1.5.3 Alternating Laser Excitation

spFRET experiments are particularly sensitive to artifacts related to the photophysical stability of the fluorescent labels. Photobleaching is the irreversible loss of fluorescence and limits the observation time of the fluorophore. A fluorophore typically emits $\sim 10^5$ photons before bleaching. Photoblinking is a reversible loss of fluorescence, where the fluorophore exists transiently in a dark state. When the acceptor fluorophore blinks, this can be mistaken for a loss of FRET, and therefore as nucleosome dynamics. Removing oxygen from the sample by using ‘oxygen scavenging systems’ and adding triplet state quenchers like trolox increases the photostability of the dyes.

Figure 1.5 (facing page) – Examples of single-pair FRET microscopes. **a:** Widefield TIRF microscope. DM, dichroic mirror; AOTF, Acousto Optical Tunable Filter; EF, Emission Filter; CCD, Charge Coupled Device. TIR excitation is achieved by displacing the excitation beams relative to the optical axis. The resulting fluorescence (orange) from immobilized molecules is collected by the objective, and filtered through an emission filter. Donor (green) and acceptor (red) fluorescence are simultaneously imaged on separate areas of the CCD chip using a dichroic mirror wedge. **b:** Fluorescence microscope with confocal geometry. AOM, Acousto Optical Modulator; PH, Pinhole; SPAD, Single-Photon Avalanche Diode. The resulting fluorescence from freely diffusing molecules in the excitation volume is collected by the objective, filtered through an emission filter, and spatially filtered through a pinhole. Donor and acceptor fluorescence are imaged on different SPADs using a dichroic mirror. In both **a** and **b**, a red and a green laser are alternated (green and red boxes) at a frequency that is synchronized to the fluorescence detection. Alternating Laser Excitation (ALEX) allows to simultaneously determine the FRET efficiency E and the label stoichiometry S for every particle. **c:** 2D E, S -histogram, revealing the presence of four different populations: donor- (D) or acceptor- (A) only species (due to incomplete labeling or photobleaching or –blinking), and doubly labeled species with high or low FRET. The first two can be excluded from the analysis.



A powerful tool to monitor the presence and integrity of both labels is Alternating Laser EXcitation (ALEX), introduced by Kapanidis et al. [43]. The laser to excite the donor is rapidly alternated by a laser that directly excites the acceptor. This second laser monitors the presence and integrity of the acceptor, and reveals blinking events. With ALEX, the label stoichiometry S can be determined simultaneously with the FRET efficiency E :

$$S = \frac{I_A^{Dex} + I_D^{Dex}}{I_A^{Dex} + I_D^{Dex} + I_A^{Aex}},$$

where I_A^{Dex} and I_D^{Dex} are the acceptor and donor intensities when excited at the donor excitation wavelength, and I_A^{Aex} the acceptor intensity when excited directly at the acceptor excitation wavelength. Nucleosomes with only a donor will have $S = 1$, and acceptor-only species $S = 0$. Properly folded nucleosomes with both fluorescent labels will have a high E and a S close to 0.5. Unwrapped nucleosomes and free DNA will have a low E and S close to 0.5 (see figure 1.5). ALEX allows to distinguish subpopulations based on label stoichiometry, and select the ones of interest or follow changes in population sizes in time. Thus ALEX can be particularly useful for spFRET experiments in nucleosomes, where eliminating artifacts due to photoblinking and D-only species is crucial for the correct interpretation of DNA breathing dynamics.

Next to the fluorescence intensity of the D and A labels, other information can be obtained, for example fluorescence lifetime and anisotropy. The simultaneous detection and analysis of these parameters, known as Multiparameter Fluorescence Detection (MFD) [44], allows to resolve heterogeneity in the sample via photophysical behavior.

1.6 DNA breathing studied with spFRET

Li & Widom investigated the conformational equilibrium of FRET-labeled nucleosomes under varying salt concentrations and in the presence of site-specific DNA binding proteins with bulk spectroscopy [35] (see figure 1.6 and 1.4a and b). Salt-induced loss of FRET shows that the equilibrium between wrapped and partially unwrapped states depends on the salt concentration. The resulting equilibrium constant (unwrapped/wrapped nucleosomes) under physiological conditions ($\sim 0.1 - 0.15$ M ionic strength), is $K_{eq} = 0.02 - 0.1$. This means a nucleosome is partially unwrapped for 2-10% of the time. Addition of LexA decreases the FRET efficiency, and drives the equilibrium to the unwrapped state, inhibiting rebinding of the DNA to the octamer. These bulk measurements set the stage for spFRET applications that aim at resolving the rates of (un)wrapping and possible heterogeneities in the nucleosome populations.

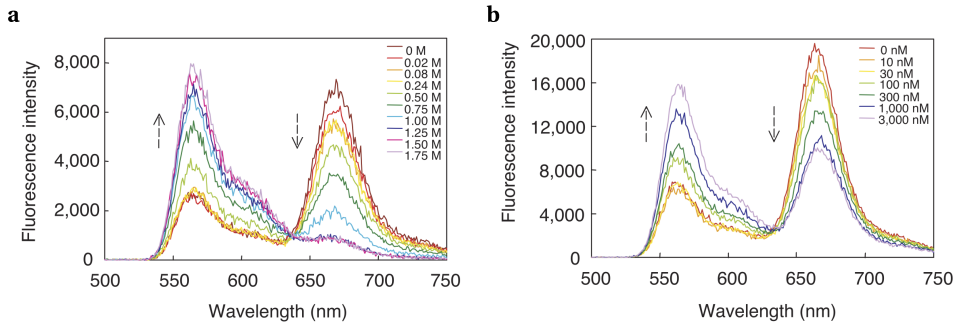


Figure 1.6 – a: FRET decrease upon increasing [NaCl], indicating unwrapping of the nucleosomal DNA; **b:** Titration of LexA to nucleosomes with a LexA recognition site 15 bp inside the nucleosomal DNA. Unwrapping of nucleosomal DNA upon specific protein binding. (Adapted by permission from Macmillan Publishers Ltd: Nature Structural and Molecular Biology [35], copyright 2004).

Li et al. performed FCS and stopped-flow FRET experiments on mononucleosomes (construct of figure 1.4b) freely diffusing in solution [36]. To resolve DNA breathing, its contribution has to be extracted from the correlation curve. A common way to do this is to measure an additional sample with only the diffusion, e.g. a D-only sample. The thus obtained diffusion correlation curve can be divided out, leaving the kinetics contribution. The resulting lifetimes are 250 ms and 10-50 ms for the closed and the open states, respectively. This method is very sensitive to the concentrations of both sample and reference. Also, by changing samples one risks introducing artifacts associated with changes in the observation volume. Therefore, Torres & Levitus developed a different approach to obtain kinetics information from correlation curves [45]. They show that from a single sample, the ratio of any two correlation curves cancels out the diffusion term. Reanalysis of the same data led to on/off times of 1.2 s and 50 ms, respectively (figure 1.7).

DNA breathing dynamics measured with TIRF microscopy on immobilized nucleosomes was first reported by Tomschik et al. [39]. They observed long-range DNA breathing of more than 35 bp (figure 1.4e), which they refer to as ‘opening’. The reported on- and off-times are 2-5 s and 100-200 ms, respectively, depending on the ionic strength. These results were later re-interpreted as photoblinking of the acceptor [46]. In a later study by Koopmans et al., immobilized nucleosomes with the label positions at the nucleosome exit were measured using ALEX (figure 1.4f) [40]. It was shown that trolox [47] suppressed acceptor blinking. Another issue that affects breathing is the presence of the surface. Of all the immobilized nucleosomes, only 10% appeared intact, with both a donor and acceptor label and high FRET, and only 3% of these show FRET fluctuations related to DNA breathing. Apparently the presence of the surface

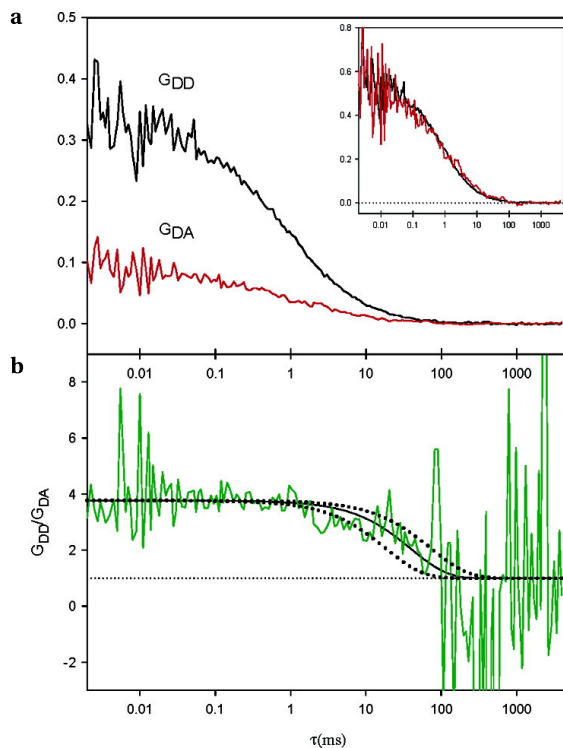


Figure 1.7 – a: Experimental donor-autocorrelation $G_{DD}(\tau)$ (black) and donor-acceptor crosscorrelation $G_{DA}(\tau)$ (red) FCS curves, from donor- and acceptor labeled nucleosomes (inset: normalized G_{DD} and G_{DA}); **b:** The ratio between the two divides out the contribution of diffusion and leaves the contribution of conformational dynamics. (Reprinted with permission from [45]. Copyright 2007 American Chemical Society.)

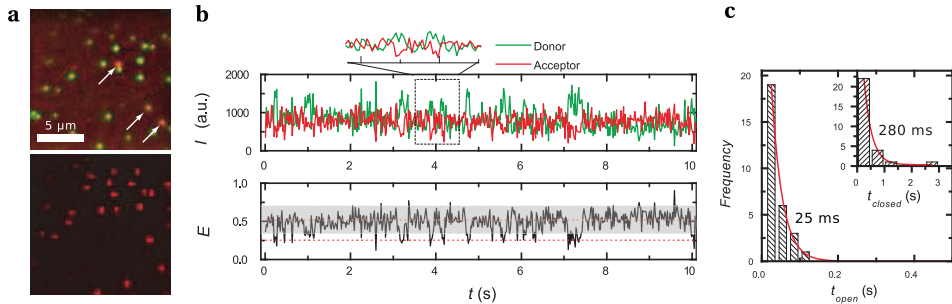


Figure 1.8 – Dynamics of nucleosomes immobilized on a starPEG surface. **a**: single-molecule fluorescence image of immobilized nucleosomes. Top: false color representation of donor and acceptor channel images, excited at 514 nm. The arrows point at molecules that featured high FRET efficiency. The majority of the molecules however did not show FRET and appears in green. Bottom: the same field of view excited at 636 nm, allowing for unambiguous identification of acceptor fluorophores (adapted with permission from Springer Science+Business Media [40]). **b**: Fluorescence intensity time trace (top) and corresponding FRET efficiency time trace (bottom). The FRET efficiency fluctuated between a high and a low FRET state, corresponding to a closed and an open nucleosome conformation, respectively. The grey bar indicates a 96% confidence interval for the photon and instrument noise. **c**: Histograms of the lifetime of the open and closed (inset) state. The solid lines are exponential fits to the data, yielding lifetimes of 25 ms for the open state and of 280 ms for the closed state (copyright Wiley-VCH Verlag GmbH & Co. KGaA. Reproduced with permission from [41])

impairs nucleosome integrity and probably also the dynamics of DNA breathing, despite surface passivation with polyethylene glycol (PEG). In a subsequent study, nucleosome integrity was investigated in relation to immobilization on either BSA, PEG, starPEG (6-arm PEG that forms cross-links), and in polymer gels [41]. StarPEG coating prevented nonspecific tethering most effectively, leaving 25% of the immobilized nucleosomes intact. Time traces with 10 ms time resolution show lifetimes of closed and open states of 280 ms and 25 ms, respectively (figure 1.8). This is in good agreement with Li et al. [36], while the closed state lifetime is short compared to the 1.2 s reported by Torres and Levitus [45].

Gansen et al. investigated the effect of salt concentration, nucleosome concentration and crowding agents on nucleosome stability [37] by burst analysis of freely diffusing single nucleosomes (figure 1.4c and d). When working with low concentrations, essential to observe individual nucleosomes, they show that nucleosomes dissociate at low concentrations and at high salt (NaCl), but that ~ 0.2 mg/ml BSA maintains nucleosome integrity for up to 300 mM NaCl. In fact, BSA is more effective than adding unlabeled nucleosomes, a common way to increase the nucleosome concentration while keeping the labeled nucleosome concentration low. A thorough quantitative analysis

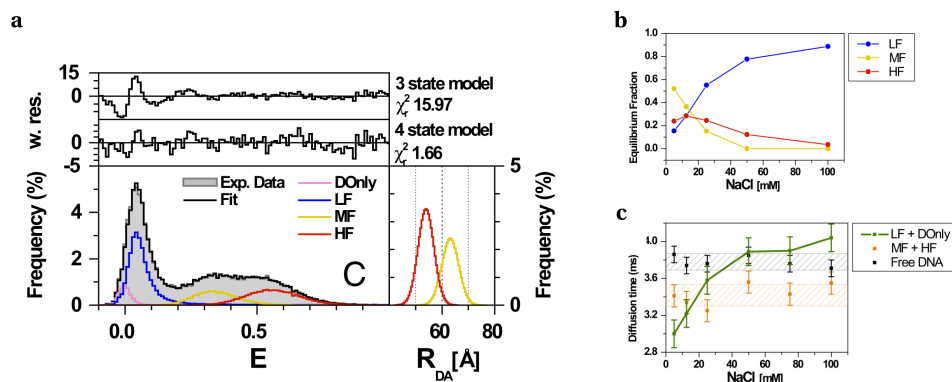


Figure 1.9 – a: FRET efficiency histogram of nucleosomes in 25 mM NaCl. Probability Distribution Analysis shows 4 different species: D-only, Low FRET (LF), medium FRET (MF), and high FRET (HF); **b:** Equilibrium fractions of LF, MF, and HF as a function of NaCl concentration; **c:** FCS correlation times of the subpopulations as a function of NaCl concentration. (Reproduced from [38].)

of FRET histograms of mononucleosomes is presented in [38]. Probability distribution analysis (PDA), combined with multiparameter fluorescence detection (FRET efficiency, lifetimes, and anisotropy) and FCS reveals at least four different subspecies with different FRET efficiency: three nucleosome species, with high (~ 0.5), medium, (~ 0.32) or low (close to zero) FRET, and a D-only population. Salt dependent stability analysis of these species identified these populations as intermediates in nucleosome disassembly. Based on these observations, a model is proposed for stepwise dissociation: first unwrapping from the ends, than dimer loss, and finally complete dissociation (figure 1.9).

In [42], Koopmans combined spFRET, ALEX, Polyacrylamide Gel Electrophoresis (PAGE) and FCS to resolve conformational heterogeneity of mononucleosomes with labels positioned at both DNA exits and 27 bp inside (figure 1.4f). Burst analysis of nucleosomes with different label positions reveals that transient DNA unwrapping occurs progressively from both ends, while nucleosomes remain stably associated. Equilibrium constants for breathing dynamics depend on the position in the nucleosome: $K_{eq} = 0.2 - 0.6$ at the nucleosome ends, and ~ 0.1 for 27 bp inside. Also it is shown that 50-100 mM monovalent salt promotes both reversible nucleosome breathing kinetics and irreversible nucleosome disassembly at low nucleosome concentrations (100-200 pM). For the first time, FCS was applied on selected bursts. By selecting a specific subpopulation, diffusion times can be related to the hydrodynamic radius of this specific population (figure 1.10).

Overall, bulk and single-molecule FRET measurements have shed light on the con-

formational dynamics of canonical nucleosomes. The approaches agree on the characteristic equilibrium constant between wrapped and unwrapped states, showing that nucleosomes are open 10 – 20 % of the time. spFRET experiments have the advantage that they reveal much more detailed information on nucleosome dynamics, such as transition rates and conformational heterogeneities. Multiple subpopulations have been distinguished, allowing the selection of specific populations of interest. Within these populations, FRET distributions reveal the presence of multiple states. The transition rates between the open and the closed conformation have been determined, resolving a lifetime of the open state of ~ 25 ms.

1.7 DNA sequence effects

Having established the canonical dynamic breathing of DNA, spFRET also provides unique possibilities to reveal more subtle effects that are responsible for modulation of DNA accessibility. Nucleosome constructs for spFRET experiments have so far been reconstituted on strong nucleosome positioning sequences. DNA sequence itself may influence nucleosome stability and DNA breathing dynamics. Gansen et al. compared 601 and 5S rDNA positioning sequences with spFRET on freely diffusing nucleosomes [32]. The 5S rDNA nucleosome is more destabilized by salt and dilution than nucleosomes based on the 601 positioning sequence.

Kelbauskas et al. compared nucleosomes with 5S, MMTV, and GAL10 DNA, the last two derived from promotor regions [48, 49]. Bulk FRET and FCS experiments in 3 % agarose gels on nucleosomes with FRET labels at the nucleosome exit or ~ 30 bp inside the nucleosome show enhanced dynamics in nucleosomes based on DNA from promotor regions compared to 5S DNA. The destabilization they observe at sub-nM concentrations is only pronounced for nucleosomes with labels at the nucleosome exit, suggesting that the destabilization is caused by H2A-H2B dimer release. The resulting open/closed times are 34/41, 58/40 and 82/36 ms for 5S, MMTV, GAL10 DNA based nucleosomes, respectively.

Thus nucleosome stability is directly linked to the affinity of the sequence to the octamer, and it is likely that DNA sequences that have a lower affinity exhibit more pronounced DNA breathing. This may help to direct nucleosomes to preferred positions along the genome.

1.8 Histone modifications

With the advent of spFRET experiments on nucleosomes, the link between histone modifications and nucleosome integrity and conformational dynamics can be directly investigated. Gansen et al. show that nonspecific chemical acetylation of histone oc-

tamers decreases nucleosome stability by opening the nucleosome structure starting at the DNA ends by comparing the FRET distributions for nucleosomes with FRET labels at the DNA exit and with FRET labels 40 bp inside the nucleosome [38].

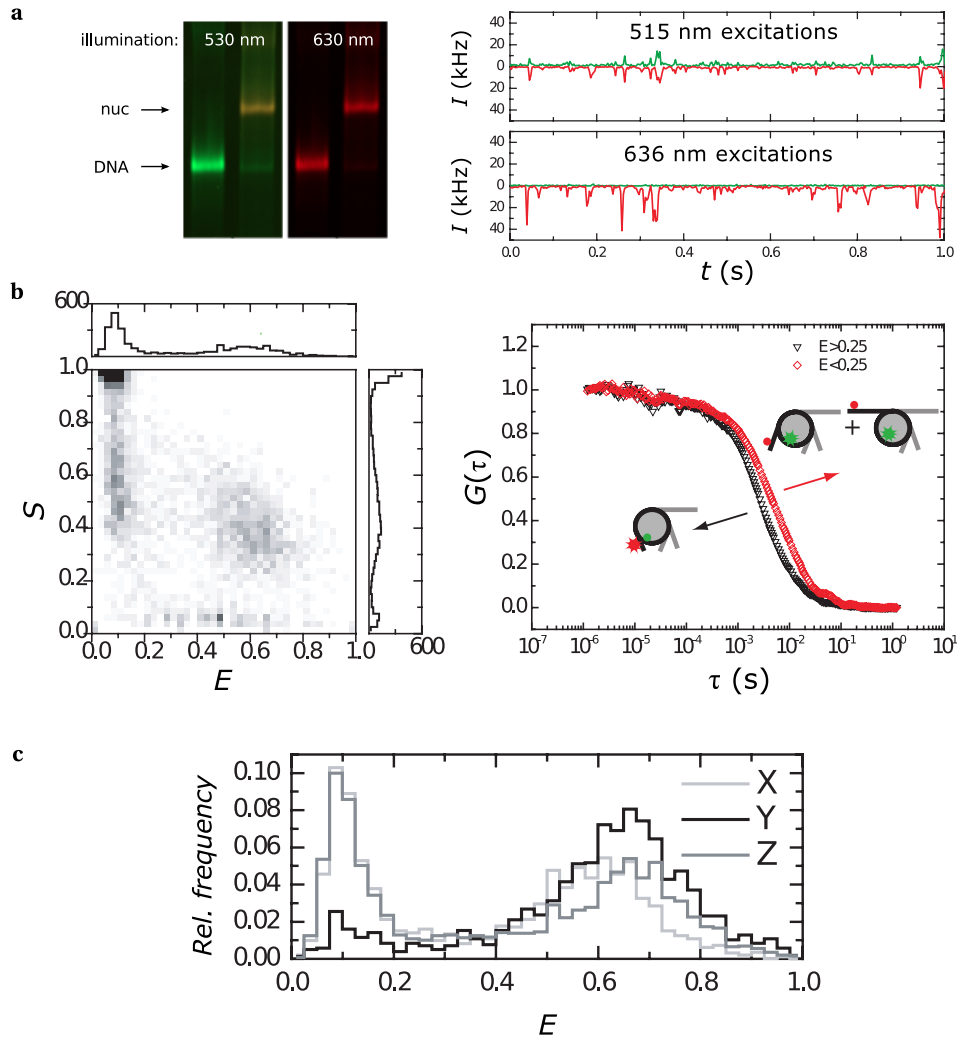
Specific acetylation of H3 K56, in the globular core, is expected to enhance DNA breathing. Neumann et al. developed a method to produce stoichiometric site-specific acetylated recombinant histones [50]. To investigate the effect of histone acetylation at H3 K56 on DNA breathing we compared nucleosomes reconstituted with recombinant xenopus histones without modifications, and recombinant *Xenopus* histones with acetylation at H3 K56. The FRET distributions were determined for both end-labeled and internally labeled nucleosomes (see figure 1.4f) using ALEX and confocal microscopy on freely diffusing nucleosomes. 13 % of the unmodified nucleosomes unwrap for 30 bp or more, and 11 % unwrap for at least 60 bp (figure 1.11). Acetylation at H3 K56 doubles the fraction that is unwrapped by 30 bp or more to 28 %, and increases the fraction that unwraps at least 60 bp with 3 % to 14 %. The FRET efficiency of the high-FRET population decreases upon acetylation. Taken together, acetylation at H3 K56 increases DNA breathing of the first ~30 bp 7-fold but hardly affects unwrapping further into the nucleosome. H3 K56 is well positioned to regulate DNA breathing, due to its position close to the exit of the nucleosome. Other modifications may have an equally important effect on enhancing or reducing DNA dynamics in the nucleosome.

1.9 Nucleosome remodeling

spFRET experiments are not only informative for quantifying DNA dynamics intrinsic to the nucleosome, they are also very well suited to probe the kinetic pathway of nucleosome remodeling.

Yang and Narlikar described a FRET based assay to follow real-time changes in

Figure 1.10 (facing page) – a: DNA and nucleosomes in a 5 % polyacrylamide gel. DNA and nucleosomes end up at different positions in the gel. The nucleosome band shows FRET when excited at 530 nm (orange color). The nucleosome band is directly placed on the confocal microscope setup. On the right a fluorescence time trace showing bursts of single nucleosomes. **b:** Results from burst analysis of nucleosomes with labels in position X (see figure 1.4f). Left: E, S -histogram, showing four distinct populations. Right: FCS analysis for selected bursts (autocorrelation with $I_1 = I_2 = J_A^{Dex} + J_D^{Dex}$), showing a different diffusion time for high- and low-FRET populations due to their different hydrodynamic radius. **c:** E -histograms of selected bursts ($0.2 < S < 0.8$). A low FRET population can clearly be observed for all three labeling positions. The low FRET population is 38 % for X and Z, and 10 % for Y, indicating progressive and pronounced nucleosome unwrapping from both ends. (Reprinted from [42], Copyright 2007, with permission from Elsevier.)



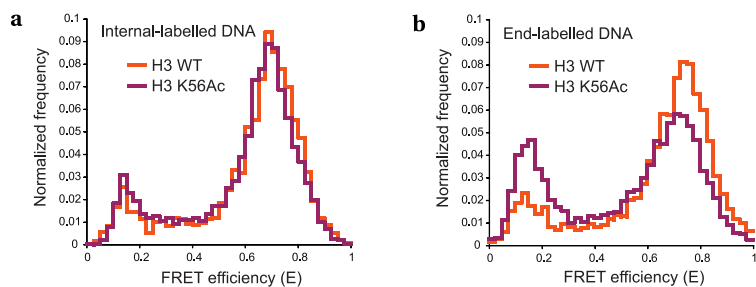


Figure 1.11 – E -histograms for nucleosomes with unmodified histones (H3 WT, orange) and histones acetylated at H3 K56 (H3 K56Ac, purple). Nucleosomes with the FRET labels at position X (**a**) and at position Y (**b**) (see figure 1.4f). The increase of the low-FRET population and the shift of the high-FRET population to a slightly lower FRET efficiency for the end-labelled nucleosomes shows that acetylation at H3 K56 promotes unwrapping of the first ~ 30 bp of the nucleosomal DNA. (Reprinted from [50] Copyright 2009, with permission from Elsevier.)

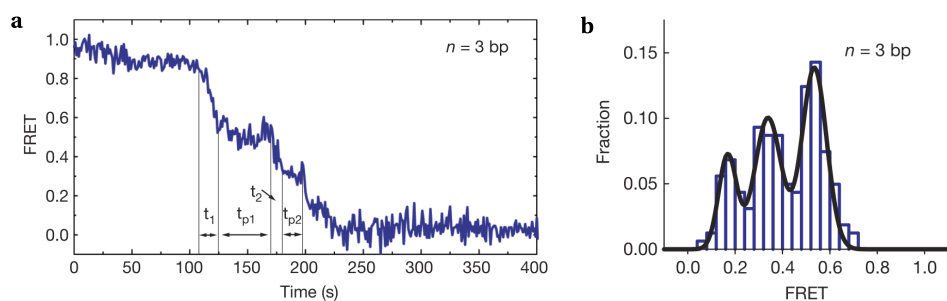


Figure 1.12 – ACF-catalyzed translocation of a single nucleosome. **a**: FRET time trace of an immobilized nucleosome after addition of ACF and ATP at $t=0$, showing kinetic pauses; **b**: FRET distribution of the pauses from time traces of many nucleosomes, revealing well-defined pauses. (Adapted by permission from Macmillan Publishers Ltd: Nature [51] copyright 2009.)

FRET due to nucleosome remodeling with a donor on the DNA and an acceptor on one of the histones [52]. They measured the ensemble donor or acceptor fluorescence intensity with a time resolution of 1 s during 6 minutes after activation of a SNF2h remodeler by adding ATP. Their nucleosome design is applicable to single-molecule experiments as well.

Blosser et al. recently reported the remodeling of nucleosomes by individual ACF complexes (ATP-dependent chromatin assembly and remodeling factor) [51] (label positions as in figure 1.4a, with D and A interchanged). With spFRET they directly monitored remodeling by ACF on individual immobilized nucleosomes. FRET-pair-labeled nucleosomes that initially show a high FRET signal gradually lose FRET when the histone octamer is repositioned with respect to the DNA by ACF. Translocation by ACF pauses at regular intervals of 7 or 3-4 bp (see figure 1.12). The binding, translocation, and dwell times of ACF are all ATP-dependent, revealing distinct roles of ATP during remodeling. It was also shown that ACF is highly processive, and can move nucleosomes in both directions along DNA before dissociating from the nucleosome.

1.10 DNA accessibility in nucleosome arrays

Restriction enzyme accessibility studies by Poirier et al. on longer arrays [53] surprisingly show that similar enzymatic accessibility to nucleosomal DNA can be observed in the arrays compared to mononucleosomes. Nucleosome positioning dramatically influences the accessibility of target sites inside nucleosomes, while chromatin folding dramatically regulates access to target sites in linker DNA between nucleosomes.

Though single nucleosomes provide excellent substrates to study DNA dynamics, *in vivo* nucleosomes always exist in the context of chromatin. In a combined bulk FRET, stopped flow, and FCS study, Poirier et al. quantified DNA accessibility in nucleosomal arrays [54] (figure 1.13). In this work, conformational dynamics of array compactness and site exposure inside the central nucleosome are probed on arrays of three nucleosomes. Bulk FRET and protein binding assays show that proteins can bind to sites in the central nucleosome of a compacted array, driven by site exposure in the central nucleosome, with rather similar kinetics to these of a single nucleosome. Array dynamics was probed on a construct where the DNA on the first and the third nucleosome was labeled. In this way, a high FRET signal is obtained when the array compacts, induced by adding Mg^{2+} . FRET-FCS and stopped-flow FRET analysis show that the short arrays show rapid spontaneous conformational dynamics and that protein binding can drive decompaction of the arrays. Based on these results, they propose a model for array dynamics with four different conformational states that have lifetimes ranging from microseconds to seconds. This study shows that spFRET has the potential to address structural dynamics beyond a single model nucleosome.

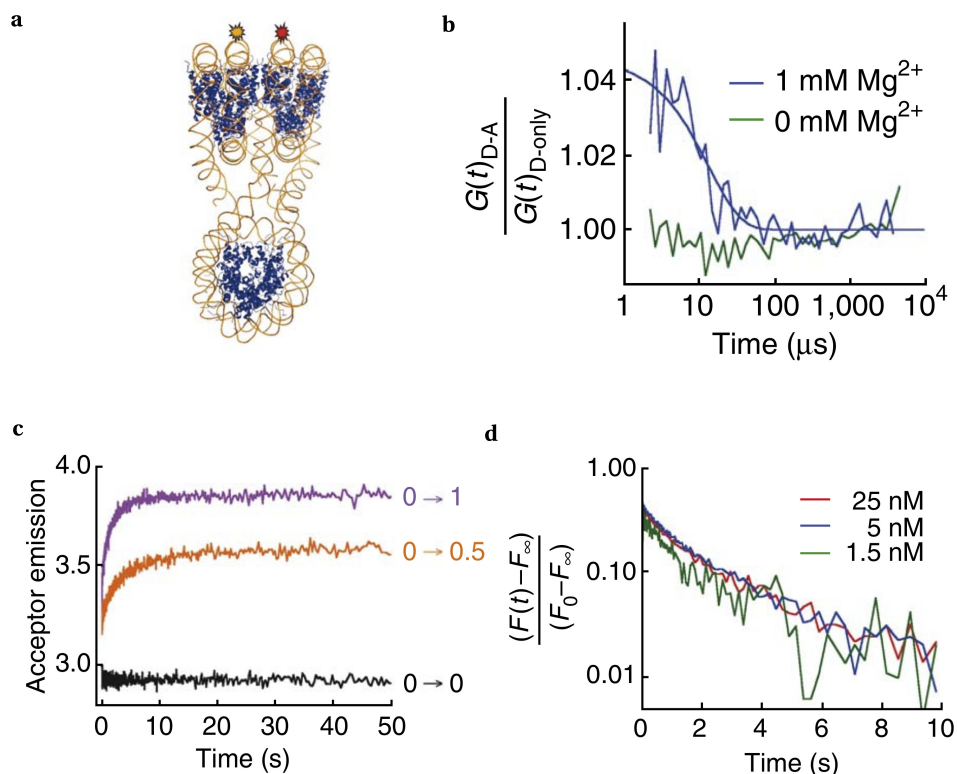


Figure 1.13 – Conformational dynamics of arrays of three nucleosomes. **a:** Three-nucleosomal construct; **b:** Ratio of the donor autocorrelation curves of a sample containing both labels and a donor-only sample isolates kinetics from diffusion fluctuations. Curves for compacted (blue) and extended (green) arrays. An exponential decay with a decay time of $\sim 10^{-5}$ s remains, indicating fluctuations between compact and less compact conformations on this timescale; **c:** stopped-flow FRET analysis of array compaction. Acceptor emission upon donor excitation during array compaction upon rapid mixing with Mg^{2+} (final concentrations 0, 0.5, or 1 mM) is followed. The large instantaneous increase in FRET indicates an array compaction on a timescale faster than $\sim 10^{-3}$ s (mixing dead time), while the further increase of compactness occurs on a timescale of ~ 2 s. **d:** Quantitative analysis of array compactness measured by FRET at different array concentrations. $F(t)$, F_0 , and F^∞ : acceptor fluorescence intensity at time (t), time 0 or at long times, respectively. Rate constants are independent of array concentration, ruling out aggregation effects. (Adapted by permission from Macmillan Publishers Ltd: Nature Structural and Molecular Biology [54] copyright 2009.)

1.11 Conclusions

Nucleosomes have been studied extensively by spFRET experiments. Restriction enzyme assays, bulk FRET and spFRET studies on mononucleosomes have revealed their conformation and dynamics. Here we have shown that despite experimental, instrumental, and biological differences employed in various studies, a coherent picture emerges of a dynamic nucleosome where spontaneous DNA breathing from the nucleosome ends provides access to the nucleosomal DNA. Nucleosomes are open 10 % of the time for tens of milliseconds. Nucleosome stability and DNA breathing can be modulated by DNA sequence and post-translational modifications of the histones. Translocation of nucleosomes along DNA by remodelers and conformational dynamics of higher order chromatin structures has been followed by spFRET. In the near future we can expect studies on more elaborate structures, that more closely resemble the *in vivo* chromatin organization. Integration of force spectroscopy and FRET will make the direct observation of dynamics under controlled force or torque conditions possible, conditions also established by the dynamic ensemble of many nucleosomes in the nucleus. When detailed mechanical behavior of mononucleosomes, arrays of two or a few nucleosomes, longer arrays, and the behavior of native chromatin in living cells have all been investigated, the combined data will provide the structural basis for epigenetic regulation mechanisms.

CHAPTER 2

Making spFRET experiments with nucleosomes succeed

Ruth Buning and John van Noort

2.1 Introduction

Probing nucleosomes with spFRET (single-pair Fluorescence, or Förster, Resonance Energy Transfer) can be very informative and seems straightforward. The Förster radius is generally in the order of 5 nm, ideal for measuring the dynamics of nucleosomes that have a diameter of ~ 10 nm. Nucleosomal DNA (or histones) can be labeled with a FRET-pair, reconstituted into nucleosomes and subsequently diluted to pmol concentrations to measure donor and acceptor intensities in single nucleosomes with confocal microscopy. The resulting FRET efficiency distributions should then reveal variations in nucleosome conformation.

In practice, the experiments and the interpretation of their results are far from trivial. Nucleosome instability during storage and sample preparation, sample heterogeneity, and simplifications in the analysis of fluorescence data can introduce artifacts or obscure the underlying conformational behavior of nucleosomes. All studies on single nucleosomes that aimed to discover nucleosome conformational dynamics in varying conditions and environments have encountered similar challenges regarding dilution, buffer conditions and surface interactions, for example as published in [37, 41, 55, 56].

Under optimal conditions nucleosomes remain stable, i.e. they do not dissociate, show the same behavior over the duration of the experiment, and measurements are reproducible. Experiments are preferably done in conditions where nucleosome behavior can be detected that has some biological relevance. Sample preparation of nucleosomes for single-molecule experiments is however not straightforward. Copying the protocols from one experiment to another is not always possible, for example when using nucleosomes with a different histone composition. Nevertheless, we saw that nucleosomes under optimal conditions can be stable for years (figure 2.1), depending on the specific histone composition, nucleosome concentration, and buffer conditions. In this chapter, we describe the caveats that we encountered during the single-molecule experiments described in this thesis, and present solutions or suggestions how to deal with them.

2.2 Reconstitution of nucleosomes with FRET pairs

2.2.1 DNA substrate

All DNA substrates described in this thesis are obtained by PCR (Polymerase Chain Reaction) and contain the 601 nucleosome positioning sequence [33]¹ (see figure 2.2).

¹CTGGAGAATCCCGGTGCCGAGGCCGCTCAATTGGTCGTAGACAGCTCTAGCACCGCTTAAACGCACGT-ACGCGCTGTCCCCCGCGTTTTAACCGCCAAGGGGATTACTCCCTAGTCTCCAGGCACGTGTCAGATATATACATCCTGT

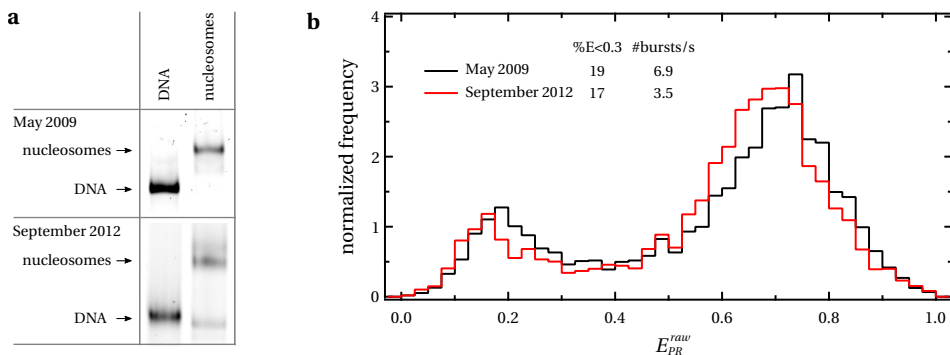


Figure 2.1 – The same nucleosome reconstitution measured twice, with an interval of more than three years. **a**: Acceptor fluorescence image of a 5 % polyacrylamide gel with DNA and reconstituted nucleosomes. After three years, a small fraction of free DNA can be observed. **b**: FRET efficiency distribution inside the nucleosome bands shown in **a**. Population sizes with and without FRET have not changed (error margin 4 %). Shifts in FRET efficiency values are due to re-alignment of the setup. Nucleosomes were reconstituted with chicken erythrocyte histone octamers.

Fluorescent labels are easily incorporated by using fluorescently labeled primers in the PCR reaction.

Label positions that allow for the detection of nucleosomal DNA unwrapping from the nucleosome ends require the use of long, i.e. about 80 bp, primers. A detailed protocol for choosing label positions and the PCR reaction can be found in [34]. PCR reactions with primers this long are likely to produce suboptimal yields and/or by-products. The PCR products were therefore always analyzed with gel electrophoresis. If, despite optimizing the PCR conditions and standard PCR purification procedures, unwanted by-products remain, the desired product can be extracted from the gel after electrophoresis. However, UV illumination, used for imaging of DNA to facilitate the excision of gel bands, can cause nicks in the DNA. DNA substrates containing only one of the fluorescent labels, for example the free primers or substrates where one of the fluorophores is bleached, may strongly bias ensemble measurements, though do not interfere with spFRET experiments that use Alternating Laser Excitation (ALEX). It is therefore not necessary to remove these side products for spFRET experiments. Nevertheless, the long primers and the resulting nonuniform mixture of PCR products require special attention during PCR and gel analysis.

If the desired DNA construct is significantly longer than the 147 bp that forms the nucleosome core, a single PCR is not sufficient to incorporate both labels within the nucleosome. We obtained DNA fragments containing more than ~50 bp linker DNA in addition to the fluorescently labeled nucleosome positioning sequence by ligation of multiple PCR products. To minimize losses due to the formation of alternative ligation

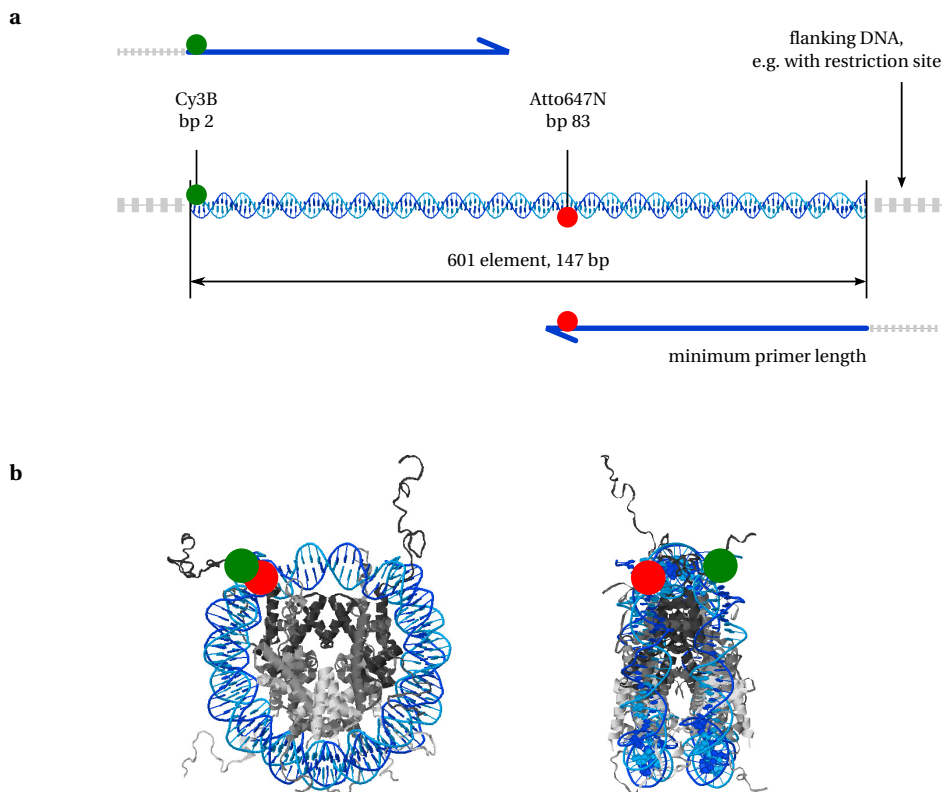


Figure 2.2 – a: DNA construct for mononucleosomes. All constructs described in this thesis are based on the 601 positioning sequence. The 147 bp of nucleosomal DNA are shown, with flanking DNA in grey dashes. The flanking DNA can contain restriction sites to allow subsequent digestion and ligation, or biotin or antidigoxigenin for immobilization. Fluorescent labels are incorporated in the nucleosomal DNA by PCR with fluorescently labeled primers. The fluorescent labels are ~24 nm apart in the DNA substrate, yielding no FRET. In reconstituted nucleosomes, the labels are only several nm apart, resulting in FRET efficiencies above 0.5. Label positions can be chosen at other locations in the nucleosome, different than shown here, to reveal DNA breathing more internally to the nucleosome. Unless mentioned otherwise, the nucleosome constructs presented in this chapter are fluorescently labeled at the positions indicated here. **b:** Top and side view of the crystal structure of the nucleosome core particle (1KX5, [12]), consisting of 147 bp DNA wrapped around the histone octamer, including FRET labels.

products, we used non-palindromic restriction sites.

spFRET on nucleosomes puts high demands on the homogeneity of the samples, as one wants to unequivocally attribute differences in FRET to conformational changes rather than different sample compositions. The more complicated DNA constructs required more digestion and ligation steps. Every digestion, ligation and purification step has a limited yield and causes loss of material. Five steps with 90 % yield already result in a loss of 40 % of the initial material. Therefore, a compromise was found between the purity of the sample and the amount of material.

Other methods to obtain DNA substrates include: annealing of multiple oligomers [57], restriction of the desired fragment from plasmids, or purification from native DNA, though the latter two methods lack the possibility to make use of modified oligomers to incorporate fluorophores. Alternative to fluorescently labeling the DNA molecule with a donor and an acceptor fluorophore, one or two of the labels could be placed on the histones [35, 36, 58, 59]. However, since all histones are present in duplo in each nucleosome, this method yields also complex mixtures.

Thus, though well established and straightforward techniques can be used to prepare DNA substrates for spFRET nucleosomes, the large number of preparation steps and the incomplete yields of each step make it far from straightforward to prepare enough homogeneous DNA material for reconstitution of FRET-labeled nucleosomes.

2.2.2 Nucleosome reconstitution

Nucleosomes can be reconstituted from DNA and histone octamers by salt gradient dialysis as described in [34]. DNA and histone octamers (HO) were mixed in various molar ratios to optimize the reconstitution yield. A high quality reconstitution product contains negligible amounts of bare DNA, which manifests itself as a single sharp band of reconstituted nucleosomes after native polyacrylamide gel electrophoresis (PAGE). The optimal molar ratio [DNA substrate]:[HO] is determined empirically and lies typically between 1:1 and 1:2 for mononucleosomes. Too high [HO] results in the formation of aggregates and acceptor quenching, shown in bulk fluorescence spectra (see figure 2.8).

Not only the molar ratio [DNA substrate]:[HO], also the total amount of DNA in the reconstitution reaction determines the quality of the reconstitution product. In general, the higher the total DNA concentration, the higher the reconstitution quality. For better reconstitution yields, competitor DNA is often added to the reconstitution reaction. Competitor DNA acts as a 'buffer' to capture superfluous HO to prevent the formation of aggregates. High DNA concentrations also help to minimize negative effects imposed by low concentrations and surface interactions (see sections 2.4.1 and 2.4.3). In our experience, a minimum of 100 nM of DNA substrate and a total amount of DNA (substrate plus competitor DNA) of 1-4 μg in 40 μl is optimal.

Before spFRET, we analyzed the reconstitution quality with ensemble methods. We determined the average FRET efficiency of the sample with bulk fluorescence spectroscopy. We used polyacrylamide gel electrophoresis (PAGE) to determine the relative concentrations of bare DNA and nucleosomes. All fluorescently labeled species, as well as their FRET efficiencies, can be visualized when the polyacrylamide gel is imaged with a fluorescence imager. While PAGE analysis clearly resolves subpopulations in the sample, it can affect nucleosome integrity, as discussed in section 2.3. Bulk fluorescence measured in a cuvette minimally disturbs the sample and proved to be an easy and quick reconstitution check. The combination of the two techniques yields a full, though ensemble averaged, characterization of the reconstitution.

When the DNA ligation contains side-products, and/or the reconstitution quality is too low, one could purify fully reconstituted nucleosomes from incomplete nucleosomes and bare DNA by ion exchange chromatography [60], gel electrophoresis or sucrose gradient purification [33, 61]. However, since 50-99% of material can be lost in such purification processes, even larger amounts of start material are required. Alternatively, single-molecule experiments can be performed directly inside the gel, without extraction of nucleosomes, using the gel to separate nucleosomes from other species [42, 62].

2.3 Nucleosomes in a polyacrylamide gel

Nucleosome reconstitutions were analyzed with 5% native polyacrylamide gel electrophoresis (PAGE). A sample of 2-8 μ l of reconstitution product was loaded on the gel (typically 29:1 bis:acrylamide, 0.2 \times TB, Amersham Bioscience Hoefer SE 400 vertical gel slab unit). The gel was run at 19 V/cm at 7 $^{\circ}$ C for 90-120 minutes to separate nucleosomes from free DNA. We used fluorescence imaging for fast and accurate determination of the relative amounts of material in the bands as well as their FRET efficiencies (see section 2.6). Subsequently, we did spFRET experiments in the same gel. In some cases we observed disruptive effects of the polyacrylamide gel on the nucleosomes (see figure 2.3). Nucleosome concentrations in the gel typically drop below a nM, as measured by the burst rate, which would lead to dilution-driven dissociation. At this point it is not clear what determines the delicate balance between dilution driven dissociation, gel matrix induced disruption, and the effect of the gel matrix acting as a crowding agent, which would help to prevent dilution-driven dissociation to some extent.

Disruption inside the gel appeared to be very much dependent on the histone content. Nucleosomes reconstituted with chicken erythrocyte histone octamers (HO) and recombinant *Xenopus* Leavis HO showed slightly enhanced dissociation in the gel in some cases. Nucleosomes reconstituted with recombinant *Arabidopsis thaliana* HO showed severe dissociation in the gel. However, *Arabidopsis thaliana* nucleosomes

containing H2A.Z instead of H2A were more stable, as shown in figure 2.3b. Thus, in-gel spFRET experiments cannot be interpreted unambiguously.

2.4 Sample preparation for spFRET

2.4.1 Dilution to single-molecule concentrations

To measure single nucleosomes in a confocal microscope, the concentration of (fluorescently labeled) nucleosomes should be in the order of pM. Such sub-nM concentrations of nucleosomes and low ionic strengths however, seem to be quite remote from the conditions found *in vivo*. Moreover, dilution to sub-nM concentrations promotes dissociation of the nucleosomes [56,63]. Addition of crowding agents to the buffer and low ionic strengths prevent this dissociation. A straightforward solution to measure spFRET is to use a high concentration of nucleosomes (10-100 nM), where only a fraction of the nucleosomes is fluorescently labeled. A study that uses this principle to combine bulk and single-molecule measurements under exactly the same conditions is described in detail in [63]. In the experiments described in this thesis, we follow this strategy and keep the nucleosome concentration relatively high by adding unlabeled nucleosomes to the sample. The unlabeled nucleosomes should have the same histone composition as the labeled nucleosomes in such experiments, because histone proteins, especially the H2A-H2B dimers, can exchange between nucleosomes.

Single-molecule experiments inside a polyacrylamide gel have similar constraints. The nucleosome concentration in the band should be low enough to detect individual nucleosomes. Unlabeled nucleosomes can also be added to the gel, but they should run together with the labeled nucleosomes and should therefore have the same DNA length and position of the nucleosome. Single-molecule experiments in solution do not require identical DNA in the labeled and unlabeled nucleosomes and can therefore more easily be diluted. In both methods it is important to be aware of undesired nucleosome dissociation.

The labeled nucleosome concentration after reconstitution can be determined by the bulk fluorescence signal of the acceptor (neglecting dissociation and incomplete reconstitution). This is not necessarily the same as the DNA input concentration. In general, the nucleosome concentration is much lower after reconstitution as nucleosomes are lost during the reconstitution reaction due to sticking to surfaces. The labeled nucleosome concentration in the spFRET sample can be estimated from the burst rate. Typically, five bursts per second, with an average burst duration of 2 ms and a detection volume of a femtoliter, corresponds to ~20 pM. Thus, labeled nucleosomes can and need to be diluted with unlabeled nucleosomes to pM concentrations for spFRET.

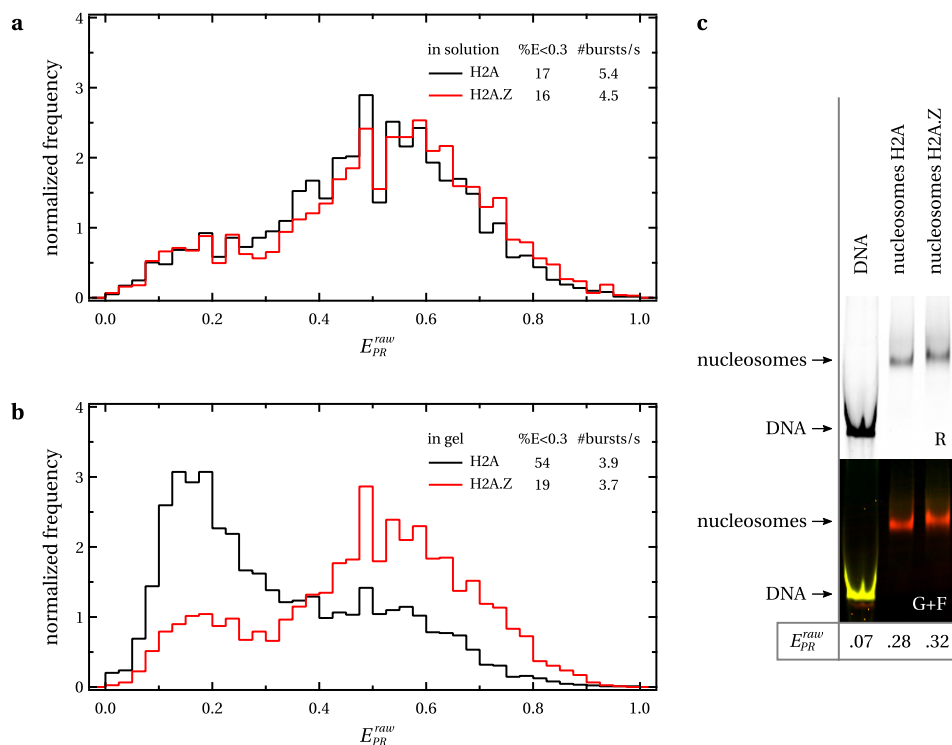


Figure 2.3 – FRET efficiency distributions of mononucleosomes reconstituted with canonical H2A or the variant H2A.Z of *Arabidopsis Thaliana* histones. **a**: single-molecule experiments in solution; **b**: single-molecule experiments in 5% PA gel shown in **c**. Where we expect a smaller population without FRET in the gel due to separation from free DNA, the population without FRET is highest in the gel which we attribute to disruption of the nucleosomes after electrophoresis. Nucleosomes containing H2A are more susceptible to disruption in the gel than nucleosomes containing H2A.Z. The data shown here is for nucleosomes with FRET labels 27 bp from the nucleosome exit.

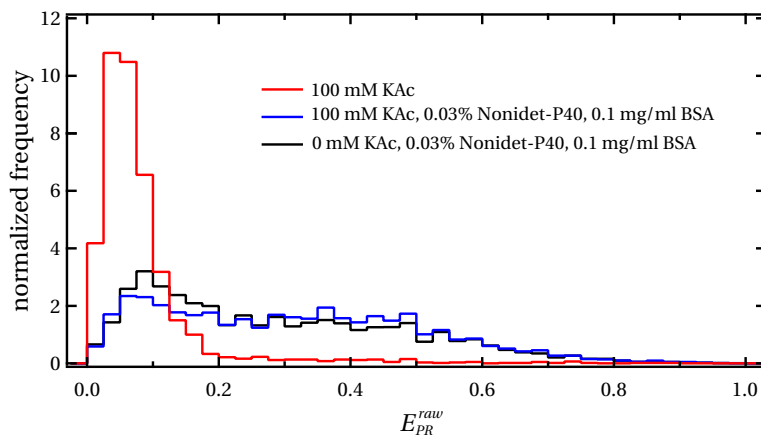


Figure 2.4 – FRET efficiency distribution of mononucleosomes in solution at zero and at 100 mM monovalent salt. Addition of BSA and Nonidet P-40 prevents dissociation at 100 mM salt. Nucleosome concentration is around 10 pM.

2.4.2 Buffer conditions

Buffer conditions have a large effect on both the nucleosome integrity, and the optical performance of the fluorescent dyes. Typically, nucleosomes are kept in 10 mM Tris.HCl pH 8. Depending on the desired measurement conditions, mono- or divalent salts can be added. For example, nucleosome-nucleosome interactions require the presence of several mM magnesium ions (see chapter 5 of this thesis). However, at sub-nM nucleosome concentrations, 100 mM of monovalent salt, approaching *in vivo* conditions, can be enough to lose all FRET, indicating dissociation of the nucleosomes.

This problem is relieved by adding Nonidet P-40 and BSA, as shown in figure 2.4. BSA acts as a crowding agent to prevent dilution-driven dissociation. The anionic detergent Nonidet P-40 (also known as IGEPAL CA-630) has been found to increase the reproducibility of experiments with nucleosomes, indicating a stabilizing effect, and to prevent nucleosome precipitation [42, 55]. In this thesis, we used 0 or 50 mM NaCl, as a compromise between stability and physiological relevance.

To prevent photobleaching and -blinking of the fluorophores, an oxygen scavenger system was added to the nucleosome sample. We initially used catalase, glucose oxidase and glucose, combined with trolox. We found however that the addition of trolox only was sufficient to yield negligible amounts of photobleaching and -blinking events. Therefore, the catalase, glucose oxidase and glucose was usually omitted.

Buffer conditions inside a polyacrylamide gel are restricted by the physical properties of the gel. Proteins like BSA, catalase and glucose oxidase can not freely enter the gel matrix. Nonidet P-40 is also not compatible with in-gel experiments. Salts and

trolox can on the other hand be used without problems. However, the addition of moderate salt concentrations (10-500 mM) in absence of BSA and Nonidet P-40 leads to nucleosome dissociation, which could only be prevented by high levels of unlabeled nucleosomes (~100 nM) in the corresponding gel band.

Overall, the stability constraints of nucleosomes require careful optimization of the buffer conditions, which can be different for different nucleosome types and measurement methods.

2.4.3 Surface effects

During sample preparation and experiments, nucleosomes are exposed to surfaces like eppendorf tubes, pipet-tips, dialysis tubes for reconstitutions and microscope slides. Such surface exposure has a detrimental effect, as nucleosomes stick and/or dissociate near a surface [41]. The resulting drop in nucleosome concentration can be as large as tens of percents, and can in turn result in additional, dilution-driven, dissociation. The lower the initial nucleosome concentration, the larger the relative effect of the surfaces. Especially when working with concentrations below 10 nM and with relatively large surface areas (pipetting, ~ μ l sample volumes), it was essential to minimize surface interactions by using non-stick or silanized tubes and pipet-tips. Vortexing and shaking of nucleosome samples during transport further increased surface exposure and was avoided when possible. An example of (dilution driven) dissociation caused by increased surface exposure is shown in figure 2.5.

spFRET with nucleosomes in solution was measured 25 μ m above the microscope slide surface. This height however was not always sufficient to prevent surface induced dissociation of nucleosomes. Surface passivation by coating with starPEG was effective to prevent surface driven dissociation, as shown in figure 2.6. Interestingly, we found that the susceptibility of nucleosomes to surface interactions depends on the HO origin. It was therefore important to always evaluate the effects of surfaces on nucleosome stability.

2.5 Single-molecule fluorescence spectroscopy

2.5.1 Confocal setup

Single molecules were imaged with a home-built confocal microscope equipped with a 60 \times water-immersion objective (NA=1.2, Olympus), as schematically depicted in figure 2.7a (see also [42]). A 515 nm diode pumped solid state laser (Cobolt) and a 636 nm diode laser (Power Technology) were used as excitation sources. The lasers were alternated at 20 kHz by analog modulation, either directly (636 nm), or with an AOM (515 nm; Isomet). The beams were spatially filtered with a single-mode fiber, and

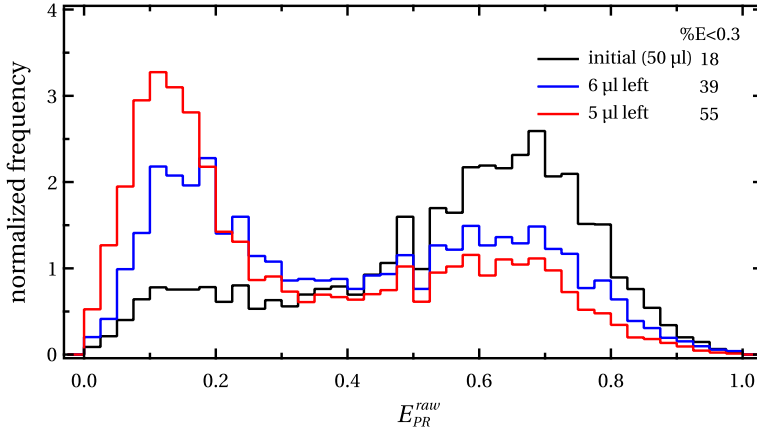


Figure 2.5 – FRET efficiency distribution of mononucleosomes stored in normal eppendorf tubes after reconstitution. The initial volume was about 50 μl . The population of nucleosomes without FRET increased dramatically when the total volume was reduced to a few μl . The lower volume in the tube results in relatively more surface-exposure, enhancing surface-induced dissociation. All measurements in 10 mM Tris.HCl pH 8.0, 0.1 mg/ml BSA, 0.03 % Nonidet P-40 and 2 mM trolox (no salt).

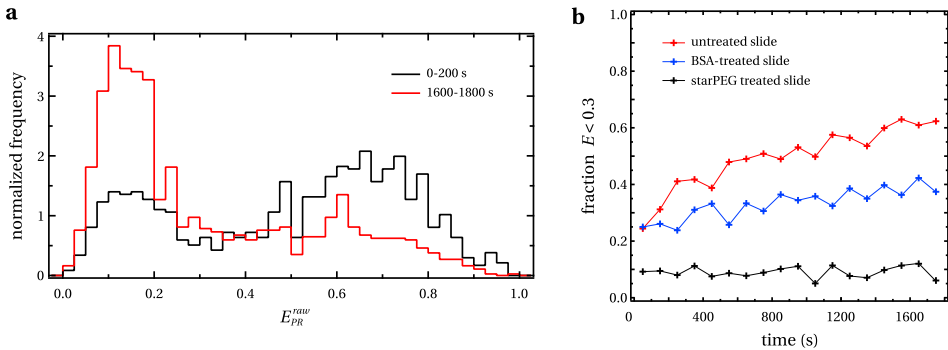


Figure 2.6 – Increase of population of nucleosomes without FRET due to interactions with the surface of the microscope slide during a 30 minute single-molecule measurement of mononucleosomes. **a:** FRET efficiency histogram of the first and last 200 seconds of measurement on an untreated microscope slide. **b:** fraction of bursts with a proximity ratio below 0.3, as a function of time after the start of the measurement. The fraction without FRET increases on an untreated slide. Slides incubated with BSA partly prevent dissociation. On starPEG coated slides [64, 65], the fraction without FRET is stable over the measurement time (and longer, data not shown). All measurements in 10 mM Tris.HCl pH 8.0, 0.1 mg/ml BSA, 0.03 % Nonidet P-40, 2 mM trolox, 50 mM NaCl, and a 5-10-fold excess of unlabeled nucleosomes.

focussed 25 μm above the glass-buffer interface by the objective. The excitation powers were in the order of 10 μW . The collected fluorescence was spatially filtered with a 50 μm pinhole in the image plane, and was split into a donor and an acceptor channel by a dichroic mirror (640dcxr, Chroma). The fluorescence was filtered with emission filters (hq570/100m for the donor channel, hq700/75m for the acceptor channel, Chroma) to minimize crosstalk, and was imaged on the active area of single photon avalanche photodiodes (SPCM AQR-14, Perkin-Elmer). The photodiodes were read out with a TimeHarp 200 photon counting board (Picoquant GmbH). Figure 2.7b shows an example of a fluorescence time trace with bursts of individual nucleosomes. In a typical experiment, data was collected for 30 minutes in which 2000-10000 bursts of fluorescence were detected.

2.5.2 Single-molecule burst selection

A burst selection algorithm is needed to distinguish fluorescence events from background. Bursts of fluorescence were detected using the method described in [66]. A burst was assigned if a minimum of 50 photons arrived subsequently, with a maximum interphoton time of 100 μs . If the maximum interphoton time is taken too small, single bursts can be split, resulting in double counts and bursts with relatively low numbers of photons, leading to broadening of the FRET efficiency histograms. Lowering the minimum number of photons per burst increases the number of bursts detected, but may lead to the detection of false positives and again broadening of the FRET histograms. If it is taken too high, bursts will be missed.

2.5.3 Caveats in spFRET

Though the principle of burst detection and classification seems to be straightforward, it can be prone to multiple complications. Burst selection criteria were chosen to minimize false negatives, i.e. missed bursts, and false positives, i.e. fluctuations in background intensity mistakenly marked as bursts, which would both lead to broadening and shifting of FRET distributions.

Another artifact arises when individual particles pass the detection volume multiple times. This will be detected as multiple bursts and leads to double (or more) counts of the same particle, which is undesired. It can however be turned to an advantage and used as a tool to detect dynamics at timescales longer than the diffusion time (~ 2 ms in solution, ~ 4 ms in gel), with so-called recurrence analysis of single particles (RASP), developed by Hoffmann et al [67]. Here we ignored possible multi-passage bursts.

Making use of Alternating Laser EXcitation (ALEX), we determined not only the FRET efficiency, but also the label stoichiometry for every burst [43]. This allows sorting into doubly labeled (Donor (D) + Acceptor (A)) and Donor-only and Acceptor-only

bursts. D-only and A-only bursts can then be excluded from subsequent analysis. Artifacts due to the presence of D-only and A-only populations resulting from photo-bleaching are avoided in this manner. Although ALEX allows to select for D+A labeled particles, it can not distinguish between nucleosomes without FRET (that are partially unwrapped) and free DNA. The amount of free DNA should therefore be negligible, or accurately determined by for example gel electrophoresis (which is not straightforward, as described in section 2.3).

We determined for every burst the mean FRET efficiency and label stoichiometry from all photons in the burst. When all caveats are properly taken care of, the observed distribution can be split into separate populations with differing FRET efficiencies, reflecting different conformations of the nucleosome. This variation can be either static or dynamic. A burst analysis technique that resolves static from dynamic heterogeneity is presented by Tomov et al. [68]. Here, we did not discriminate between static and dynamic differences in FRET. Based on previous work [41] we anticipate the lifetimes of the open and closed conformation of the nucleosome to be 25 and 280 ms, which are both larger than the diffusion limited window of 2-4 ms we can measure here.

2.6 Quantitative comparison of multiple FRET techniques

Though different measurement techniques have different requirements for sample preparation, which may have a large effect on the measured FRET, we nevertheless aimed for a quantitative comparison of FRET efficiencies across setups.

2.6.1 Bulk fluorescence spectroscopy

The average FRET efficiency, as determined from the ensemble fluorescence spectrum, gives a general indication of the yield of the nucleosome reconstitution reaction. The sample does not need to be diluted and could be recovered from the cuvette after measuring. A typical bulk fluorescence spectrum of mononucleosomes with Cy3B and ATTO647N is shown in figure 2.8. Typically, we record two emission spectra: emission from 535 to 735 nm with donor excitation (515 nm) and emission from 635 to 735 nm with direct acceptor excitation (615 nm).

We determined the FRET efficiency from the enhanced fluorescence of the acceptor using the ratio_A method [28]:

$$E_{\text{ratio}A} = \frac{\epsilon_{615}^A}{\epsilon_{515}^D} \frac{F_{515}^A}{F_{615}^A} - \frac{\epsilon_{515}^A}{\epsilon_{515}^D} \frac{d^+}{d^+} \quad (2.1)$$

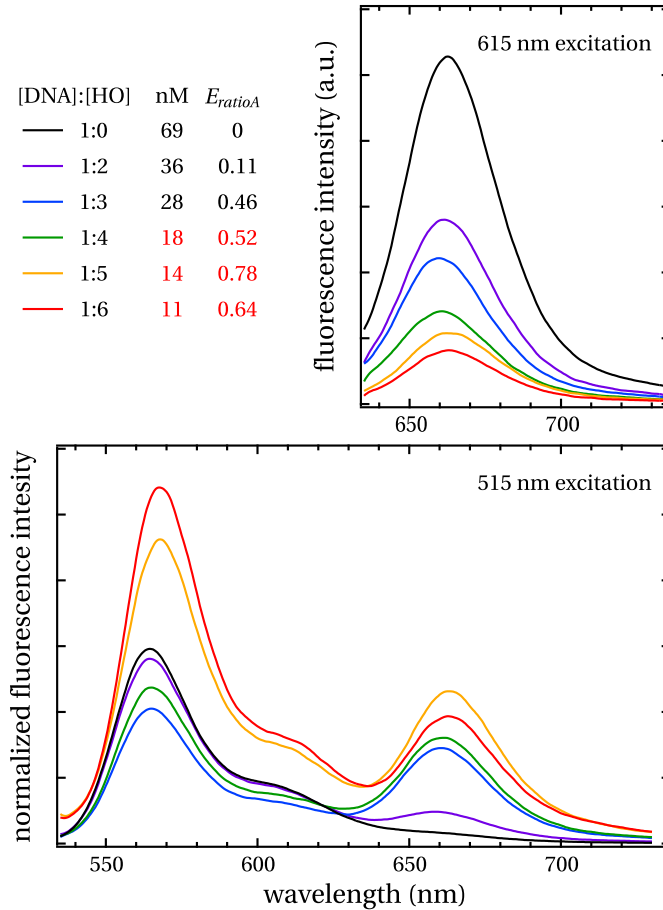


Figure 2.8 – Bulk fluorescence spectra of mononucleosome reconstitutions. The concentration is determined from the peak fluorescence intensity with excitation at 615 nm (direct acceptor excitation). The fluorescence spectra for 515 nm excitation are normalized by dividing by the peak fluorescence intensity for 615 nm excitation. The FRET efficiency is determined from the peak intensities with excitation at 515 nm via equation 2.1. For high histone octamer (HO) concentrations, the 615 nm spectra do no longer provide an accurate concentration estimation. The nucleosome concentration is underestimated, as shown by the normalized 515 nm spectra, which lie above the lower [HO] spectra over the entire wavelength range. FRET efficiencies calculated from these spectra are not reliable, indicated by values in red. Note also the shift of the acceptor fluorescence peak to higher wavelength, like the peak for bare DNA. The optimal [DNA] to [HO] ratio depends on multiple factors, including the absolute DNA concentration and the amount of competitor DNA and can differ from what is shown here.

where $\epsilon_{\lambda}^{A/D}$ is the donor or acceptor extinction coefficient at wavelength λ , F_{λ}^A the fluorescence intensity of the acceptor when excited at wavelength λ , and d^+ the fractional labeling coefficient of the donor. The fluorescence intensity of the acceptor was determined from its maximum value, which is at approximately 663 nm. To obtain the acceptor fluorescence when excited at the donor wavelength, F_{515}^A , the donor fluorescence at 663 nm, which was previously determined from the fluorescence at 663 nm of a donor-only sample and was typically found to be $0.11 \cdot F_{515}^D$, was subtracted. d^+ was determined from DNA and fluorophore absorption peaks in an absorption spectrum of the labeled DNA.

The fluorescence intensity of the acceptor for direct acceptor excitation is a measure for the acceptor concentration, which can be calibrated with an absorption spectrum. If the amount of acceptor-only species (e.g. free primers) and free DNA in the sample is negligible, the acceptor concentration directly gives the nucleosome concentration in the sample.

At high histone octamer concentrations, the total acceptor concentration seems to drop, as shown in fluorescence spectra for direct acceptor excitation (figure 2.8). This is possibly due to the formation of aggregates accompanied by acceptor quenching. This leads to an underestimation of the nucleosome concentration and incorrect FRET efficiency calculation and normalization of 515 nm excitation spectra.

2.6.2 PAGE and spFRET

The definitions and descriptions how to determine FRET efficiencies and correction factors found in this section are all based on Lee et al. [31].

2.6.2.1 Definitions of FRET efficiencies and label stoichiometries

Photon streams and correction factors In any FRET experiment with excitation and detection at both the donor (D) and acceptor (A) wavelength, four experimental photon streams exist:

- D-emission upon D-excitation: I_{Dex}^{Dem}
- A-emission upon D-excitation: I_{Dex}^{Aem}
- D-emission upon A-excitation: I_{Aex}^{Dem}
- A-emission upon A-excitation: I_{Aex}^{Aem}

The A-emission upon D-excitation consists mainly of photons due to FRET (I^F), but leakage of donor photons into the acceptor channel and direct excitation of the acceptor by the donor excitation wavelength also contribute to this signal:

$$I_{Dex}^{Aem} = I^F + l \cdot I_{Dex}^{Dem} + d \cdot I_{Aex}^{Aem} \quad (2.2)$$

The correction factors l for leakage and d for direct excitation depend on absorption cross sections, quantum efficiencies and detection efficiencies of the dyes and the detection system and can be experimentally determined from D- and A-only fractions or samples, as explained in detail in [31]:

$$l = \frac{I_{Dex}^{Aem}}{I_{Dex}^{Dem}} \quad \text{for a D-only population} \quad (2.3)$$

$$d = \frac{I_{Dex}^{Aem}}{I_{Aex}^{Aem}} \quad \text{for an A-only population} \quad (2.4)$$

Correction factor l is defined by the detection efficiencies of D-emission in the D- and A-channel, and is thus instrument-dependent. Correction factor d is determined by the photon counts of A-emission upon D- and A-excitation, and is therefore dependent on the laser intensities. Therefore, d must be determined for every measurement (series) separately, since laser intensities were varied to minimize bleaching effects and to balance the donor and acceptor signal intensities.

FRET efficiency The absolute FRET efficiency is given by:

$$E = \frac{I^F}{I^F + \gamma I_{Dex}^{Dem}} = \frac{I_{Dex}^{Aem} - l I_{Dex}^{Dem} - d I_{Aex}^{Aem}}{I_{Dex}^{Aem} - l I_{Dex}^{Dem} - d I_{Aex}^{Aem} + \gamma I_{Dex}^{Dem}} \quad (2.5)$$

where γ is a detection correction factor involving quantum yields (ϕ) and detection efficiencies (η) of donor and acceptor [69, 70]:

$$\gamma = \frac{\phi_A \eta_{Aem}^A}{\phi_D \eta_{Dem}^D} \quad (2.6)$$

η_{Dem}^D and η_{Aem}^A are the detection efficiencies of D-emission in the D-detection channel and A-emission in the A-detection channel.

Taking $\gamma = 1$ gives the proximity ratio:

$$E_{PR} = \frac{I^F}{I^F + I_{Dex}^{Dem}} = \frac{I_{Dex}^{Aem} - l I_{Dex}^{Dem} - d I_{Aex}^{Aem}}{I_{Dex}^{Aem} - l I_{Dex}^{Dem} - d I_{Aex}^{Aem} + I_{Dex}^{Dem}} \quad (2.7)$$

The proximity ratio is often used instead of the absolute E to circumvent determination of γ . If only relative changes in the FRET efficiency histogram are of interest, the proximity ratio suffices. Differences between E and E_{PR} as a function of γ are most

pronounced for intermediate FRET values. To increase the resolution for low- E samples, Gansen et al. [32] developed an approach that deliberately lets γ deviate from 1. Note that the expression for E_{PR} still involves the corrections for leakage and direct excitation. Without these correction factors, we get the most simplified expression for the FRET efficiency:

$$E_{PR}^{raw} = \frac{I_{Dex}^{Aem}}{I_{Dex}^{Aem} + I_{Dex}^{Dem}} \quad (2.8)$$

which can be directly calculated from the experimental photon streams, but depends heavily on the experimental conditions.

Label stoichiometry Accurate FRET measurements require dual labeling of every molecule in the sample. This can not always be achieved, especially for spFRET, in which bleaching occurs frequently. We therefore measure the label stoichiometry S in each measurement. Similar to the expressions for the FRET efficiency, Lee et al. [31] defined an E -independent stoichiometry ratio S_γ ; a crosstalk-corrected stoichiometry ratio S , and a raw stoichiometry ratio S^{raw} :

$$S_\gamma = \frac{I^F + \gamma I_{Dex}^{Dem}}{I^F + \gamma I_{Dex}^{Dem} + I_{Aex}^{Aem}} = \frac{I_{Dex}^{Aem} - l I_{Dex}^{Dem} - d I_{Aex}^{Aem} + \gamma I_{Dex}^{Dem}}{I_{Dex}^{Aem} - l I_{Dex}^{Dem} - d I_{Aex}^{Aem} + \gamma I_{Dex}^{Dem} + I_{Aex}^{Aem}} \quad (2.9)$$

$$S = \frac{I^F + I_{Dex}^{Dem}}{I^F + I_{Dex}^{Dem} + I_{Aex}^{Aem}} = \frac{I_{Dex}^{Aem} - l I_{Dex}^{Dem} - d I_{Aex}^{Aem} + I_{Dex}^{Dem}}{I_{Dex}^{Aem} - l I_{Dex}^{Dem} - d I_{Aex}^{Aem} + I_{Dex}^{Dem} + I_{Aex}^{Aem}} \quad (2.10)$$

$$S^{raw} = \frac{I_{Dex}^{Aem} + I_{Dex}^{Dem}}{I_{Dex}^{Aem} + I_{Dex}^{Dem} + I_{Aex}^{Aem}} \quad (2.11)$$

Correction factor γ The correction factor γ can be experimentally determined from the relation between E_{PR} and S for two or more populations measured under identical conditions, ideally within a single measurement. The slope (Σ) and intercept (Ω) of the linear relation between E_{PR} and $1/S$ define γ :

$$1/S = \Omega + \Sigma E_{PR} \quad (2.12)$$

$$\gamma = (\Omega - 1)/(\Omega + \Sigma - 1) \quad (2.13)$$

The correction factor γ , defined in equation 2.6, depends on the quantum yields, and thus on the local environment of the fluorophores (e.g. pH, temperature, incorporation site of the fluorophore), and on the detection efficiencies, which depend on

the optical alignment of the setup and the properties of optics, filters and the detectors used. Therefore, accurate comparison of experimental FRET efficiencies requires a fresh determination of γ for every setup, and even for every measurement series when the alignment or experimental factors have been altered.

2.6.2.2 Determination of correction factors

spFRET For the single-pair FRET experiments, determination of the correction factors is quite straightforward. The ability of ALEX to recover D-A stoichiometry enables sorting of D-only, A-only and D-A species. Population sorting allows determination of all correction factors needed in a single measurement. The sorting capability of ALEX allows accurate determination of the FRET efficiency, independent of instrumental factors (like excitation intensity and optical components/alignment). All data necessary is available from a single measurement.

l follows from the D-only population: calculate l (eq. 2.3) for every burst and take the mean.

d follows from the A-only population: calculate d (eq. 2.4) for every burst and take the mean.

γ follows from two or more D+A populations with different FRET efficiency. After correcting for l and d , calculate E_{PR} (eq. 2.7) and S (eq. 2.10) for every burst and take the mean. A linear fit to $1/S$ versus E_{PR} gives γ via slope and intercept (eqs. 2.12 and 2.13).

Gel electrophoresis For the polyacrylamide gel electrophoresis (PAGE) experiments described in 2.3, the correction factors can be estimated when a D-only and an A-only band is present in the gel.

l follows from a D-only band: calculate l (eq. 2.3) from the integrated fluorescence intensities of the band (after background-subtraction).

d follows from an A-only population: calculate d (eq. 2.4) from the integrated fluorescence intensities of the band (after background-subtraction).

γ follows from two or more D+A bands with differing FRET efficiency. After correcting for l and d , calculate E_{PR} (eq. 2.7) and S (eq. 2.10) for every band. A linear fit to $1/S$ versus E_{PR} gives γ via slope and intercept (eqs. 2.12 and 2.13).

A caveat when determining the correction factors for PAGE experiments is that the D-only and A-only fractions within D+A bands are unknown, which leads to an underestimation of γ . D-only and A-only populations can originate from bleaching of one of the fluorophores during the electrophoresis and/or imaging process.

2.6.2.3 Comparison of γ across setups without absolute γ determination

The ratio between the values of γ for two different setups or measurement series can be determined without knowledge of the absolute γ values if a FRET standard with fixed FRET efficiency is measured in both setups. It is required that the D-only population is either absent (i.e. by population sorting with ALEX-spFRET) or (assumed to be) the same for both setups/measurement series.

The absolute FRET efficiency (eq. 2.5) must be identical for both datasets (subscripts 1 and 2):

$$E = \frac{I_1^F}{I_1^F + \gamma_1 I_{Dex,1}^{Dem}} = \frac{I_2^F}{I_2^F + \gamma_2 I_{Dex,2}^{Dem}} \quad (2.14)$$

Rearrangement of eq. 2.7 gives:

$$\frac{1}{E_{PR}} - 1 = \frac{I_{Dex}^{Dem}}{I^F} \quad (2.15)$$

Rearrangement of eq. 2.14 and substitution of eq. 2.15 gives:

$$\frac{1}{E} - 1 = \gamma_1 \frac{I_{Dex,1}^{Dem}}{I_1^F} = \gamma_1 \left(\frac{1}{E_{PR,1}} - 1 \right) = \gamma_2 \left(\frac{1}{E_{PR,2}} - 1 \right) \quad (2.16)$$

from which follows:

$$\frac{\gamma_1}{\gamma_2} = \frac{E_{PR,2}(1 - E_{PR,1})}{E_{PR,1}(1 - E_{PR,2})} \quad (2.17)$$

2.7 Conclusions

During our spFRET investigations of nucleosomes in various conditions we encountered several difficulties. Here, we described the procedures for the preparation of nucleosome samples, the detection of spFRET with confocal fluorescence spectroscopy and the analysis of FRET efficiencies, and how we have dealt with these difficulties.

Under non-optimal conditions, complete dissociation of nucleosomes into histones and DNA, or partial dissociation into dimers and hexa- or tetramers occurs. Both are irreversible and should be avoided. Non-optimal conditions include dilution to sub-nM concentrations, high ionic strengths and surface effects, and depend on the specific histone composition and probably also the DNA sequence. Based on our experience, described in this chapter, we conclude that essential conditions for good measurements include:

- 100 % reconstitution yield (no bare DNA)
- reconstitution at high DNA concentration ($\sim\mu\text{g}/\mu\text{l}$), and high volumes ($>40\ \mu\text{l}$) (relatively less surface)
- measurement in solution
- addition of BSA & Nonidet P-40
- a total (labeled + unlabeled) nucleosome concentration $> 10\ \text{nM}$
- the use of treated surfaces: non-stick tubes and passivated slides in spFRET experiments

If not only the distribution of subpopulations, but also the FRET efficiencies or label distances are desired, correction factors to the raw FRET efficiency have to be taken into account. The data and considerations presented in this chapter will help future researchers design and carry out spFRET experiments on nucleosomes and have been the basis for all experiments presented in this thesis.

CHAPTER 3

A method for genetically installing site-specific acetylation in recombinant histones defines the effects of H3 K56 acetylation

Heinz Neumann, Susan M. Hancock, Ruth Buning, Andrew Routh, Lynda Chapman, Joanna Somers, Tom Owen-Hughes, John van Noort, Daniela Rhodes, and Jason W. Chin

Based on: Molecular Cell, vol. 36, no. 1, pp. 153-163, 2009

Abstract

Lysine acetylation of histones defines the epigenetic status of human embryonic stem cells, and orchestrates DNA replication, chromosome condensation, transcription, telomeric silencing, and DNA repair. A detailed mechanistic explanation of these phenomena is impeded by the limited availability of homogeneously acetylated histones. We report a general method for the production of homogeneously and site-specifically acetylated recombinant histones by genetically encoding acetyl-lysine. We reconstitute histone octamers, nucleosomes and nucleosomal arrays bearing defined acetylated lysine residues. With these designer nucleosomes we demonstrate that, in contrast to the prevailing dogma, acetylation of H3 K56 does not directly affect the compaction of chromatin, and has modest effects on remodeling by SWI/SNF and RSC. Single-molecule FRET experiments reveal that H3 K56 acetylation increases DNA breathing 7-fold. Our results provide a molecular and mechanistic underpinning for cellular phenomena that have been linked with K56 acetylation.

3.1 Introduction

The post-translational acetylation of chromatin on the ϵ -amine of lysine residues in histone proteins defines the epigenetic status of human embryonic stem cells, and is a crucial regulator of DNA replication, chromosome condensation, transcription, and DNA repair in model organisms [24, 71–75]. Acetylation may alter nucleosome or chromatin structure and function directly, or act to recruit other factors to the genome [24, 72] via interaction with bromodomain containing proteins [76] and other potential acetyl-lysine binding modules [77].

It is emerging that modifications in the globular core of histones play crucial roles in regulating the structure and function of chromatin and controlling biological function [78]. H3 K56 acetylation is a particularly important modification in the globular core of H3 [79–81] that is conserved from yeast to humans [82]. Numerous reports have demonstrated its role in DNA repair and replication, regulation of transcription and chromatin assembly [77, 80, 81, 83–94]. K56 is located on the first α -helix of H3 and makes a water-mediated contact close to the DNA at the entry-exit point on the nucleosome [12]. This has led to the proposal that K56 acetylation modulates the binding of the DNA in the nucleosome. Though H3 K56 acetylation is clearly important in defining epigenetic status, and regulating transcription, replication and repair it has not been possible to experimentally and quantitatively test the mechanistic proposals for how K56 acetylation might affect these complex cellular phenomena [77–79, 81, 83, 85, 87–90, 93] since it has not been possible to synthesize homogeneously acetylated H3 K56.

Current methods to introduce site-specific acetylation into recombinant histones include enzymatic post-translational modification and native chemical ligation [22, 95]. Core histones consist of a structural domain and a long N-terminal tail, and chemical ligation provides an approach suitable for introducing modification into histone tails. For example, the role of H4 K16 acetylation in antagonizing chromatin compaction was demonstrated with histones modified at the N-terminal tail produced by native chemical ligation [22]. This method remains challenging however, requires the synthesis of large quantities of peptide thioester, has not been demonstrated for acetylation in the structured core of histones, and yields small quantities of acetylated protein. Enzymatic post-translational acetylation of histones has also proved challenging [23]. The acetyl-transferase enzymes are large complexes that are difficult to purify. Moreover enzymatic acetylation does not yield homogeneous samples, as acetylation at the desired site is not quantitative and rarely exceeds 30 %, and in vitro acetylation at other sites leads to heterogeneous samples [23]. We recently reported proof-of-principle experiments in which we demonstrated the production of a homogeneously acetylated protein using an aminoacyl-tRNA synthetase and tRNACUA pair that we created by directed evolution. This pair directs the incorporation of acetyl-lysine in re-

sponse to an amber codon in the gene of interest encoded on a plasmid in *E. coli* [96]. While this system is in principle applicable to the production of homogeneously and site-specifically acetylated histones, its utility has previously only been demonstrated in a single case with MnSOD, a small non-histone enzyme.

We report an improved method for genetically encoding site-specific and homogeneous acetylation of histones in *E. coli*. This method has permitted the production of histones modified in the core of the protein, enabling us to produce recombinant histone H3 that is acetylated on K56 in milligram quantities, for the first time. We have assembled histone octamers, nucleosomes and chromatin arrays that bear this modification and investigated the effect of H3 K56 acetylation on nucleosome and chromatin structure and function: we have examined the effect of H3 K56 acetylation on nucleosome stability, transient unwrapping of DNA from single nucleosomes, chromatin compaction and nucleosome remodeling by SWI/SNF and RSC to test the mechanistic hypotheses on the role of this modification that have been proposed on the basis of cellular experiments.

3.2 Results

3.2.1 Production of site-specifically acetylated histones

We recently described an acetyl-lysyl-tRNA synthetase (AckRS)/tRNACUA pair that is derived from the *M. barkeri* (Mb) pyrrolysyl-tRNA synthetase/tRNACUA pair [96]. The AckRS/tRNACUA pair directs the incorporation of acetyl-lysine in response to the amber codon with high translational efficiency and fidelity to produce homogeneously acetylated protein. To improve the efficiency of this system further we made a library, which randomizes residues L266, A267, L270, Y271, L274 in acetyl-lysyl-tRNA synthetase (figure 3.1) and selected for improved efficiency of acetyl-lysine incorporation as previously described [96]. These selections yielded an improved synthetase, which contains a single L266M mutation with respect to AckRS-1. We named the new synthetase AckRS-3. Expression of myoglobin-his6 incorporating acetyl-lysine at position 4 from a myoglobin gene bearing an amber codon at position 4 demonstrates the improvement in protein expression using the new AckRS-3/tRNACUA system.

In order to synthesize acetylated histone H3 we further created a vector which contains the MbtRNACUA gene and an N-terminally hexahistidine tagged histone H3 downstream of a T7 promoter (Supplementary figure 1). We introduced an amber codon at position 56 and transformed this vector into BL21 *E. coli* bearing AckRS-3. Cells were supplemented with 10 mM acetyl-lysine and 20 mM nicotinamide (to inhibit the *E. coli* deacetylase CobB) at OD 0.7, and protein expression induced by addition of IPTG 30 minutes later. Like unmodified histone H3, the H3 K56Ac is over-expressed

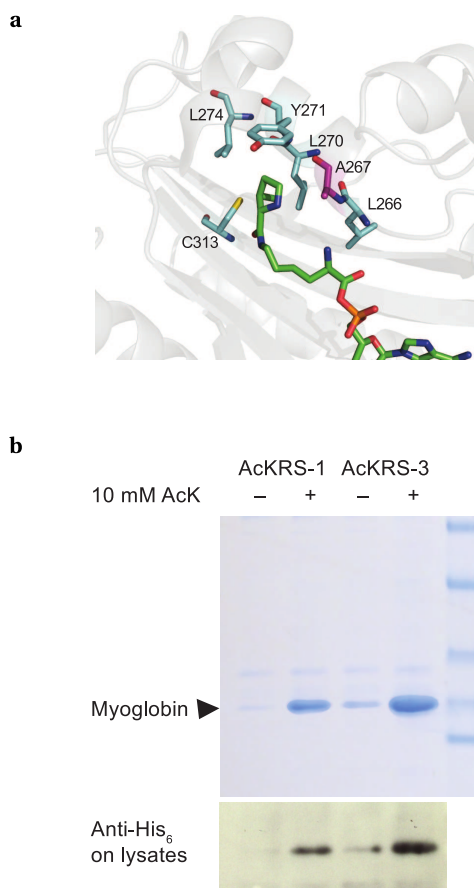


Figure 3.1 – Selection of an improved acetyl-lysyl-tRNA synthetase/tRNACUA pair for the incorporation of acetyl-lysine in recombinant proteins. **a:** The active site of *M. mazei* PylRS bound to pyrrolysine (figure created using Pymol (www.pymol.org) and pdb file 2Q7H). The residues mutated relative to the wild-type sequence are shown as sticks. Residues in cyan are mutated in the progenitor AcKRS-1 and were randomized again in the new library, A267 (magenta) was only included in the new library. **b:** Characterization of a more efficient acetyl-lysyl-tRNA synthetase/tRNACUA pair. Myoglobin-His6 was expressed in *E. coli* DH10B from pMyo4TAG PylT [96] (containing a hexa-histidine tagged myoglobin gene with an amber codon at position 4 and the gene encoding MbtRNACUA) in the presence or absence of 10 mM acetyl-lysine using either pBK AcKRS-1 or pBK AcKRS-3. The proteins were purified by Ni²⁺ chromatography and analyzed by 4-12 % SDS-PAGE or detected in total lysates by Western blot with an anti-His6 antibody.

and found in inclusion bodies (figure 3.2b). Histone H3 K56Ac was purified by denaturing Ni-NTA chromatography with a yield of 2 mg per liter of culture. Subsequent cleavage with TEV protease cleanly removed the N-terminal His6-tag. Electrospray ionization mass spectrometry (figure 3.2c) demonstrates the homogeneous incorporation of a single acetyl-lysine residue and MS/MS confirms that the amino acid is incorporated at the genetically encoded site. By simply moving the position of the amber codon in the H3 gene we have made several other important acetylated variants of H3, including H3 K14Ac, K23Ac and K27Ac. To further demonstrate the generality of the method, we have expressed and characterized other histones containing acetylated lysines at specific positions H2B K5 and K20, and H2A K9 (figure 3.2b and Supplementary figure 2).

We assembled H3 K56Ac into histone octamers with H2A, H2B and H4 using standard methods of refolding with a comparable efficiency to unmodified H3 [97] indicating that acetylation does not affect octamer formation *in vitro* (figure 3.2d). We used these H3 K56Ac-containing histone octamers to assemble nucleosomes with DNA. The efficiency of octamers formation with unacetylated H3 and H3 K56Ac were comparable (figure 3.2e), again indicating that acetylation does not affect the efficiency of nucleosome formation.

3.2.2 H3 K56Ac does not affect salt-dependent nucleosome stability

The structure of the nucleosome core particle shows that H3 K56 is in an α -helix that binds the last 10 bp of DNA at the entry/exit site and H3 K56 itself makes a water-mediated contact between H3 K56 and the phosphate backbone of the DNA [12]. Several groups have proposed that K56 acetylation affects the stability of the nucleosome or DNA breathing on the nucleosome and suggested that this provides a structural, mechanistic and energetic basis for observed cellular phenomena [78, 79, 81, 89]. However, there is no experimental data on the effect of this modification on nucleosome stability or DNA breathing. To investigate the effect of H3 K56 on nucleosome stability we first compared the equilibrium stability as a function of NaCl concentration for nucleosomes containing H3 K56Ac and unacetylated H3 by fluorescence resonance energy transfer (FRET) using previously established assays and fluorophore positions [35].

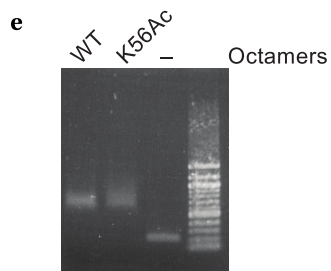
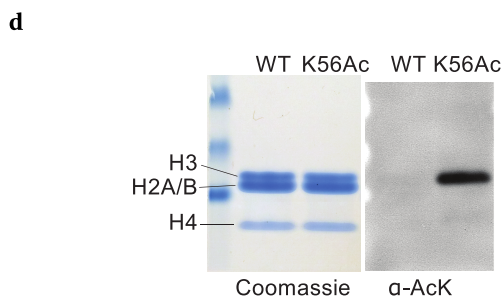
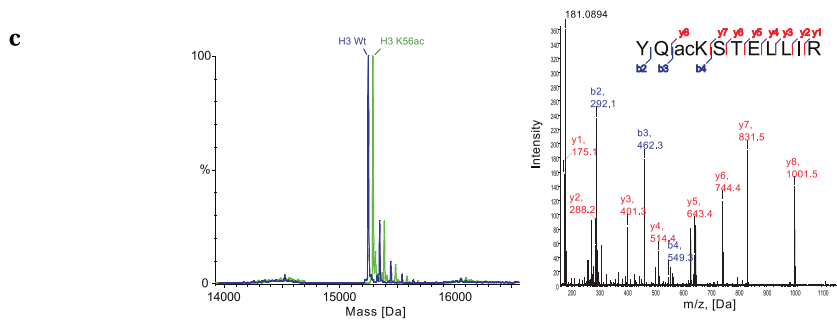
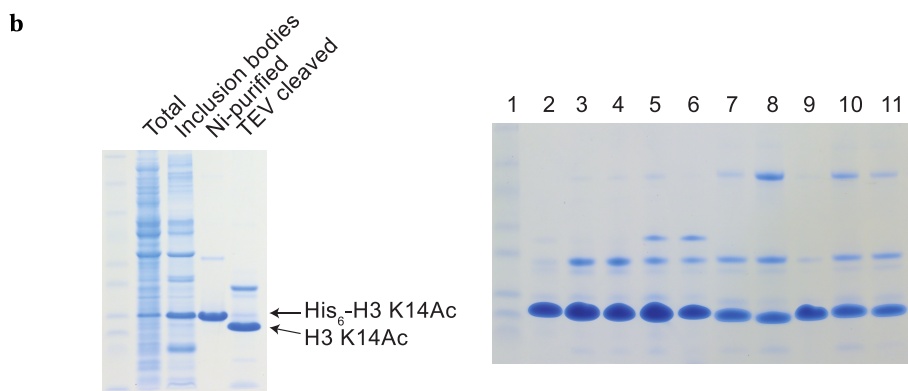
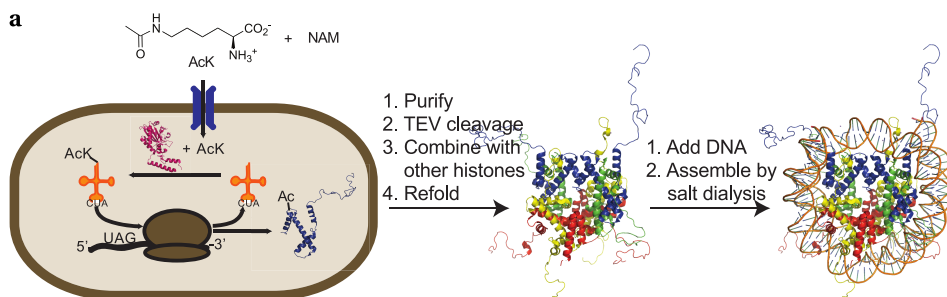
We placed a Cy3 FRET donor on the 5' end of a 147 bp DNA nucleosome positioning sequence [33] and quantitatively labelled a K119C mutant of H2A with a Cy5 maleimide to create a FRET acceptor (Supplementary figure 3). We assembled nucleosomes with the Cy3 labelled DNA and octamers that contained the Cy5 labelled H2A and either H3 K56Ac or unacetylated H3 (figure 3.3a and b). In each nucleosome there are two Cy5 fluorescently labelled H2A molecules, however only one of these H2A molecules is close enough to the Cy3 on the DNA to contribute significantly to FRET [35]. At

high NaCl concentrations, where the nucleosome is dissociated, excitation of the Cy3 donor leads to strong emission centered on 565 nm, consistent with Cy3 fluorescence and negligible acceptor emission centered on 670 nm, as expected in the absence of FRET (figure 3.3c). At low NaCl concentrations where the nucleosome is intact, excitation of the Cy3 donor leads to a decreased donor emission at 565 nm and an increased Cy5 acceptor emission at 670 nm consistent with a FRET signal. To assess the stability of H3 K56 acetylated nucleosomes we followed the emission of donor and acceptor fluorophores as a function of [NaCl] for nucleosomes bearing H3 K56 acetylation and nucleosomes bearing unmodified H3 (figure 3.3d). We find that acetylated and non-acetylated nucleosomes show comparable stability to NaCl through a range of concentrations that cover partial unwrapping of the DNA, dissociation of H2A/H2B dimers and dissociation of H3/H4 dimers. These data indicate that acetylation of H3 K56 does not have a substantial effect on nucleosome stability, but the error in the assay does not allow us to distinguish small effects in partial unwrapping of the DNA that result from DNA breathing.

3.2.3 H3 K56Ac increases DNA breathing in mononucleosomes

To investigate the partial unwrapping of the DNA resulting from the spontaneous transient breathing of DNA from the histone core [35], we used a recently developed combination of single pair FRET (spFRET), Alternating Excitation (ALEX) selection and native PAGE [42]. Nucleosomes reconstituted on a nucleosome-positioning element DNA, containing a Cy3B-ATTO647N FRET pair, were separated from free DNA using native PAGE. The nucleosome-containing band was excised from the gel and imaged in a con-

Figure 3.2 (facing page) – The expression and purification of site-specifically acetylated histones and the assembly of histone octamers and nucleosomes. **a:** Schematic illustration showing the recombinant expression of site-specifically acetylated recombinant histones in *E. coli* and their reconstitution into histone octamers and nucleosomes. **b:** (Left) The expression, purification and TEV cleavage of histone H3 K14Ac is followed by SDS PAGE, (Right) Purified and TEV cleaved site-specifically acetylated histones. (1) molecular weight marker, (2) H3 WT, (3) H3 K14Ac, (4) H3 K23Ac, (5) H3 K27Ac, (6) H3 K56Ac, (7) H2A WT, (8) H2A K9Ac, (9) H2B WT, (10) H2B K5Ac, (11) H2B K20Ac. **c:** Electrospray ionization mass spectrometry demonstrates that the protein is homogeneously acetylated and MS/MS of tryptic peptides identifies the site of acetylation is at lysine 56, as genetically encoded. The smaller peak to the right of the main peak is 98 Da heavier and corresponds to a phosphate from buffer associated with the histone. **d:** H3 K56Ac assembles into octamers with comparable efficiency to unmodified H3. Denaturing (4-12 %) SDS-PAGE of assembled octamers. The acetylation of H3 in the octamer is confirmed by Western blot with an anti-acetyl-lysine antibody. **e:** Reconstitution of unmodified octamers and octamers bearing H3 K56Ac into nucleosomes with 197 bp 601 DNA. Nucleosomes and free DNA were resolved by 0.8 % agarose gel and stained with ethidium bromide.



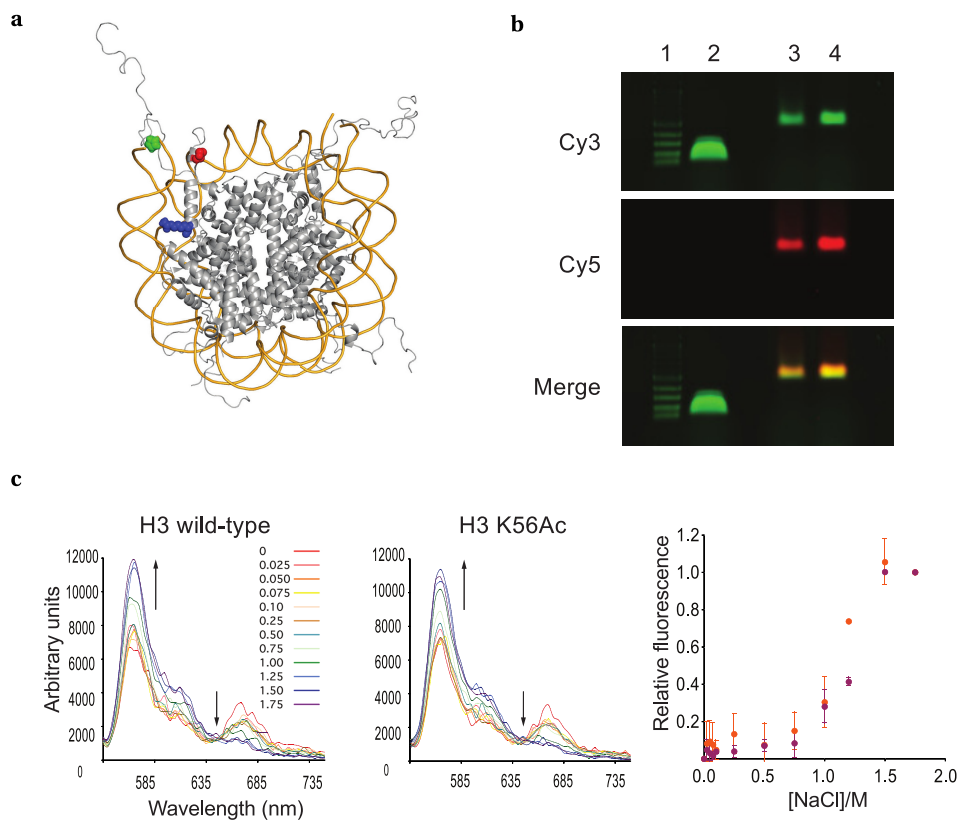


Figure 3.3 – Nucleosome stability and dynamic partial unwrapping of nucleosomal DNA measured by FRET using three-way labelled nucleosomes. **a:** Schematic of the nucleosome highlighting the locations of the fluorescence donor Cy3 (green) at the 5' end of the DNA, the acceptor dye Cy5 (red) coupled to histone H2A K119C, and the site of acetylation, H3 K56Ac (blue). The figure was created using the pdb file 1KX5 and pymol (www.pymol.org). **b:** Analysis of nucleosome reconstitution by 0.8% agarose gel electrophoresis, where lane 1 = 100 bp DNA ladder, lane 2 = naked Cy3-labelled DNA, lane 3 = Cy5-labelled H2A K119C nucleosome reconstitution with wild-type H3, lane 4 = Cy5-labelled H2A K119C nucleosome reconstitution with H3 K56Ac. **c:** The salt-induced dissociation of nucleosome core particles can be monitored by FRET. (Left) Increasing [NaCl] from 0 (red) to 1.75 M (violet) leads to decreased FRET emission from Cy5 and increased Cy3 emission (arrows). Excitation wavelength was set at 515 nm. (Right) Equilibrium dissociation curves were obtained by monitoring changes in fluorescence donor and acceptor emission at 565 and 670 nm, respectively. Data were normalized using the upper and lower plateau values as baselines, with wild-type nucleosomes in orange and H3 K56Ac nucleosomes in magenta. The data represent the mean values and the error bars represent ± 1 standard deviation.

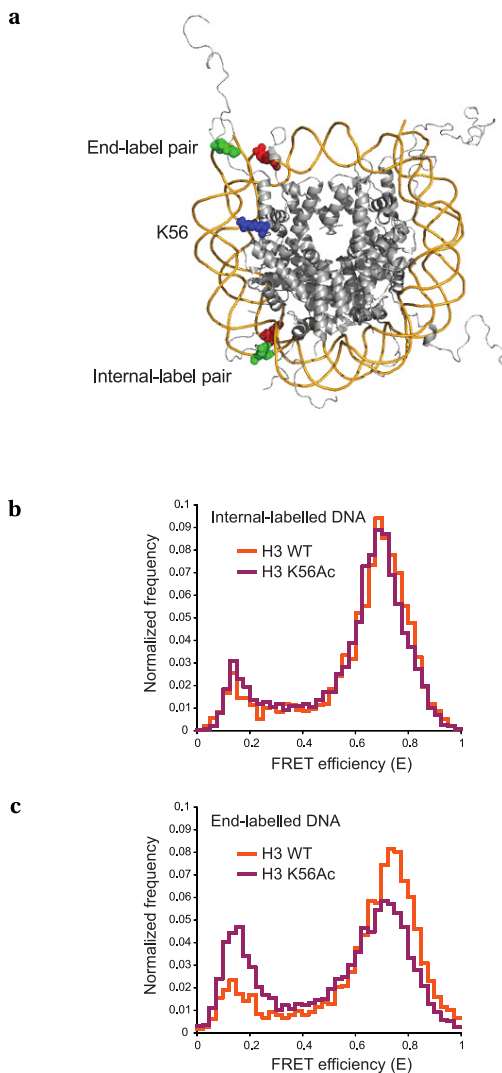


Figure 3.4 – spFRET experiments on transient unwrapping of DNA and DNA breathing demonstrate that K56 acetylation promotes local unwrapping near the entry-exit points of the nucleosome. **a**: Schematic of the labeling positions on the nucleosome DNA. The end-label fluorophore pair (Cy3/Atto647N) is close to the entry exit point of the nucleosome at position -2 and the internal-label pair is at -27 from the entry exit point. The position of K56 is shown in blue. The figure was created using the pdb file 1KX5 and pymol (www.pymol.org). **b and c**: spFRET efficiency measured for nucleosomes reconstituted with internally- or end-labelled DNA, respectively, using a combination of native PAGE, ALEX and FCS as described in the experimental section.

focal microscope using rapidly alternating green and red excitation. Resulting photon bursts were separated into a green and a red channel. The fluorescence of each nucleosome that diffuses through the focus was analyzed for both FRET efficiency and fluorescent label stoichiometry. Finally, a distribution of FRET efficiencies was generated from individual nucleosomes that have both the donor and acceptor label. Using these stringent selections we identified complexes that were folded into nucleosomes and contained both fluorescent labels. By examining this population we were able to accurately assess the transient DNA conformations of individual nucleosomes.

To measure the effect of H3 K56 acetylation on DNA breathing we used two label pairs. The first label pair was positioned 2 bp from the end of the DNA on the nucleosome and within 7 bp of the K56 location (end-label, -2 position), and was located near the positions labelled in our bulk FRET experiments. The second label pair was positioned 27 bp from the end of the nucleosomal DNA and 20 bp internally to the K56 binding position (internal-label, -27 position) (figure 3.4a).

For the unmodified nucleosomes, 11 % of the DNA is unwrapped (FRET efficiency < 0.3) at the internal-position and 13 % of the DNA is unwrapped at the end-position (figure 3.4b and c) in the first turn of DNA. For H3 K56 acetylated nucleosomes the fraction of nucleosomes in which the DNA is unwrapped at the end-position is doubled to 28 % while the fraction of nucleosomes in which the DNA is unwrapped at internal-position only increases 3 %, from 11 % to 14 %. These data clearly indicate that H3 K56 acetylation is sufficient to cause a local increase in spontaneous DNA breathing at the entry exit point of the DNA on the nucleosome. This effect may increase the accessibility of nucleosomal DNA to other factors such as nucleosome remodeling complexes. Assuming that unwrapping of the end-positions is required for unwrapping the internal pair only 2 % (13 %-11 %) of unacetylated nucleosome cores are unwrapped only at the end-label position in the first turn of the DNA. In contrast acetylated nucleosome cores are 14 % (28 %-14 %) unwrapped only at the end label position. Comparison of the fraction of nucleosomes unwrapped only at the end-label position suggests that acetylation increases DNA breathing within the last turn of DNA on the nucleosome core 7-fold.

3.2.4 Formation of higher-order chromatin structure in nucleosome arrays is unaffected by H3 K56Ac

Compaction is a pre-requisite for heterochromatin formation. Mutation of H3 K56 to a non-charged residue causes defects in silencing at telomeres [89], where K56 acetylation is normally less abundant [93]. Moreover, failure to deacetylate K56 may lead to defective silencing at telomeres [93]. These experiments suggest that H3 K56Ac may mediate, directly or indirectly, the compaction state of chromatin.

To investigate the direct effect of H3 K56Ac on chromatin compaction we recon-

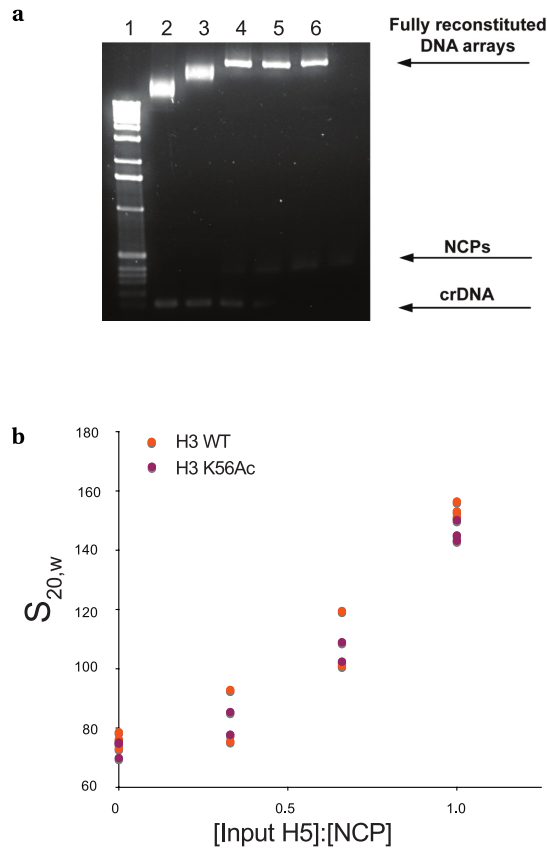


Figure 3.5 – Assembly and sedimentation analysis of nucleosome arrays bearing homogeneously acetylated nucleosomes. **a:** Titration of purified histone H3 K56Ac octamers to assemble chromatin arrays containing 61 repeats of 197 bp of the 601 nucleosome positioning DNA sequence. A retarded gel shift indicates loading of the DNA array with histone octamers. Excess histone octamer forms nucleosome core particles (NCPs) with competitor DNA (crDNA). Conditions of lane 4 were used to reconstitute DNA arrays in subsequent experiments. **b:** DNA arrays were reconstituted with saturating amounts of histone octamer and with increasing amounts of H5 linker histone in order to induce compaction. Chromatin arrays were folded in 1 mM MgCl₂, 10 mM TEA pH 7.4 and the degree of the compaction was measured quantitatively by sedimentation velocity analysis.

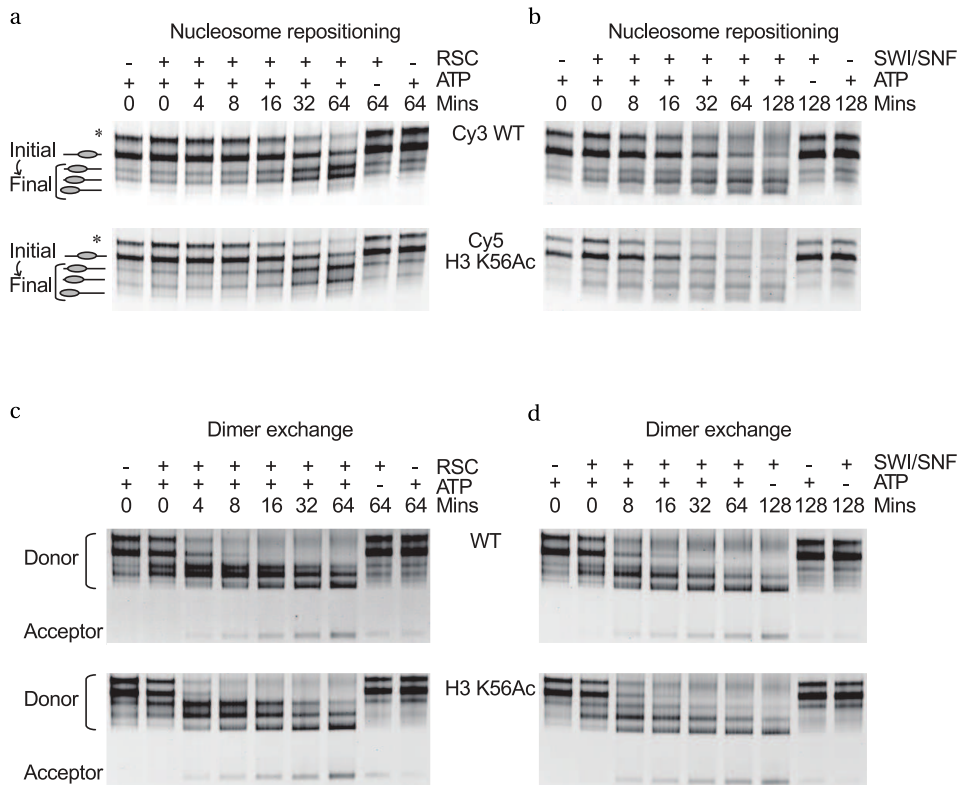
stituted nucleosome arrays, by assembling histone octamers containing H3 K56Ac or unmodified H3, on 61 repeats of the 197 base pair 601 nucleosome positioning DNA sequence with increasing amounts of H5 linker histone (figure 3.5a) [98, 99]. These chromatin arrays were then folded in 1 mM MgCl₂ and 10 mM TEA, pH 7.4. Sedimentation velocity analysis (figure 3.5b) of the H3 K56Ac arrays reveals a compaction profile that is essentially indistinguishable from that of the arrays bearing wild-type H3. Our results suggest that H3 K56Ac has little effect on the compaction of the chromatin fibre, and support the view that its effect on compaction suggested from *in vivo* experiments is either mediated by additional factors or is context dependent.

3.2.5 The effect of H3 K56Ac on chromatin remodeling

Chromatin immunoprecipitation (CHIP) experiments demonstrated a correlation between H3 K56Ac and SWI/SNF recruitment to activated promoters [81]. Since SWI/SNF contains a bromodomain, we investigated the effect of K56 acetylation on the direct recruitment of SWI/SNF. We did not detect any difference in binding of K56 acetylated nucleosomes and non-acetylated nucleosomes to SWI/SNF (using electrophoretic mobility shift assays, data not shown), indicating that recruitment of SWI/SNF to K56 acetylated nucleosomes is either context dependent or is mediated by another factor. Similarly we did not observe enhanced binding of the acetylated nucleosomes to RSC or Bdf1, which also contain bromodomains (data not shown). These experiments demonstrate that H3 K56Ac is not sufficient to directly recruit these remodelers.

It was proposed previously that H3 K56Ac modulates chromatin remodeling by

Figure 3.6 (facing page) – a and b: H3 K56 acetylated nucleosomes cause minimal alteration to the initial rate of RSC or SWI/SNF repositioning. Competitive repositioning assays were performed using 1 pmol each of H3 K56Ac and wild-type nucleosomes, 1 mM ATP and 41 fmol of RSC (**a**) or 115 fmol of SWI/SNF (**b**). A representative native PAGE gel of the repositioning assay is shown for each remodeler. The initial rate estimate for repositioning of H3 K56Ac nucleosomes relative to wild-type for RSC was 1.2 fold \pm 0.1 (mean \pm standard error of the mean) and for SWI/SNF 1.4 fold \pm 0.2. Each experiment was repeated in triplicate. * indicates the P position. WT, wild-type. **c and d:** H3 K56Ac and wild-type nucleosomes exhibit equivalent remodeler driven dimer transfer. Remodeler dimer transfer was performed using 0.25 pmol of donor nucleosomes assembled with Cy5 labeled H2A onto 54A18 DNA fragments, 0.75 pmol of wild-type tetrasome acceptor assembled on 0W0 DNA fragments, 1 mM ATP and 83 fmol RSC (**c**) or 230 fmol SWI/SNF (**d**). For each dimer transfer experiment, a representative Cy5 scan of the native PAGE gel is shown. Both RSC and SWI/SNF caused a 1.2-fold increase of the percentage of dimer transfer for H3 K56Ac nucleosomes relative to wild-type at the finish of their respective time courses. As the standard error of the mean was large in both cases, 0.1 and 0.2 for RSC and SWI/SNF, respectively, there was no significant change in the percentage of dimer transfer. Each experiment was repeated in triplicate.



SWI/SNF by facilitating access to the DNA at the entry-exit gate [78]. A H3 K56R mutant failed to recruit SWI/SNF as judged by ChIP analysis and failed to activate histone gene transcription [81]. To investigate the effect of H3 K56Ac on remodeling by SWI/SNF and RSC, we compared the remodeling of nucleosomes containing H3 K56Ac and unmodified nucleosomes (figure 3.6a and b). SWI/SNF repositioned H3 K56Ac-containing nucleosomes 1.4 fold \pm 0.2 faster than unmodified control nucleosomes (figure 3.6a), whereas RSC repositioned the acetylated nucleosomes 1.2 fold \pm 0.1 faster than unmodified nucleosomes (figure 3.6b). This observation is also consistent with the data obtained using H3 K56Q mutated nucleosomes, which were repositioned \sim 1.3-fold faster than wild-type nucleosomes [100]. Collectively, these observations show that histone H3 K56 acetylation has a small effect (\sim 20%) on nucleosome redistribution by RSC and SWI/SNF. However, given that the effects of H3 K56Ac on *in vivo* transcriptional activation are 2- to 3-fold [81] it is possible that the modest increase in acetylation-dependent nucleosome repositioning contributes to the observed activation.

In addition to moving nucleosomes in *cis* along DNA, the Snf2 sub-family members have also been shown to displace H2A/H2B dimers from nucleosomes [101, 102]. We therefore performed ATP-dependent H2A/H2B dimer transfer assays (figure 3.6c and d) using H3 K56Ac nucleosomes to investigate whether this modification was able to influence this specific type of remodeling behavior. In brief, wild-type or H3 K56Ac nucleosomes were assembled with Cy5-labeled H2A onto Cy3-labeled 54A18 DNA fragments. A chromatin acceptor of wild-type H3/H4 tetramer assembled onto 0W0 DNA fragments was added at \sim 3 fold molar excess. Following remodeling, the samples were resolved on a native PAGE gel and the Cy5 histone dimer fluorescence monitored. ATP-dependent dimer transfer for both RSC and SWI/SNF was not greatly affected by the H3 K56Ac donor nucleosomes relative to wild-type nucleosome controls (figure 3.6c and d). Quantification of the data revealed that both RSC and SWI/SNF were no more efficient at H2A/H2B dimer transfer from H3 K56Ac nucleosomes than from unmodified nucleosomes, indicating that H3 K56Ac has a minimal effect on dimer transfer.

3.3 Discussion

We have developed the first method for the production of large quantities of histones bearing site-specifically defined and homogeneous acetylations. This method has allowed us to prepare histone H3 with 100% acetylation at K56 in the globular core of the histone for the first time. Using nucleosomes assembled with H3 K56Ac we have measured the effect of H3 K56 acetylation on nucleosome stability and DNA breathing at the entry exit points of the nucleosome. In summary, we find that whereas H3 K56Ac does not affect the compaction of chromatin fibers, it affects the nucleosome

core structure in a number of subtle ways: it increases DNA breathing at the entry-exit point of the nucleosome, and has a small effect on remodeling of mononucleosomes. It is possible that these effects may be amplified within chromatin, leading to large-scale changes in accessibility and structure. Understanding the effects of lysine acetylation on transcription, DNA replication or DNA repair requires biochemical analysis of the effect of this modification on chromatin structure [103, 104]. Peptide models have allowed the interactions of histone tail modifications to be investigated [105–111], but these experiments cannot address the direct or indirect effects of modifications on nucleosome structure, the higher order structure of chromatin or the effect of modifications on the interaction with other factors and remodelers within the context of intact chromatin. Moreover peptide models cannot be used to probe the role of the emerging modifications in the globular core of histone proteins, the most prominent of which is perhaps H3 K56 acetylation. From the outset, H3 K56 acetylation was hypothesized to strongly destabilize this DNA-histone interaction at the entry-exit [79, 81, 89, 93]. This was assumed to affect the structure of chromatin especially during compaction [89, 93] and has been implicated in silencing at telomeres [93]. The acetylation might directly affect compaction or act to recruit factors that affect the remodeling and compaction of chromatin. Our data demonstrate that H3 K56Ac is not sufficient to cause the 2- to 3-fold changes in compaction observed for H4 K16 [22, 23]. The effect of H3 K56 acetylation on silencing is therefore more subtle and must depend on the simultaneous presence of other modifications or on the modification dependent recruitment or action of other factors. Single-molecule FRET experiments on acetylated nucleosomes, which are possible for the first time with the homogeneous material produced by our method, demonstrate that H3 K56 acetylation is sufficient to cause a seven-fold increase in DNA breathing on the nucleosome. These results are consistent with the observed increase in MNase sensitivity of yeast chromatin bearing an H3 K56Q mutation [79]. Our data also support the proposal that deacetylation of H3 K56Ac by Sir2 acts to close the entry-exit gates of DNA around the histone octamer [93]. Furthermore, the 7-fold increase in DNA breathing observed in our single-molecule experiments may well explain a number of phenotypes reported for mutations in H3 K56, or the enzymes involved in its modification. For example, the Grunstein lab reported (using ChIP assays) that wild-type yeast recruited the remodeler SWI/SNF 2-3 fold more efficiently to the HTA1 promoter than an H3 K56R mutant [81]. Changes seen in gene expression levels caused by deletion of Spt10 (an enzyme required for the acetylation of H3 K56 on histone genes) are of the same magnitude and overlap with the changes seen for mutations in H3 K56 [81]. H3 K56Ac is also involved in the activation of the PHO5 promoter [91]. The loss of nucleosomes from the PHO5 promoter is slowed ~2 fold by a H3 K56R mutation. H3 K56Q mutants also affect telomeric chromatin structure leading to a 4- to 6-fold increase in the mRNA levels of a telomere proximal gene [93]. The magnitude of the physical changes resulting from H3 K56Ac are of the same order

of magnitude as the increases in, for instance, transcription, suggesting the biological processes are directly regulated by the enhanced nucleosome plasticity.

The method we present for genetically encoding acetyllysine will facilitate investigation into the roles of histone acetylation within the same nucleosome, as well as the roles of multiple acetylations on a single histone [112]. Our method of acetylation is compatible with native chemical ligation [22, 95, 113, 114], as well as methods for installing methylation analogues [115], and it will therefore be possible to introduce acetylation in combination with other histone modifications such as ubiquitylation and methylation on individual histones and nucleosomes. Combining the full arsenal of methods, synthetic and genetic, for installing histone post-translational modifications in chromatin will be increasingly important for defining the combinatorial role of modifications [103, 116], and in providing a biochemical understanding of biological phenomena.

3.4 Experimental procedures

Information on library design and selection, mass spectrometric analysis of recombinant histones and the purification of remodeling complexes can be found in the Supplementary Methods online. Standard methods and assays, such as the reconstitution of histone octamers and nucleosome arrays and their analysis by sedimentation velocity, bulk FRET and remodeling assays can be found there as well.

3.4.1 Expression and purification of acetylated histones H2A, H2B and H3

BL21 DE3 (for H3) or Rosetta DE3 (for H2A and H2B) cells were transformed with plasmid pAcKRS-3 and pCDF PyIT-1 carrying the ORF for the histone with amber codons at the desired sites. The cells were grown over night in LB supplemented with 50 $\mu\text{g/ml}$ kanamycin and 50 $\mu\text{g/ml}$ spectinomycin (LB-KS). One litter prewarmed LB-KS was inoculated with 50 ml over night culture and incubated at 37 °C. At OD600 of 0.7-0.8 the culture was supplemented with 20 mM nicotinamide (NAM) and 10 mM acetyl-lysine (AcK). Protein expression was induced 30 min later by addition of 0.5 mM IPTG. Incubation was continued at 37 °C and cells were harvested 3-3.5 hr after induction, washed with PBS-20 mM NAM and stored at -20 °C.

The pellet was resuspended in 30 ml PBS supplemented with 20 mM NAM, 1 mM PMSE, 1x PIC (Roche), 1 mM DTT, 0.2 mg/ml lysozyme and 0.05 mg/ml DNase I and incubated for 20 min with shaking at 37 °C. Cells were lysed by sonication (output level 4 for 2 min on ice). Extracts were clarified by centrifugation (15 min, 18,000 rpm, SS34) and the pellet resuspended in PBS supplemented with 1 % Triton X-100, 20 mM NAM

and 1 mM DTT. The samples were centrifuged as above and washed again, once with the same buffer then twice with the same buffer without Triton X-100. The pellet was macerated in 1 ml DMSO and incubated for 30 min at room temperature. 25 ml of 6 M guanidinium chloride, 20 mM Tris, 2 mM DTT pH 8.0 were used to extract the histone proteins from the pellet. The samples were incubated for 1 hr at 37 °C with shaking, centrifuged as above and loaded onto a pre-equilibrated Ni²⁺-NTA column (Qiagen). The column was washed with 100 ml 8 M urea, 100 mM NaH₂PO₄, 1 mM DTT pH 6.2. Bound proteins were eluted with 7 M urea, 20 mM sodium acetate, 200 mM NaCl, 1 mM DTT (pH 4.5).

The eluates containing the protein were combined and dialyzed at 4 °C against 5 mM β-mercaptoethanol (two times against the 100-fold volume). The solution was made up to 50 mM Tris/HCl pH 7.4 and supplemented 1:50 with 4 mg/ml TEV. The reaction was incubated for 5 hr at 30 °C. Afterwards, salts were removed by dialysis as above, and the protein was lyophilized.

3.4.2 Single-molecule FRET

Mononucleosomes were reconstituted on a fluorescently labelled 155 bp DNA template containing a 601 nucleosome positioning sequence as described [40]. In brief, the template DNA was prepared by PCR and was labelled with Cy3B (donor) and ATTO647N (acceptor) by incorporation of fluorescently labelled, HPLC purified primers (IBA GmbH, Göttingen, Germany). Nucleosome reconstitutions were analyzed with 5 % native poly-acrylamide gel electrophoresis (PAGE). A sample of 0.1-1 pmol was loaded on the gel (29:1 bis:acrylamide, 0.2 × TB). The gel was run at 19 V/cm at 4 °C for 80 min and visualized with a gel imager (Typhoon 9400, GE, Waukesha, WI, USA). The band corresponding to reconstituted nucleosomes was excised and put on a home-built confocal microscope equipped with a 60 × water-immersion microscope objective (NA = 1.2, Olympus, Zoeterwoude, The Netherlands) and two single photon avalanche photodiodes (SPCM AQR-14, Perkin-Elmer (EG&G), Waltham, MA, USA). The photodiodes were read out with a TimeHarp 200 photon counting board (Picoquant GmbH, Berlin, Germany). A 515 nm diode pumped solid state laser (Cobolt, Solna, Sweden) and a 636 nm diode laser (Power Technology, Little Rock, AR, USA) were alternated at 20 kHz for excitation. In a typical experiment, data was collected for 10 min and 1000-5000 bursts of fluorescence were detected. Photon arrival times in the donor and acceptor channel were sorted according to excitation period, resulting in four photon streams: I_{515}^D , donor emission during green excitation; I_{515}^A , acceptor emission during green excitation; I_{636}^D , donor emission during red excitation; and I_{636}^A , acceptor emission during red excitation. The total fluorescence emission was analyzed with a burst detection scheme as described [66]. A burst was selected if a minimum of 100 photons arrived subsequently, with a maximum interphoton time

of 100 μ s. For each burst we calculated the apparent FRET efficiency E (also known as proximity ratio): $E = N_{515}^A / (N_{515}^A + \gamma N_{515}^D)$ and the apparent label stoichiometry S : $S = (N_{515}^A + \gamma N_{515}^D) / (N_{515}^A + \gamma N_{515}^D + N_{636}^A)$, in which N_{515}^D , N_{515}^A , and N_{636}^A are the number of photons in the burst from the different photon streams, and γ is a parameter to correct for photophysical properties of the dyes, in our case equal to unity. The excitation powers were chosen such that $N_{515}^A + \gamma N_{515}^D \approx N_{636}^A$, resulting in $S \sim 0.5$ for doubly labelled nucleosomes. Only nucleosomes with $0.2 < S < 0.7$ were selected for FRET analysis.

Supplemental data

Supplemental Data include Supplemental Experimental Procedures and three figures and can be found with this article online at [http://www.cell.com/supplemental/S1097-2765\(09\)00582-6](http://www.cell.com/supplemental/S1097-2765(09)00582-6).

Acknowledgements

The authors thank the European Research Council (JWC), the Human Frontier Science Program (JWC & JvN), FOM (RB), and the Medical Research Council UK (HN, AR, LC, DR, JWC) for support. We are grateful to Sew Peak-Chew (MRC-LMB) for acquiring top-down mass spectra.

CHAPTER 4

Stability and dynamics of nucleosomes containing H2A or H2A.Z and their temperature response studied with spFRET

Ruth Buning, Anna Brestovitsky, Charles Ravarani, Philip A. Wigge, and John van Noort

Manuscript in preparation

Abstract

The incorporation of histone variants is one of the ways in which eukaryotic cells regulate their DNA activity. H2A.Z is a highly conserved histone variant involved in many transcription-related functions. In *Arabidopsis Thaliana*, H2A.Z plays an essential role in ambient temperature sensing. The mechanism by which H2A.Z does so remains however unresolved. Both enhanced and reduced nucleosome stability have been reported. Here we show that H2A.Z-containing nucleosomes are more stable than H2A-containing nucleosomes. We found in single-pair FRET experiments on individual nucleosomes that H2A.Z-containing nucleosomes have a lower unwrapping probability and are less susceptible to dissociation during gel electrophoresis, at low concentrations, and in the presence of surfaces. Ambient temperature changes between 7 and 37 °C have no detectable effect on the dynamics of H2A.Z-containing nucleosomes. Our results suggest that H2A.Z incorporation may act as a nucleosomal stability switch.

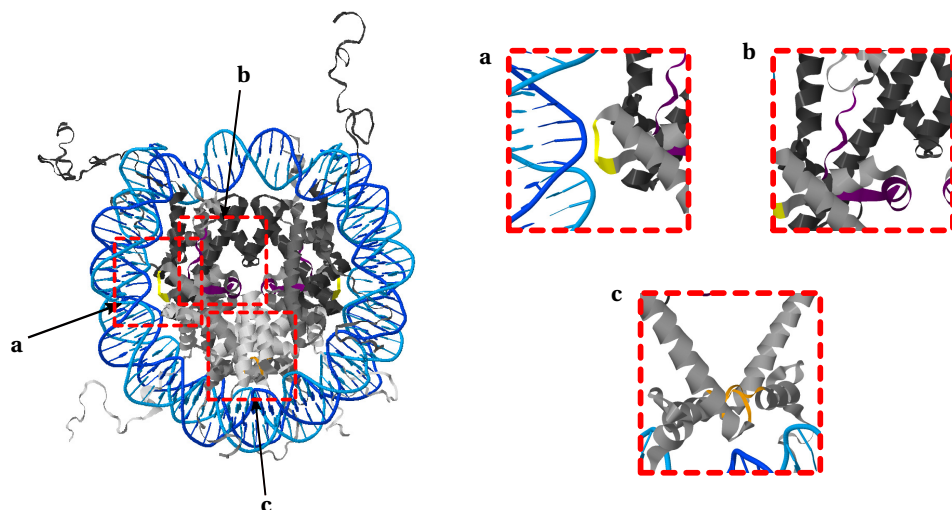


Figure 4.1 – Structural differences between H2A- and H2A.Z-containing nucleosomes. Crystal structure of the nucleosome (1KX5, [12]), with highlighted the regions where H2A and H2A.Z differ. Three regions show structural differences, which are conserved across species: **a (yellow)**: H2A(Z)-DNA contact at the second minor groove; **b (purple)**: H2A(Z) interface with H3; **c (orange)**: interface between the two copies of H2A(Z). Left: full crystal structure. Right: Zooms of the marked regions, where for clarity only the first superhelical turn of the DNA is shown, and histones H2A and H3.

4.1 Introduction

The wrapping of eukaryotic DNA into nucleosomes and higher order chromatin structures restricts access of the cellular machinery to the DNA. The amount of DNA wrapping and dynamics regulates processes like transcription. DNA wrapping itself is in its turn regulated by ATP dependent remodeling of nucleosomes and/or chromatin, post-translational modifications to the histone proteins, or the incorporation of histone variants.

H2A.Z is an H2A-variant that is highly conserved among all eukaryotes. It is found to have multiple functions, for example in transcription regulation and progression through the cell cycle, and is essential for viability in many organisms [117]. Despite multiple reports on the behavior of H2A.Z-containing nucleosomes, no univocal view on the effect of H2A.Z on the accessibility of nucleosomal DNA has emerged yet. Both stabilization [118, 119] and destabilization [120, 121] have been reported.

The sequence and structure of H2A and H2A.Z are highly conserved among species. Three regions have been identified where H2A and H2A.Z differ [117, 122], indicated in figure 4.1. First, at the H2A(Z)-DNA contact in the second minor groove, there is a

conserved substitution of a Threonine (uncharged, polar) in H2A to a Lysine (positively charged) in H2A.Z. This additional charge in H2A.Z might render the DNA-histone contact more tight, decreasing the DNA unwrapping probability. Second, H2A and H2A.Z differ structurally at their interface with H3. This might result in a different dissociation constant of the H2A/H2B dimer from the tetramer (also called dimer loss). The third structural difference is at the H2A(Z)-H2A(Z) interface. This has been suggested to be the reason why a single nucleosome can only contain either (H2A)₂ or (H2A.Z)₂ [122], since there would be steric hindrance otherwise. Heterotypic nucleosomes have nevertheless been seen *in vitro* and *in vivo* [123].

Recently, Kumar et al. [124] found that H2A.Z is essential for ambient temperature sensing in Arabidopsis Thaliana. Wild type plants develop phenotypes specific for temperature changes between 12 and 27 °C, correlated with nucleosome and H2A.Z occupancy. H2A.Z knockouts, on the other hand, fail to produce the proper temperature response. Their phenotype at low temperature resembles the wild type phenotype at high temperature. In the same paper [124], Kumar et al. show that purified Arabidopsis nucleosomes containing H2A are more accessible to restriction enzymes than H2A.Z-containing nucleosomes. They suggest that temperature-dependent unwrapping of nucleosomal DNA in H2A.Z-containing nucleosomes might serve as a direct mechanism for temperature perception in plants.

We can estimate the effect of temperature change on the unwrapping probability P_{open} for the first contact point by a simple thermodynamic model assuming two states (open and closed):

$$P_{open} = e^{\frac{\Delta G}{k_B T}} \quad (4.1)$$

where ΔG is the binding energy per contact point, T the temperature and k_B the Boltzmann constant. The binding energy per contact point is only slightly more than one $k_B T$ [15], which allows frequent spontaneous transient unwrapping of the DNA. From equation 4.1 follows that, at ambient temperatures, the unwrapping probability ($0 < P_{open} < 1$) increases about 0.012 per 10° temperature increase. Such a small increase will probably not have a profound impact on gene regulation. Experimental data on the unwrapping probability of individual nucleosomes is required to exclude or identify the unwrapping of nucleosomal DNA as a temperature-sensing mechanism.

Here, we probe the effect of the H2A.Z histone variant on nucleosome dynamics and stability with single-pair Fluorescence (or Förster) Resonance Energy Transfer (spFRET) in nucleosomes reconstituted with Arabidopsis Thaliana histone octamers. We show that H2A.Z-containing nucleosomes are more stable than H2A-containing nucleosomes: their unwrapping probability is lower, and they are less susceptible to dissociating conditions like low concentrations and the presence of surfaces. Furthermore, we show that the stability of H2A.Z-containing nucleosomes is temperature

independent, excluding H2A.Z as direct ambient temperature sensor in *Arabidopsis Thaliana*.

4.2 Materials and Methods

4.2.1 Preparation of DNA constructs

A 155 bp DNA template containing a single 601 nucleosome positioning sequence was generated by PCR, separated on agarose gel and cleaned by Qiagen gel extraction kit. The forward and reverse primers were labeled at a single position with Cy3B and ATTO647N (via amino linker with 6-carbon spacer to the base, IBA)¹. We generated three DNA constructs with a FRET pair at either of the nucleosome extremes (labels at position X or Z), or at a position 27 bp from one nucleosome end (Y) (see figure 4.2a). In all DNA constructs the donor and acceptor were separated by 76-81 bp (~24 nm). A DNA template without fluorescent labels was constructed as well to reconstitute unlabeled nucleosomes².

4.2.2 Preparation of histone octamers

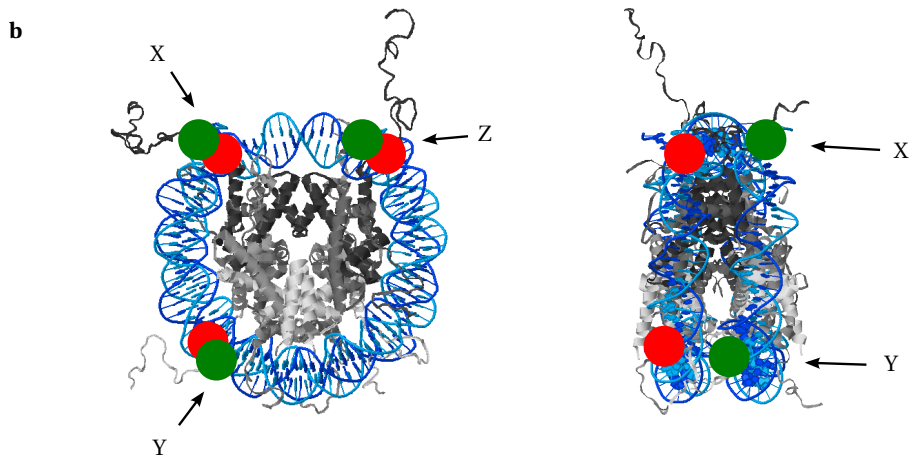
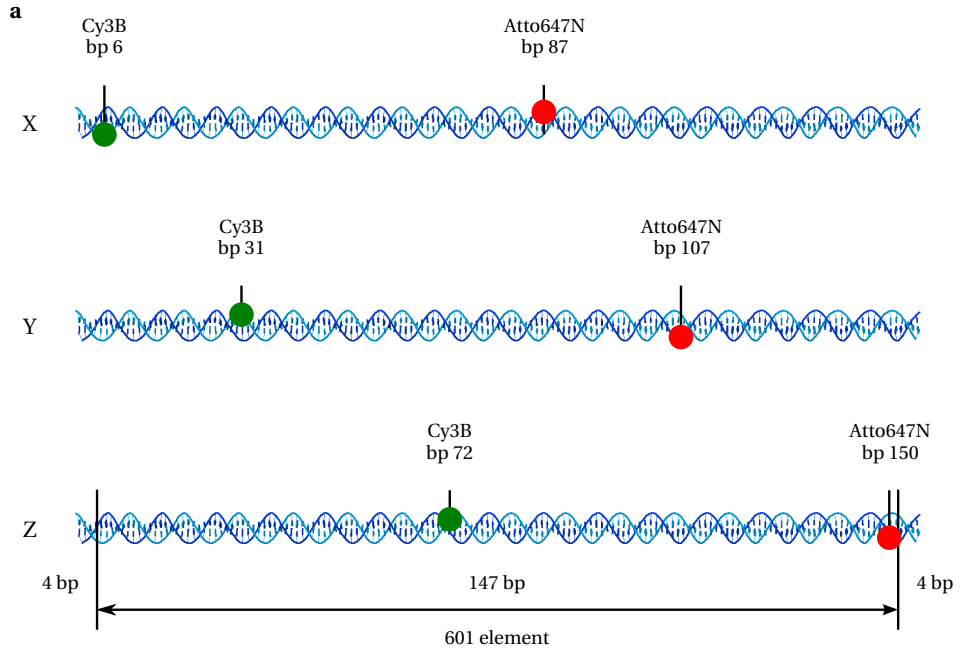
Wild type (WT) *Xenopus laevis* and *Arabidopsis Thaliana* H2A, H2A.Z, H2B, H3 and H4 histones were expressed in *E. coli* and purified as described previously [23]. Recombinant histone octamers were reconstituted from purified histones by refolding an equimolar mixture of each of the four denatured histone by dialysis against a buffer containing 2 M NaCl. The intact histone octamers were fractionated from histone tetramers and hexamers by size-exclusion chromatography as described [23].

¹PCR primers were as follows (5'→3'), modified bases for either construct X, Y or Z indicated in bold: TTGGCT(Cy3B,X)GGAGAATCCCGGTGCCGAGGCCGCT(Cy3B,Y)CAATTGGTCGTAGACAGCTCTAGCACCG-CTTAAACGCACGT(Cy3B,Z)ACGCGCTG and TTGGAC(ATTO647N,Z)AGGATGTATATCTGACACGTGCCTGGAGACTAGGGAGTAAT(ATTO647N,Y)CCCCTTGGCGGTAAAACGC(ATTO647N,X)GGGGACAGC.

²PCR primers for the 155 bp non-labeled DNA construct were as follows (5'→3'): TTGGCTGGAGAATCCCGGT and TTGGACAGGATGTATATCTGAC.

Figure 4.2 (facing page) – Constructs used for the experiments described in this chapter.

a: The 155 bp DNA construct, indicating the position of the 601 positioning element and the fluorescent labels. Constructs X, Y and Z differ only in label positions. The donor and acceptor labels are separated by ~80 bp, preventing FRET in bare DNA. The labels are only several nm apart for fully reconstituted nucleosomes, allowing efficient FRET. **b:** Top and side view of the crystal structure of the nucleosome core particle (1KX5, [12]), consisting of 147 bp DNA wrapped around the histone octamer. The positions of the fluorescent labels for the different constructs X, Y and Z are indicated.



4.2.3 Nucleosome reconstitution

DNA and histone octamers containing either H2A or H2A.Z were mixed in various molar ratios in TE (1 mM EDTA, 10 mM Tris.HCl pH 8.0) and 2 M NaCl. Nucleosomes were reconstituted by salt gradient dialysis against 0.85, 0.65, 0.5 and finally 0 mM (figures 4.4 and 4.8) or 50 mM (other figures) NaCl, all buffered with TE in a total volume of 40 μ l at a labeled DNA concentration around 200 nM. Competitor DNA, 147 bp unlabeled random sequence DNA (produced with PCR), was included in the reconstitution reaction at concentrations between 100 and 200 nM. After reconstitution, the products were transferred to non-stick tubes (Ambion), and BSA and Nonidet-P40 were added to concentrations of 0.1 mg/ml and 0.03 % w/v, respectively.

4.2.4 Polyacrylamide gel electrophoresis

Nucleosome reconstitutions were analyzed with 5 % native polyacrylamide gel electrophoresis (PAGE). A sample of 2 μ l of reconstitution product was loaded on the gel (37.5:1 acrylamide:bis (30 %, BioRad), 0.2 \times TB, BioRad Mini-PROTEAN Tetra Cell (83 \times 73 \times 0.75 mm, figures 4.3 and 4.4) or Amersham Bioscience Hoefer SE 400 vertical gel slab unit (140 \times 140 \times 1.5 mm, figures 4.7 and 4.8)). The gel was run at 300 V at 7 $^{\circ}$ C for 90-120 minutes (figures 4.3 and 4.4) or at 200 V on ice for 30 minutes (other figures) to separate nucleosomes from free DNA. The fluorescence was imaged with a gel imager (Typhoon 9400, GE). Red: excitation at 633 nm, emission detected at 670 nm; Green: excitation at 532 nm, emission detected at 580 nm; FRET: excitation at 532 nm, emission detected at 670 nm (all 30 nm bandpass). Gel images were analyzed with ImageJ software to determine the relative intensities of the bands. Raw FRET efficiencies in the gel were calculated using equation 4.2 (see section 4.2.7). Gels with unlabeled nucleosomes were post-stained with ethidium bromide and imaged with an UV imager.

4.2.5 spFRET sample preparation

Nucleosomes in solution were diluted 100-300 \times in a buffer containing 10 mM Tris.HCl pH 8.0, 0.1 mg/ml BSA, 0.03 % Nonidet-P40, 2 mM trolox, and 50 mM NaCl. The final concentration of labeled nucleosomes was 50-100 pM, estimated from the measured burst rate in the single-molecule experiments. Unlabeled nucleosomes were added in a 5-10 \times excess to fluorescently labeled nucleosomes, both with the same histone composition. We used non-stick tubes (Ambion) for nucleosome dilutions. Microscope slides (#1.5, Menzel) were cleaned and passivated by coating with star PEG [64] as described in [34] to minimize interactions with the surface. We placed a 2-well culture insert (Ibidi), cleaned by sonication in ethanol, on the slide to get two confined chambers to prevent spreading of the sample over the entire slide. With the insert, two samples could be mounted on the setup simultaneously. First, we loaded 25 μ l of

buffer containing only unlabeled nucleosomes in the wells. After incubating 5-10 minutes, we added 25 μl of buffer with both unlabeled nucleosomes and twice the final concentration labeled nucleosomes. Samples and slides were equilibrated on ice or at room temperature (depending on the measurement temperature) before mounting.

Nucleosomes in gel were imaged at single-molecule concentration by excising the nucleosome band from the gel. The gel slice was placed on an (untreated) glass cover slide. A drop of 30 μl buffer (10 mM Tris.HCl pH 8.0, 2 mM trolox) was used to match the refractive index of the gel and to prevent drying of the gel during the experiment.

After mounting or after changing the temperature of the setup, we allowed 30 minutes for temperature equilibration. To verify that this is sufficient, we monitored the photon statistics during the equilibration, which stabilized after 10-15 minutes.

4.2.6 Single-molecule fluorescence microscopy

Single molecules were imaged with a home-built confocal microscope as described in chapter 2 and [42]. Excitation sources at 515 nm and 636 nm were alternated at 20 kHz. The beams were focussed 25 μm (for in-solution measurements) or 50 μm (for in-gel measurements) above the glass-buffer interface. The excitation power was 12 μW for 515 nm excitation, and 8 μW for 636 nm excitation. The experiment was kept at a specific temperature by circulating thermostated water through a heating device mounted on the objective and the sample stage. In a typical experiment, data was collected for 30 minutes (unless stated otherwise) in which 2000-10000 bursts of fluorescence were detected.

4.2.7 Single-molecule data analysis

Bursts of fluorescence were detected using the method described in [66]. A burst was assigned if a minimum of 50 photons arrived subsequently, with a maximum inter-photon time of 100 μs . Photon arrival times in the donor (D) and acceptor (A) channel were sorted according to excitation wavelength, resulting in four photon streams: D-emission upon D-excitation: I_{Dex}^{Dem} , A-emission upon D-excitation: I_{Dex}^{Aem} , D-emission upon A-excitation: I_{Aex}^{Dem} , A-emission upon A-excitation: I_{Aex}^{Aem} .

For each burst, we estimated the FRET efficiency by the sensitized-acceptor emission method [69, 70]. Following the definitions as proposed and discussed in detail by Lee et al. [31], we calculated the raw FRET efficiency E_{PR}^{raw} and label stoichiometry S^{raw} from the total number of photons in the burst for the different photon streams:

$$E_{PR}^{raw} = \frac{I_{Dex}^{Aem}}{I_{Dex}^{Aem} + I_{Dex}^{Dem}} \quad (4.2)$$

$$S^{raw} = \frac{I_{Dex}^{Aem} + I_{Dex}^{Dem}}{I_{Dex}^{Aem} + I_{Dex}^{Dem} + I_{Aex}^{Aem}} \quad (4.3)$$

Doubly labeled nucleosomes were selected for further analysis by taking only bursts with $0.2 < S^{raw} < 0.8$. Histograms of the FRET efficiencies of these bursts show the distribution of FRET efficiencies in the sample. Histograms were normalized to a total area below the curve of 1 to allow comparison of different measurements. The fraction without FRET (representing open or (partly) dissociated nucleosomes) was determined by taking the area below the histogram for $E_{PR}^{raw} < 0.3$.

4.3 Results

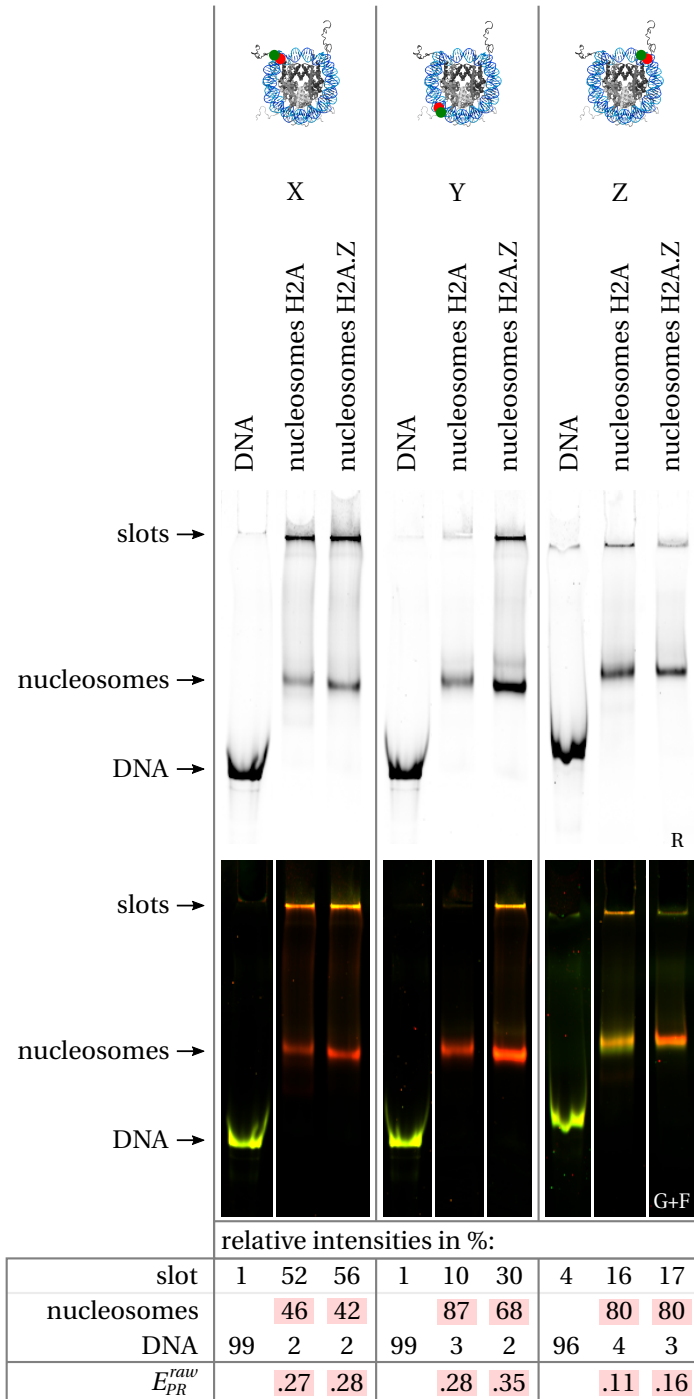
4.3.1 Gel electrophoresis reveals near 100 % reconstitution yield

Native gel electrophoresis separates free DNA from nucleosomes. Fluorescence images of polyacrylamide gels with reconstitution products, as in figure 4.3, show that the reconstitution efficiency is near 100 %. Besides a band shift of reconstituted nucleosomes with respect to bare DNA, fully reconstituted nucleosomes can also be distinguished based on their FRET efficiency, which is apparent in the fluorescence gel images as well. From observing the gel, some differences between H2A- and H2A.Z-containing nucleosomes already become clear:

H2A-containing nucleosomes run slightly higher than H2A.Z-containing nucleosomes, due to their weight and charge difference (for *Arabidopsis Thaliana*: 13.8 kDa and +8.4 for H2A, 14.3 kDa and +12.5 for H2A.Z, at pH=8.0 [125, 126]), possibly in combination with conformational differences like DNA breathing.

Conformational differences should be reflected in FRET differences. Indeed, H2A-containing nucleosomes show slightly less FRET than H2A.Z-containing nucleosomes, indicating a more compact conformation for H2A.Z-containing nucleosomes. The

Figure 4.3 (facing page) – Fluorescence images of 5 % polyacrylamide gels with reconstituted mononucleosomes. For every construct (X/Y/Z), a compilation of sections from the same gel is displayed (indicated by white space between the lanes). Top (R): acceptor fluorescence upon direct acceptor excitation. Bottom (G+F): false color overlay of donor and acceptor (FRET) fluorescence upon donor excitation. Reconstituted nucleosomes show FRET, in contrast to bare DNA. On the very bottom, the relative intensities of the bands in each lane from the direct acceptor excitation image are displayed, providing a measure for the relative concentrations of the different components (free DNA, nucleosomes, aggregates) present in the sample. Percentages are approximate within a few percent. Numbers corresponding to mononucleosome bands are highlighted, and the FRET efficiency calculated from the green and FRET intensities of the bands is indicated in the bottom row.



FRET efficiency difference for the nucleosomes with the labels at position Y indicates that conformational differences between H2A and H2A.Z-containing nucleosomes in this gel are larger than the breathing of the first 30 bp of the nucleosomal DNA only [127].

While the fluorescent label positions X and Z are both at the second bp from the nucleosome exit, Z nucleosomes show significantly less FRET. Also, the nucleosome band has a small side band, that shows no FRET. We attribute this asymmetry to the non-palindromic 601 sequence, the only asymmetric component in the nucleosome constructs. Either both sides are not equally stable wrapped, or positioning is favored towards one of the DNA ends.

There is a significant amount of material left in the slots. Aggregates were however no problem for single-molecule experiments. Reconstitutions were spun down before the single-molecule measurements, and no signs of aggregates were present in the single-molecule data.

4.3.2 spFRET in gel shows H2A.Z-nucleosomes are more stable

Making use of the separating power of gel electrophoresis, we performed single-molecule FRET experiments inside the nucleosome band in a 5 % polyacrylamide gel. Figure 4.4a shows the fluorescence image of the gel used for these single-molecule experiments. The FRET efficiencies in the gel are reproducible within ~3 %. Figure 4.4b shows the FRET efficiency distributions of the nucleosome bands measured within two hours after gel imaging. Nucleosomes with labels at position Y show significantly more FRET than nucleosomes with labels at position Z. For both label positions, H2A.Z-containing nucleosomes show a larger high-FRET population, in accordance with the higher FRET efficiency measured from the gel image.

The same nucleosome bands were measured again four hours later. In these four hours, the FRET distribution of H2A-containing nucleosomes has hardly changed, still ~40 % of the nucleosomes shows no FRET. The fraction without FRET for H2A.Z-containing nucleosomes, on the other hand, has doubled from ~20 to ~40 % to resemble the distribution of H2A-containing nucleosomes. The nucleosomes appear to dissociate inside the gel at a timescale of a few hours. This dissociation occurs more slowly in H2A.Z-containing nucleosomes, which apparently are more stable than H2A-containing nucleosomes. The dissociation seems to reach a steady state after 2 hours for H2A-containing nucleosomes and 6 hours for H2A.Z-containing nucleosomes.

4.3.3 FRET distributions are temperature independent

Since the nucleosomes used in this study dissociate inside a polyacrylamide gel within a few hours, we proceeded with single-molecule experiments in solution. This was

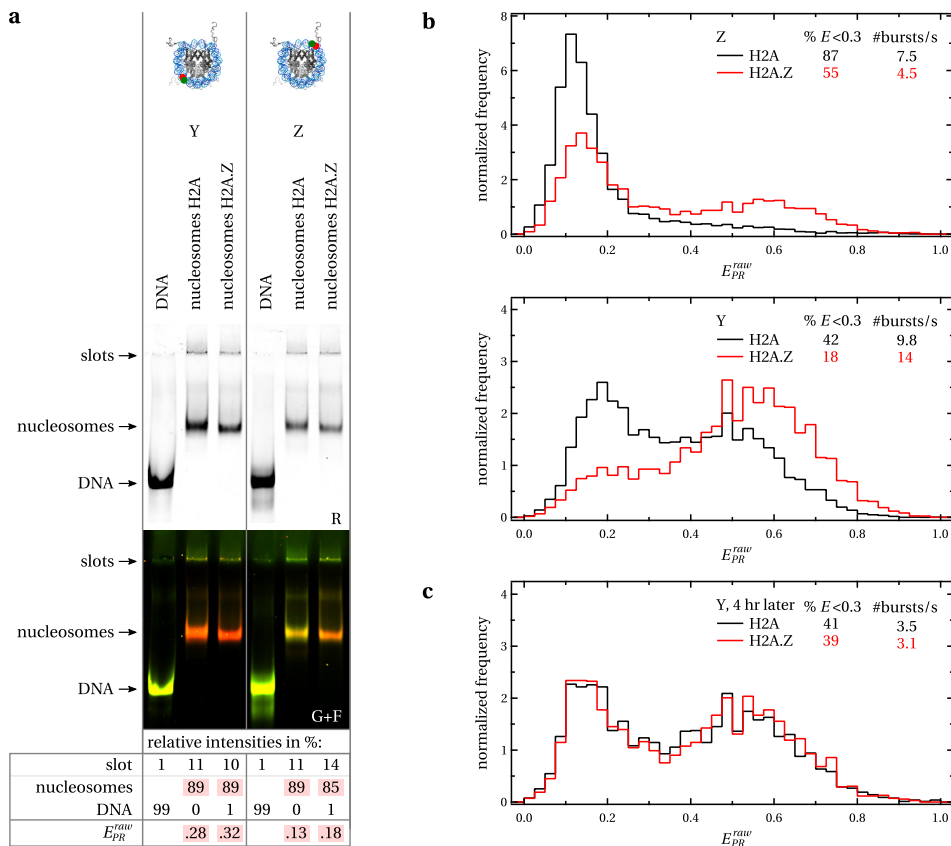


Figure 4.4 – Single-molecule FRET experiments inside a polyacrylamide gel. **a**: Fluorescence images of a 5% polyacrylamide gel with reconstituted nucleosomes with labels at positions Y or Z. Top (R): acceptor fluorescence upon direct acceptor excitation. Bottom (G+F): false color overlay of donor and acceptor (FRET) fluorescence upon donor excitation. The nucleosome bands are cut from the gel right after imaging and placed on the single-molecule fluorescence microscope. **b**: FRET efficiency distributions of nucleosomes in the gel showed in a. The fraction without FRET is much larger for Z nucleosomes than for Y nucleosomes. For both Z and Y nucleosomes, the H2A-containing nucleosomes show a larger population without FRET than the H2A.Z-containing nucleosomes. **c**: Same bands measured again 4 hours later. The fraction without FRET for H2A.Z-containing nucleosomes has increased to resemble the distribution of H2A-containing nucleosomes. Single-molecule data was collected for 15 minutes.

possible because the reconstitution yield was close to 100 %. In contrast to our observations inside the gel, on passivated slides and with optimal buffer conditions the fraction of nucleosomes without FRET remained relatively constant over more than six hours (figure 4.5).

A sample of H2A- and a sample of H2A.Z-containing nucleosomes in buffer were placed simultaneously on the single-molecule fluorescence microscope and measured subsequently at 7, 22, 37 and again at 7 °C. The result is shown in figure 4.5. There is a slight increase in the fraction of nucleosomes without FRET during the course of the measurement. The fraction size did not return to its initial value when resetting the temperature to 7 °C, indicating that the small change in distribution is temperature-independent and rather reflects nucleosome instability over time.

The single-molecule data of nucleosomes with labels at position X suggest small differences in stability between H2A- and H2A.Z-containing nucleosomes. H2A-containing nucleosomes show on average a slightly larger population without FRET, and also more variation in fraction size. The FRET distribution of H2A.Z-containing nucleosomes is more narrow and shows more intermediate values. Based on the almost equal number of bursts per second, this is not a concentration-dependent artifact.

4.3.4 spFRET measurements on nucleosomes depend critically on slide passivation

We repeated the experiments for nucleosomes with labels at position X described in section 4.3.3 and shown in figure 4.5b after approximately one and two weeks. During this period, the reconstitutions were stored at 4 °C. From these stored reconstitutions, a new sample was diluted on the day of measurement. The fraction of nucleosomes without FRET increased for both H2A- and H2A.Z-containing nucleosomes in a linear fashion, which extrapolates to a minimum value at the date of slide passivation (see figure 4.6). This observation suggests that the increase of nucleosomes without FRET is caused by a decrease in starPEG-coated slide quality. A decrease in quality of the starPEG coating after a few days is expected [64, 65]. While we did not observe an effect of the age of starPEG coated slides on single-molecule FRET experiments on nucleosomes with histones from chicken erythrocytes or recombinant *Xenopus Laevis* histones, the *Arabidopsis Thaliana* histones used in this study are apparently more susceptible to surface conditions. FRET-loss due to decreased surface quality is an undesired artifact, but it also enhances the initially small difference between H2A- and H2A.Z-containing nucleosomes, where H2A.Z-containing nucleosomes appear less susceptible to destabilization by surface interactions than H2A-containing nucleosomes.

The fact that the fraction without FRET for Y nucleosomes is after nine days still

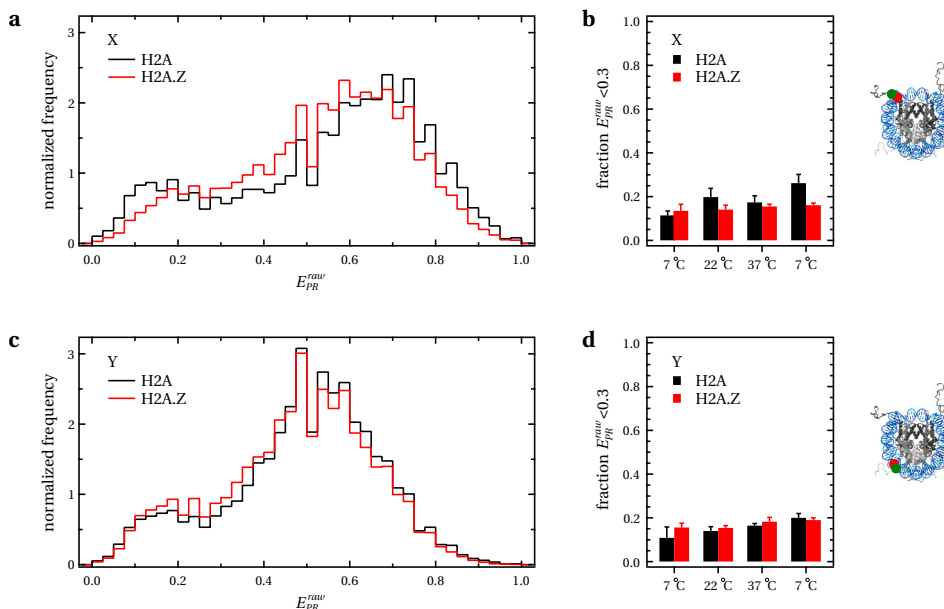


Figure 4.5 – FRET efficiency distributions at different temperatures of H2A- and H2A.Z-containing nucleosomes in solution with labels at position X (a, b) or at position Y (c, d). A sample of H2A- and a sample of H2A.Z-containing nucleosomes in buffer were placed simultaneously on the single-molecule fluorescence microscope and measured subsequently at 7, 22, 37 and again 7 °C. **a, c**: Combined histograms of the measurements at different temperatures. **b, d**: Fraction of bursts with FRET efficiency below 0.3 at different temperatures. Error bars represent standard deviations of the values for 100 s intervals of the 1800 s measurements.

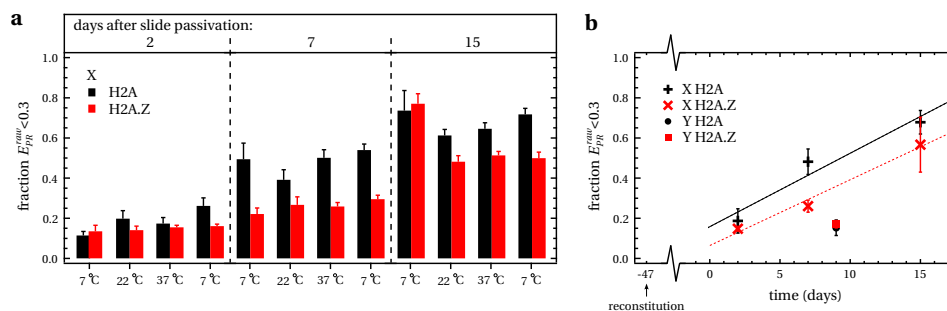


Figure 4.6 – Loss of FRET in time. **a:** Fraction of bursts with FRET efficiency below 0.3 at different temperatures. The experiment is repeated twice after several days, in which the fraction without FRET increased for both H2A- and H2A.Z-containing nucleosomes. Error bars represent standard deviations of the values for 100 s intervals of the 1800 s measurements. **b:** Fraction of bursts with FRET efficiency below 0.3 as a function of number of days after slide passivation. Data points represent averages of the four measurements at different temperatures shown in a, error bars the standard deviations, dashed lines linear fits. Reconstitution occurred 48 (H2A) or 46 (H2A.Z) days before slide passivation.

much lower than for X nucleosomes, suggests that the loss of FRET in X nucleosomes is not caused by full dissociation into free DNA and histones.

4.3.5 H2A.Z nucleosomes are more stable during extended periods of storage

To test whether nucleosomes destabilized during storage or measurement, we performed gel electrophoresis with nucleosomes after 76 days of storage at 4 °C (figure 4.7). Stored nucleosomes still show near 100 % reconstitution yield. The amount of free DNA is negligible; besides nucleosome bands there is only material in the slots. While bands with H2A.Z-containing nucleosomes are still nice and sharp, the H2A-containing nucleosome bands appear different: more smeared and shifted upwards. Whether this degradation of H2A-containing nucleosomes has happened during storage or is an artifact caused by the gel, is not entirely clear, but it shows again a different behavior for H2A- and H2A.Z-containing nucleosomes, where H2A.Z-containing nucleosomes are more stable.

We also loaded nucleosome samples recovered from the setup after the last single-molecule experiment (15 days after slide passivation, figure 4.6) on the gel. The samples that were run on the gel after single-molecule experiments show significant amounts of free DNA, indicating full dissociation of (part of the) nucleosomes. The nucleosomes that were not fully dissociated show the same gel pattern as the stored nucleosomes. Whether the dissociation happened during the single-molecule experi-

ment or during gel electrophoresis is not clear, because the reduced nucleosome concentration of single-molecule samples, despite loading of the maximum amount of material in the gel, makes nucleosomes unstable in gel electrophoresis conditions, as discussed in chapter 2.

4.3.6 *Xenopus* H2A.Z nucleosomes also more stable

In addition to experiments with nucleosomes reconstituted with *Arabidopsis Thaliana* (AT) histones, we performed experiments with nucleosomes reconstituted with *Xenopus Leavis* (XL) histone octamers. *Xenopus Leavis* histones are commonly used in *in vitro* studies. The XL nucleosomes appeared less sensitive to disrupting conditions like eppendorf tube or glass surfaces and gel electrophoresis. Despite the limited dataset for XL nucleosomes, and the multitude of factors that influence nucleosome stability as described in chapter 2, our data show that the difference between H2A- and H2A.Z XL nucleosomes follows the same trend as observed for AT nucleosomes.

We obtained fully reconstituted nucleosomes with XL histones containing either H2A or H2A.Z, as verified by gel electrophoresis (see figure 4.8a). The XL nucleosomes run faster than AT nucleosomes due to their weight and charge difference (for *Xenopus Leavis*: 14.0 kDa and +15.4 for H2A, 13.5 kDa and +12.5 for H2A.Z; for *Arabidopsis Thaliana*: 13.8 kDa and +8.4 for H2A, 14.3 kDa and +12.5 for H2A.Z (pH=8.0) [125, 126]). Also, conformational differences can give rise to variations in running speed: a more compact structure will experience less gel resistance and hence run faster. The FRET efficiency of XL nucleosomes is much higher than of AT nucleosomes, reflecting a more compact conformation and/or higher stability.

Three independent single-molecule measurements inside a polyacrylamide gel reveal FRET distributions of H2A- and H2A.Z-containing nucleosomes. Although the fraction of nucleosomes without FRET shows a correlation with the local nucleosome concentration (see figure 4.8b), these measurements suggest that H2A.Z-containing nucleosomes are more stable than H2A-containing nucleosomes for XL as well as for AT.

FRET efficiency distributions of XL-H2A.Z-containing nucleosomes in solution at 7, 22, and 37 °C are shown in figure 4.8c. The FRET efficiency of the high FRET population is higher than for AT nucleosomes, indicating a more compact conformation for XL nucleosomes. Though the same sample is measured at increasing temperatures, the distribution is constant and is thus temperature-independent.

4.4 Discussion

This is the first time that temperature dependent stability of H2A.Z-containing nucleosomes is measured at the single-molecule level. We have reconstituted nucleosomes

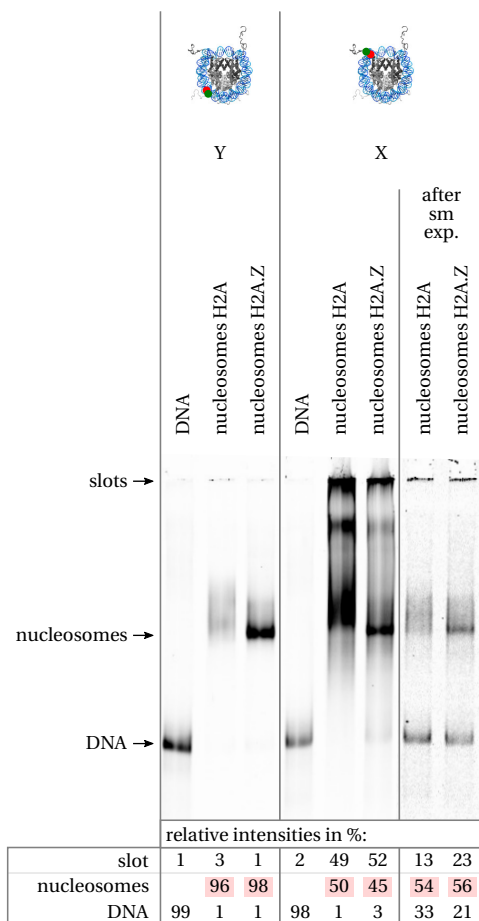


Figure 4.7 – Fluorescence image (direct acceptor excitation) of polyacrylamide gel with nucleosomes, 76 days after reconstitution. The two lanes on the right show the sample that was used for the last single-molecule experiments (15 days after slide passivation). The contrast of these lanes is increased in order to make the 100 times less concentrated material visible. The bands of H2A-containing nucleosomes are smeared compared to gel images made shortly after reconstitution, whereas the bands of H2A.Z-containing nucleosomes are still sharp. Nucleosome samples that have been measured in the single-molecule fluorescence microscope contain a significant amount of free DNA, indicating full dissociation.

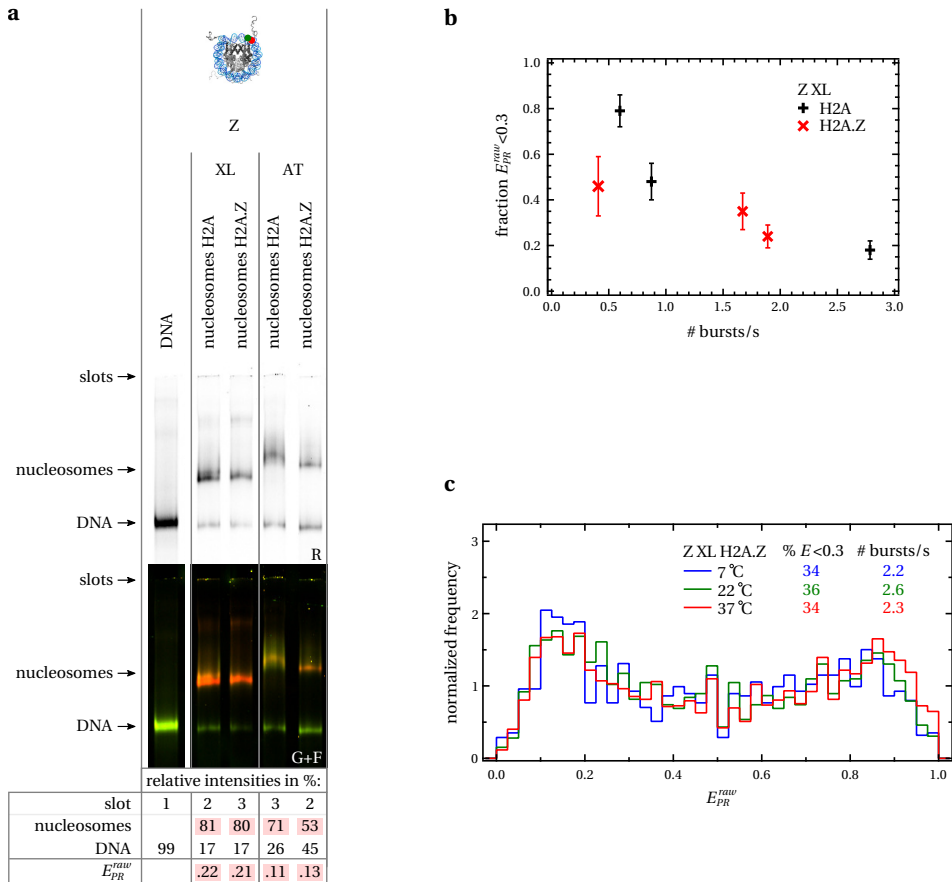


Figure 4.8 – Nucleosomes reconstituted with *Xenopus Leavis* histones. **a**: Fluorescence images of a 5% polyacrylamide gel with reconstituted nucleosomes with labels at position Z. Nucleosomes with either *Xenopus Leavis* (XL) or *Arabidopsis Thaliana* (AT) histones. Displayed is a compilation of two sections from the same gel, indicated by whitespace between the lanes. Top (R): acceptor fluorescence upon direct acceptor excitation. Bottom (G+F): false color overlay of donor and acceptor (FRET) fluorescence upon donor excitation. **b**: Fraction of nucleosomes without FRET as a function of number of bursts per second for three independent single-molecule measurements of XL nucleosomes inside a polyacrylamide gel at 22 °C. Error bars represent standard deviations of the values for 200 s intervals of the 1800 s measurements. **c**: FRET efficiency distributions of XL nucleosomes in solution. The same sample is measured at three different temperatures. Single-molecule data was collected for 10 minutes.

with *Arabidopsis Thaliana* histone octamers containing either H2A or H2A.Z with practically 100% reconstitution yield. We have investigated their FRET efficiencies in a polyacrylamide gel, and FRET distributions with spFRET inside the gel and in solution at different ambient temperatures.

The nucleosomes containing *Arabidopsis Thaliana* histone octamers used in this study were very sensitive to disrupting conditions. At single-molecule concentrations, the nucleosomes lose FRET in gel, upon exposure to surface, and in suboptimal buffer conditions. Nevertheless, H2A.Z nucleosomes consistently have a larger high-FRET population and are less susceptible to disrupting conditions than H2A-containing nucleosomes. The ensemble FRET (in gel) of H2A-containing nucleosomes is lower (figures 4.3 and 4.4a), they lose FRET more rapidly in gel (figure 4.4b), and are more susceptible to surface interactions and degradation during storage than H2A.Z-containing nucleosomes (figures 4.6 and 4.7). Not only *Arabidopsis Thaliana*, but also *Xenopus Leavis* histone octamers show that H2A.Z-containing nucleosomes are slightly more stable (figure 4.8).

FRET can be lost due to increased DNA breathing, dimer loss, or full dissociation into free DNA and histones, schematically depicted in figure 4.9. Comparison of the data for nucleosomes with labels at position X, Y or Z gives some insight into the possible mechanisms causing increase of the population without FRET. Nucleosomes with labels at position X or Z lose FRET for DNA unwrapping of 30 bp or more or (irreversible) dimer loss. Nucleosomes with labels at position Y lose FRET only for unwrapping of more than 60 bp, possibly accompanied by dimer loss. All constructs lose FRET upon complete dissociation.

While the ensemble FRET efficiency in gel is the same for H2A- and H2A.Z-containing nucleosomes with labels at position X and H2A-containing nucleosomes at position Y, the H2A.Z-containing nucleosomes with labels at position Y have a higher ensemble FRET efficiency. This indicates that the population of nucleosomes where more than 60 bp is unwrapped is larger in H2A-containing nucleosomes than in H2A.Z-containing nucleosomes. Z-labeled nucleosomes show a much lower FRET efficiency than X-labeled nucleosomes. We attribute this asymmetry to the non-palindromic 601 sequence, the only asymmetric component in the nucleosome constructs. Asymmetric unwrapping of 601-based nucleosomes has been reported before [128]. Asymmetry of the 601 sequence is not always found in spFRET experiments with single nucleosomes. For example, the data from Koopmans et al. [42] show equal distributions X- and Z-labeled nucleosomes with in-gel spFRET. These experiments were performed with histone octamers purified from chicken erythrocytes, from which the energy landscape for DNA unwrapping could differ from *Arabidopsis Thaliana* histones such that any differences caused by 601 asymmetry are not detectable.

The high-FRET fraction of both H2A- and H2A.Z-containing nucleosomes decreases inside a polyacrylamide gel within a few hours. Both H2A- and H2A.Z-con-

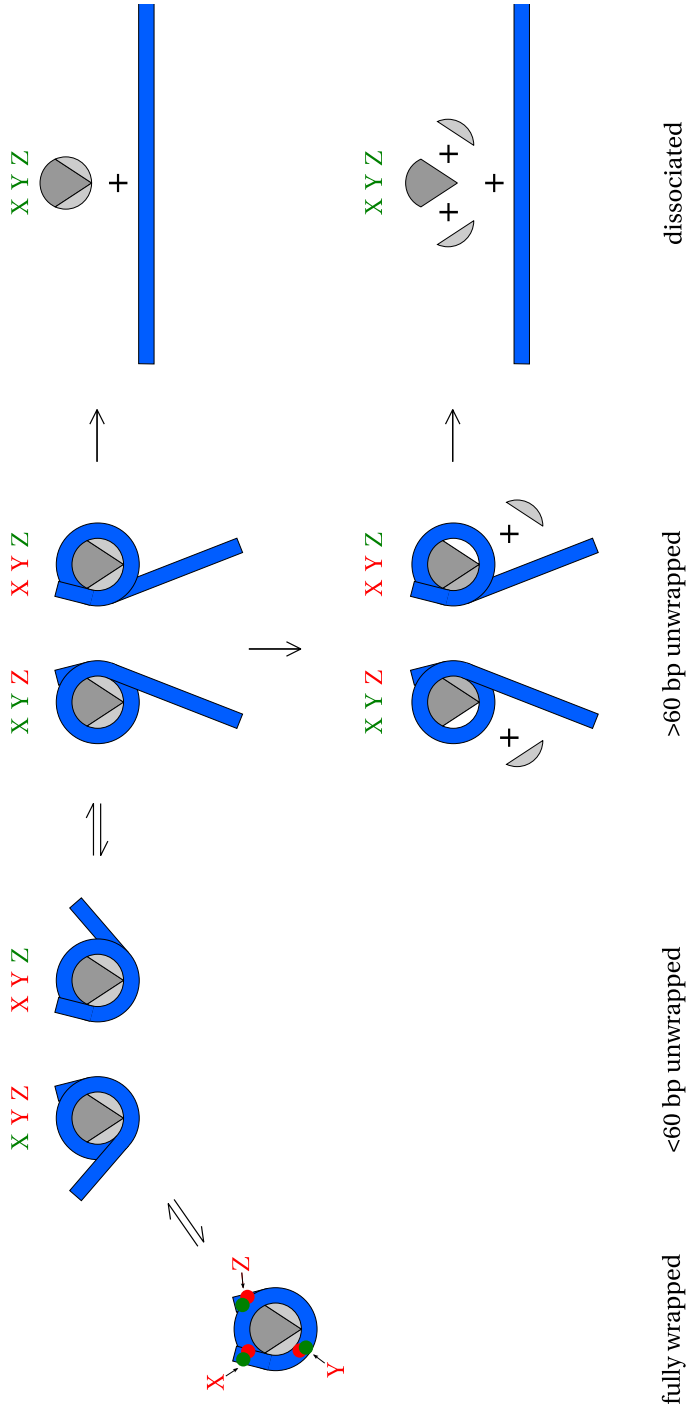


Figure 4.9 – Schematic overview of possible nucleosome conformations. Blue: DNA; dark grey: (H3/H4)₂ tetramer; light grey: H2A/H2B dimer. X, Y and Z indicate the positions of the fluorescent labels. Red: high FRET; green: no FRET.

taining nucleosomes reach the same distribution between FRET and no FRET, but H2A.Z-containing nucleosomes reach this distribution more slowly. This suggests that (at least) two populations are present, and the observed distribution is a superposition of the distributions of these two populations. The first population is constant over time and exists of intact nucleosomes with a certain unwrapping probability. The second population changes from high FRET to complete loss of FRET in a few hours, and exists of nucleosomes that dissociate irreversibly. This last population might consist of nucleosomes that initially are not properly folded and therefore lose their dimers or completely dissociate more easily, depending on whether they contain H2A or H2A.Z.

The nucleosomes used in this spFRET study lose their FRET mainly due to interactions with the microscope slide surface. The fraction of X-labeled nucleosomes without FRET increases from about 20 to 70 % within 15 days after slide passivation. This means that the quality of the slides diminishes rapidly. It is also clear that H2A.Z-containing nucleosomes suffer less from the surface interactions than H2A-containing nucleosomes. Comparison with Y-labeled nucleosomes shows however that while the no-FRET population of X-labeled nucleosomes is about doubled in 9 days, the no-FRET population of Y-labeled nucleosomes is still below 20 % (figure 4.6). Therefore, the loss of FRET in X-labeled nucleosomes is due to an increased DNA unwrapping probability or possibly (irreversible) dimer loss and not due to full dissociation into free DNA and histones.

The experimentally found differences between H2A- and H2A.Z-containing nucleosomes are of two kinds: decreased unwrapping probability and decreased dissociation probability for H2A.Z-containing nucleosomes. The decreased unwrapping probability is in agreement with the expectation based on the substitution of a Threonine in H2A to a Lysine in H2A.Z at the second minor groove of the nucleosomal DNA. Threonine is an uncharged polar amino-acid, while lysine is positively charged, resulting in an electrostatically less strong DNA-histone binding at the second contact point for H2A. A similar increase in unwrapping probability at the first DNA-histone contact point has been seen for nucleosomes where a lysine at H3 K56 has been acetylated, which also removes a positive charge [50] (see chapter 3 in this thesis). The structural difference between H2A- and H2A.Z-containing octamers at the H2A(Z)/H3 interface is probably the reason for a decreased probability for dimer loss in H2A.Z-containing nucleosomes. The third structural difference between H2A- and H2A.Z-containing nucleosomes is the H2A(Z)-H2A(Z) interface. It is possible that the H2A(Z)-H2A(Z) interactions at this interface are stronger in H2A.Z-containing nucleosomes, thus decreasing the probability for loss of one of the dimers.

The thermodynamically expected temperature effect of a few percent with 30° temperature change lies within the measurement uncertainty, and may be too small to have consequences for gene manipulation. We have found no influence of temperature on the unwrapping or dissociation probability of H2A.Z-containing nucleosomes

between 7 and 37 °C. Thus we exclude H2A.Z as a direct temperature sensor responsible for ambient-temperature dependent changes in phenotype seen in *Arabidopsis Thaliana* [124]. H2A.Z could still be indirectly involved in the ambient temperature sensing pathway via for example remodeling by an ambient temperature dependent factor.

4.5 Conclusions

We have directly measured the temperature dependent stability of H2A- and H2A.Z-containing nucleosomes at the single-molecule level. Although the nucleosomes containing *Arabidopsis Thaliana* histone octamers were very susceptible to dissociating conditions like dilution to single-molecule concentrations and the presence of surfaces, we clearly showed that H2A- and H2A.Z-containing nucleosomes behave differently. H2A.Z-containing nucleosomes are more stable and less susceptible to dilution- or surface-induced dissociation. The unwrapping probability is constant in the ambient temperature range. Thus alternative explanations need to be explored to explain the role of H2A.Z in temperature sensing *in vivo*.

Acknowledgements

We thank Prof. Dr. Jürgen Groll (Universität Würzburg) for providing the NCO-starPEG material. This work is part of the research program of the Foundation for Fundamental Research on Matter (FOM), which is part of the Netherlands Organization for Scientific Research (NWO).

CHAPTER 5

spFRET reveals changes in nucleosome breathing by neighboring nucleosomes

Ruth Buning, Wietske Kropff, Kirsten Martens, and John van Noort

Accepted for publication in Journal of Physics: Condensed Matter

Abstract

Chromatin, the structure in which DNA is compacted in eukaryotic cells, plays a key role in regulating DNA accessibility. FRET experiments on single nucleosomes, the basic units in chromatin, have revealed a dynamic nucleosome where spontaneous DNA unwrapping from the ends provides access to the nucleosomal DNA. Here we investigated how this DNA breathing is affected by extension of the linker DNA and by the presence of a neighboring nucleosome. We found that both electrostatic interactions between the entering and exiting linker DNA and nucleosome-nucleosome interactions increase unwrapping. Interactions between neighboring nucleosomes are more likely in dinucleosomes spaced by 55 bp of linker DNA than in dinucleosomes spaced by 50 bp of linker DNA. Such increased unwrapping may not only increase the accessibility of nucleosomal DNA in chromatin fibers, it may also be key to folding of nucleosomes into higher order structures.

5.1 Introduction

Chromatin consists of arrays of nucleosomes connected with 10-90 base pairs (bp) of linker DNA [129]. Interactions between these nucleosomes lead to dense higher order structures. Although the arrangement of nucleosomes and the DNA trajectory in chromatin has been investigated intensively in the past decades, the structure of chromatin remains highly debated [130]. The compact state of native chromatin under physiological salt conditions was visualized by electron microscopy (EM) more than 35 years ago [3]. The DNA trajectory in the fiber was however not visible in the EM pictures of compacted chromatin. The crystal structure of a tetranucleosome, four nucleosomes connected by 20 bp linker DNA, provides more detailed information on the arrangement of nucleosomes and DNA trajectory [131]: next-neighbors interact in a face-to-face configuration and the linker DNA is straight. A similar small array, consisting of three nucleosomes connected by 20 bp linker DNA, has been investigated with FRET (Fluorescence or Förster Resonance Energy Transfer) [54]. The array compacts under influence of magnesium, and next-neighbors appear to interact face-to-face in the same way as in the crystal structure, as demonstrated by a high FRET efficiency between the labels on next-neighboring nucleosomes. Recently, this arrangement was confirmed by cryogenic electron microscopy of 20 and 30 bp linker DNA chromatin fibers that included linker histones [132].

The interactions between nucleosomes are mediated by electrostatics and specific contacts involving flexible histone tails [133]. The unstructured tails allow for alternative orientations between nucleosome pairs that put different constraints on the linker DNA. In native chromatin, the linker length varies between 10 and 90 bp [129], which may lead to interactions between other nucleosome pairs and hence different topologies of the chromatin fiber. Indeed, EM experiments on reconstituted nucleosomal arrays with 30-90 bp linker length suggest interactions between direct neighbors [130]. The force-extension behavior of nucleosomal arrays with 50 bp linker length, as measured on single chromatin fibers using magnetic tweezers, also suggests interactions between direct neighbors [134]. From such force spectroscopy experiments, another interesting feature arises: a large increase in fiber length at a force of 4 pN indicates the disruption of nucleosome-nucleosome interactions [26, unpublished data]. This length increase is larger than what would be expected from the extension of the linker DNA only. The disruption of nucleosome-nucleosome interactions seems to be accompanied by partial unwrapping of the nucleosomal DNA, suggesting that in the condensed fiber, the nucleosomal DNA may already be partly unwrapped.

Partial unwrapping of nucleosomes in a compacted chromatin fiber would have consequences for the accessibility of nucleosomal DNA. It might even make part of the nucleosomal DNA more accessible in a folded chromatin fiber than in an individual nucleosome. Poirier et al. [53] have investigated the accessibility of nucleosomal and

linker DNA to restriction enzymes in both mononucleosomes and in nucleosomal arrays. Interestingly, they found that parts of the nucleosomal DNA in a fiber can be up to 8-fold more accessible than in mononucleosomes.

Individual nucleosomes are dynamic structures. DNA breathing, the transient unwrapping of DNA from the histone core, makes nucleosomal DNA accessible for DNA-binding proteins [25, 58]. Single-pair FRET (spFRET) [135] experiments have quantified this [127], revealing DNA breathing from both nucleosome ends. Nucleosomes are open for about 10 % of the time for tens of milliseconds [42]. DNA breathing is modulated by DNA sequence and by post-translational modifications to the histone proteins [32, 50]. So far, spFRET experiments have mainly focussed on individual nucleosomes, ignoring how nucleosome conformation and dynamics are influenced when the nucleosome is embedded in a chromatin fiber. To address this question, we focus here on (partial) unwrapping of nucleosomal DNA in nucleosomes flanked by linker DNA and/or by a second nucleosome.

We measure unwrapping of nucleosomal DNA in dinucleosomes with 50 bp linker length, because this is the average linker length found *in vivo* [129] and commonly used in chromatin fiber experiments [99, 130, 134]. The mechanical properties of the linker DNA pose constraints on the conformational freedom to position nucleosomes face-to-face, and the energy required to bend the linker DNA could be reduced by partial unwrapping of the nucleosomal DNA. We therefore expect that interactions between nucleosomes will be accompanied by DNA unwrapping from the nucleosome exit, in accordance with observations made by force spectroscopy on single chromatin fibers [26].

The energy required to bend the linker DNA depends on sterical constraints as well as on the linker DNA length. Variations of only a few bp have significant effects on the torsional energy required for positioning neighboring nucleosomes face-to-face, due to the 10.4 bp helical periodicity of DNA. Increasing the linker length with 5 bp from 50 to 55 bp is just a 1.7 nm change in length, but changes the relative orientation of two non-interacting nucleosomes by 180 degrees (see figure 5.2 for an illustration). So far, the effect of the linker length has mostly been studied for multiples of 10 bp. However, a natural preference for $10n+5$ bp linker DNA has been suggested, and observed in yeast [136–138]. Such a ‘phase offset’ may play a crucial role in the formation of chromatin higher order structure.

Not only interactions between nucleosomes determine higher order chromatin structure, the linker DNA itself may also have an effect on the DNA trajectory in the fiber by steric and/or electrostatic interactions with the nucleosome and/or other stretches of linker DNA.

Here, we describe spFRET experiments on single fluorescently labeled nucleosomes flanked by either 300 bp linker DNA or a neighboring nucleosome with 20 or 50 bp linker DNA. Moreover, we compare unwrapping in dinucleosomes with 50 and

with 55 bp linker DNA. We show that the presence of linker DNA and of a neighboring nucleosome results in a significant change in FRET distribution, depending on the linker length. The presence of linker DNA enhances unwrapping of nucleosomal DNA. In dinucleosomes with 55 bp linker DNA, interactions between the nucleosomes appear to further increase the unwrapping probability of the nucleosomal DNA.

5.2 Materials and Methods

5.2.1 Preparation of DNA constructs

A 198 bp DNA template containing a single 601 nucleosome positioning sequence was constructed by PCR. The forward and reverse primers were labeled at a single position with Cy3B and ATTO647N (via amino linker with 6-carbon spacer to the base; IBA). Primer sequences can be found in the supplementary material. The donor and acceptor were separated by 81 bp. After reconstitution, the donor (Cy3B) is located at the second base pair from the nucleosome exit. The acceptor (ATTO647N) is located 10 base pairs from the dyad, leading to a FRET efficiency larger than 0.5 for a fully folded nucleosome. The layout of the mononucleosome construct is shown in figure 5.1. Two non-palindromic restriction sites were included close to the DNA ends: BsaI and BseYI, which were subsequently used to build longer constructs by ligation.

After purification, the 198 bp construct was digested with either BsaI or BseYI and ligated to 300 bp DNA without any nucleosome positioning sequence, or DNA with a second, unlabeled, 601 nucleosome positioning sequence. If necessary, the ligated DNA product was purified from agarose gel to remove unligated product. Figure 5.2 schematically shows all nucleosome constructs described in this paper.

5.2.2 Nucleosome reconstitution

DNA and chicken erythrocyte histone octamers were mixed in various molar ratios in TE (1 mM EDTA, 10 mM Tris.HCl pH 8.0) and 2 M NaCl. Mono- and dinucleosomes were reconstituted by salt gradient dialysis against 0.85, 0.65, 0.5 and finally 0 M NaCl, all buffered with TE in a total volume of 40 μ l and a labeled DNA concentration around 50 nM. Competitor DNA, 147 bp unlabeled random sequence DNA (produced with PCR), was included in the reconstitution reaction at concentrations between 150 and 300 nM.

5.2.3 Polyacrylamide gel electrophoresis

Nucleosome reconstitutions were analyzed with 5 % native polyacrylamide gel electrophoresis (PAGE). A sample of 2-8 μ l of reconstitution product was loaded on the gel

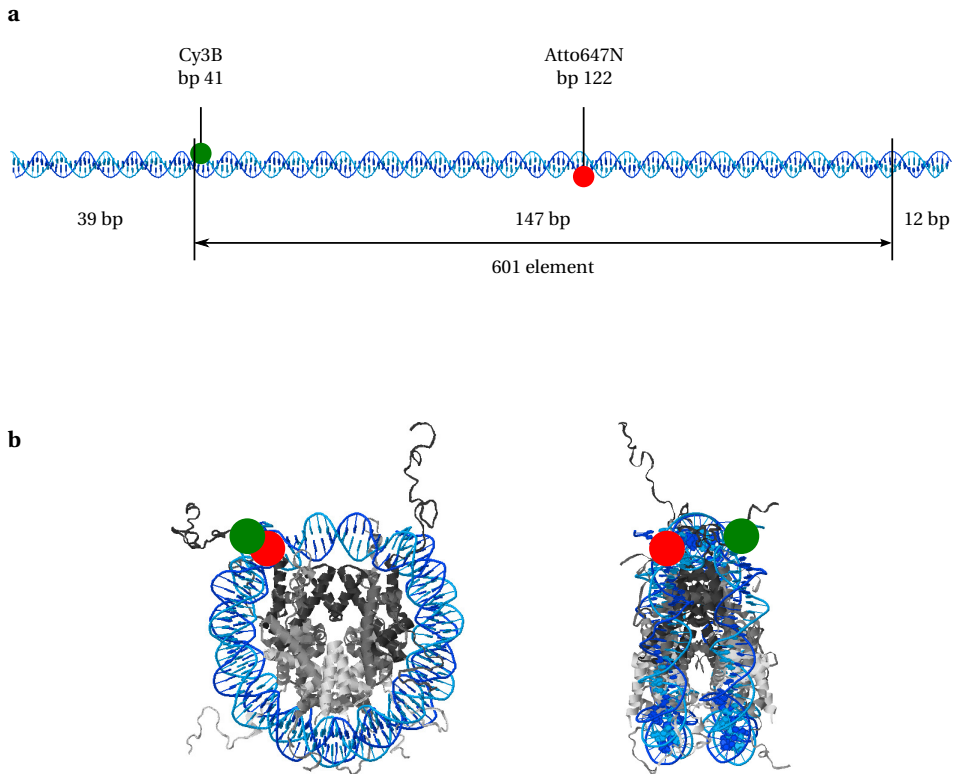


Figure 5.1 – a: The 198 bp DNA construct, indicating the position of the 601 positioning element and the fluorescent labels. **b:** Top and side view of the crystal structure of the nucleosome core particle (1KX5, [12]), consisting of 147 bp DNA wrapped around the histone octamer. The positions of the fluorescent labels are indicated.

(29:1 bis:acrylamide, $0.2 \times$ TB, Amersham Bioscience Hoefer SE 400 vertical gel slab unit). The gel was run at 19 V/cm at 7 °C for 90-120 minutes to separate nucleosomes from free DNA. The fluorescence was imaged with a gel imager (Typhoon 9400, GE Healthcare). Red: excitation at 633 nm, emission detected at 670 nm; Green: excitation at 532 nm, emission detected at 580 nm; FRET: excitation at 532 nm, emission detected at 670 nm (all 30 nm bandpass). Gel images were analyzed with ImageJ software to determine the relative intensities of the bands. The uncorrected proximity ratio (E_{PR}^{raw}), as a measure for the FRET efficiency in the bands, was calculated according to equation 5.1 (see section 5.2.6).

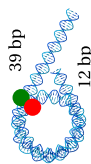
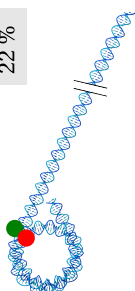
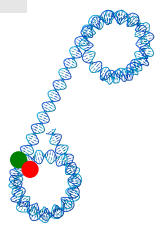
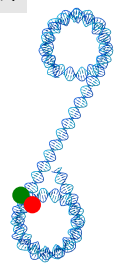
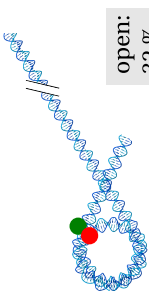
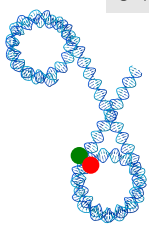
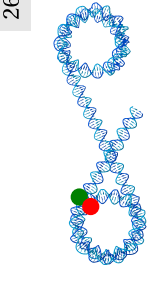
5.2.4 Sample preparation

Fluorescently labeled nucleosomes were diluted to a concentration of 50-100 pM in a buffer containing 10 mM Tris.HCl pH 8.0, 0.1 mg/ml BSA, 0.03 % Nonidet-P40 and 2 mM trolox. Where stated, 100 mM KAc and 2 mM MgAc₂ were added to the buffer. We used non-stick tubes (Ambion) for nucleosome dilutions. After 15-30 minutes of equilibration to room temperature, a drop of 50 μ l was placed on a glass coverslide (#1.5, Menzel) and imaged as described below.

5.2.5 Single-molecule fluorescence microscopy

Single molecules were imaged with a home-built confocal microscope equipped with a $60 \times$ water-immersion objective (NA=1.2, Olympus), as schematically depicted in figure 5.3a (see also [42]). A 515 nm diode pumped solid state laser (Cobolt) and a

Figure 5.2 (facing page) – Schematic overview of the constructs described in this chapter. The elementary mononucleosome (MN) contains a single 601 element, flanked by 39 bp on the side closest to the fluorescent labels, and by 12 bp on the opposite side. All other constructs are extensions of the elementary nucleosome. The mononucleosomes with 300 bp linker DNA contain a single 601 element, flanked by 300 bp either on the label side (MNI300), or on the opposite side (MNo300). The dinucleosomes (DN) contain two 601 elements, linked by 20, 50 or 55 bp linker DNA. The two 601 elements are linked via the label side (DNI50 and DNI55), or via the opposite side (DNo20, DNo50 and DNo55). Dinucleosomes linked by 20 bp linker DNA via the label side are missing due to constraints imposed by the positions of restriction sites. The percentages of open nucleosomes ($E_{PR}^{raw} < 0.3$) correspond to single-molecule measurements in 100 mM KAc. Structures shown are based on the nucleosomal DNA from the crystal structure of the nucleosome core particle (IKX5, [12]), which we extended with linear stretches of DNA with the use of [139]. The histone octamers are left out for visual clarity. Note that the images of the constructs just display a linear extension of the linker DNA, and do not reflect actual experimentally determined or theoretically predicted trajectories of the linker DNA. FRET experiments with both labels on the linker DNA rather suggest that the linker DNA is bent [140].

Elementary Mononucleosome		Dinucleosomes					
	<p>MN</p>  <p>open: 11 %</p>						
Mononucleosomes with 300 bp linker DNA		50 bp linker DNA		55 bp linker DNA			
linker DNA attached at the label side	<p>MNI300</p>  <p>open: 22 %</p>	<p>DNI50</p>  <p>open: 13 %</p>	<p>DNI55</p>  <p>open: 21 %</p>	linker DNA attached at the opposite side	<p>MNI300</p>  <p>open: 32 %</p>	<p>DNo50</p>  <p>open: 31 %</p>	<p>DNo55</p>  <p>open: 26 %</p>

636 nm diode laser (Power Technology) were used as excitation sources. The lasers were alternated at 20 kHz by analog modulation, either directly (636 nm), or with an AOM (515 nm; Isomet). The beams were spatially filtered with a single-mode fiber, and focussed 25 μm above the glass-buffer interface by the objective. The excitation power was 13 μW for 515 nm excitation, and 6 μW for 636 nm excitation. The collected fluorescence was spatially filtered with a 50 μm pinhole in the image plane, and was split into a donor and an acceptor channel by a dichroic mirror (640dcxr, Chroma). The fluorescence was filtered with emission filters (hq570/100m for the donor channel, hq700/75m for the acceptor channel, Chroma) to minimize crosstalk, and was imaged on the active area of single photon avalanche photodiodes (SPCM AQR-14, Perkin-Elmer). The photodiodes were read out with a TimeHarp 200 photon counting board (Picoquant GmbH). In a typical experiment, data was collected for 30 minutes in which 2000-10000 bursts of fluorescence were detected.

5.2.6 Single-molecule data analysis

Bursts of fluorescence were detected using the method described in [66]. A burst was assigned if a minimum of 50 photons were detected with a maximum interphoton time of 100 μs . Photon arrival times in the donor (D) and acceptor (A) channel were sorted according to excitation wavelength, resulting in four photon streams: D-emission upon D-excitation: I_{Dex}^{Dem} , A-emission upon D-excitation: I_{Dex}^{Aem} , D-emission upon A-excitation: I_{Aex}^{Dem} , A-emission upon A-excitation: I_{Aex}^{Aem} . Example data are shown in figure 5.3b.

For each burst, we estimated the FRET efficiency by the sensitized-acceptor emission method [69, 70]. Following the definitions described by Lee et al. [31], we calculated the uncorrected proximity ratio E_{PR}^{raw} and label stoichiometry S^{raw} from the total number of photons in the burst for the different photon streams:

$$E_{PR}^{raw} = \frac{I_{Dex}^{Aem}}{I_{Dex}^{Aem} + I_{Dex}^{Dem}} \quad (5.1)$$

$$S^{raw} = \frac{I_{Dex}^{Aem} + I_{Dex}^{Dem}}{I_{Dex}^{Aem} + I_{Dex}^{Dem} + I_{Aex}^{Aem}} \quad (5.2)$$

The excitation powers were chosen such that $I_{Dex}^{Aem} + I_{Dex}^{Dem} \approx I_{Aex}^{Aem}$ for doubly labeled particles, resulting in $S^{raw} \sim 0.5$. An example of a 2D E, S histogram from a typical measurement is shown in figure 5.3c. Nucleosomes containing both donor and acceptor fluorophores were selected for further analysis by taking only bursts with $0.2 < S^{raw} < 0.8$. Histograms of the FRET efficiencies of these bursts show the distribution of FRET efficiencies of the doubly labeled nucleosomes only. Bursts of two

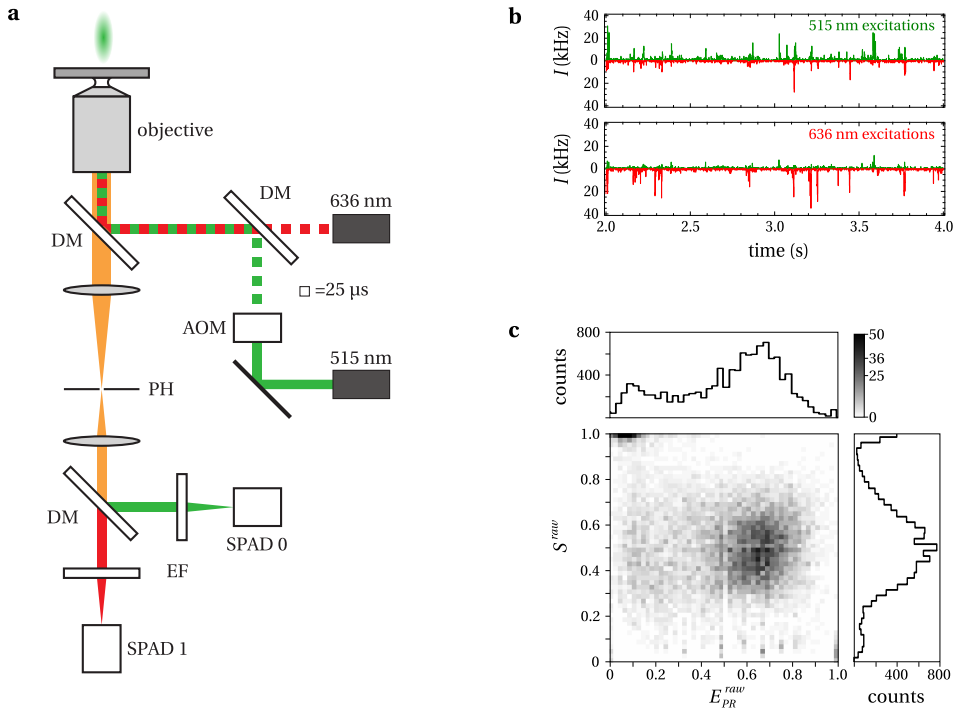


Figure 5.3 – **a**: Schematic overview of the confocal FRET microscope. DM: dichroic mirror; AOM: acousto-optical modulator; PH: pinhole; EF: emission filter; SPAD: single photon avalanche diode. **b**: Typical fluorescence intensity timetraces of the four different photon streams acquired with the setup in a. Photon arrival times are binned to 1 ms. Bursts of fluorescence arise from the passage of a single particle through the excitation volume. **c**: Typical 2D-histogram of FRET efficiency (E_{PR}^{raw}) and label stoichiometry (S^{raw}) for mononucleosomes. Four populations are distinguishable: donor only ($S^{raw} > 0.8$), acceptor only ($S^{raw} < 0.2$), doubly labeled ($0.2 < S^{raw} < 0.8$) with FRET ($E_{PR}^{raw} > \sim 0.3$) and without FRET ($E_{PR}^{raw} < \sim 0.3$).

or three measurements of the same construct and conditions were verified for reproducibility and combined to build one FRET histogram. Histograms were normalized to a total area under the curve of 1 to allow comparison of different constructs. The fraction without FRET (representing open or (partly) dissociated nucleosomes) was determined by taking the area below the histogram for $E_{PR}^{raw} < 0.3$.

Note that we did not attempt to quantify the extent of DNA unwrapping from the histone core. The limited number of photons per burst, the complications with the translation from FRET efficiency to label pair distance [31], and the possibility of conformational changes within a single burst prevent a direct calculation of the label pair distance and from that the nucleosome conformation. Alternatively, one can change the positions of the labels along the DNA to resolve the extent of DNA unwrapping [42, 50], but this requires new DNA constructs. By choosing the location of the FRET pair to be at the very end of the nucleosomal DNA, we ensure that all DNA unwrapping events of over 10 bp DNA are captured in our measurements [127]. In this paper, increased unwrapping therefore refers to more frequent breathing rather than breathing of larger stretches of nucleosomal DNA.

5.3 Results

5.3.1 Gel electrophoresis of (di)nucleosome reconstitutions

Figure 5.4 shows the fluorescence in (di)nucleosomes after native gel electrophoresis of all reconstituted nucleosomal constructs, separating free DNA from nucleosomes. The amount of free DNA is generally much smaller than the amount of reconstituted nucleosomes, confirming a high reconstitution yield. As opposed to bare DNA, nucleosomes show significant FRET, indicating reconstitution into fully wrapped nucleosomes, properly positioned on the 601 elements.

In most cases, a single sharp band of nucleosomes is present. However, sometimes a second band is visible just below the main nucleosome band. This minor band can be attributed to incomplete nucleosomes, lacking the H2A/H2B dimer(s). In all cases there is some material left in the slots, originating from aggregates, that show a small FRET signal as well.

FRET differences between constructs are readily visible in the gel: the FRET efficiency of dinucleosomes depends on the linker DNA length. 20 bp linker DNA dinucleosomes yield the highest FRET efficiency and 50 bp linked at the nucleosomal side opposite of the fluorescent labels the lowest.

Since the amount of reconstituted nucleosomes is small (1-2 pmol), we did not purify the nucleosomes after reconstitution. The consequences for the interpretation of single-molecule data will be discussed in the discussion section.

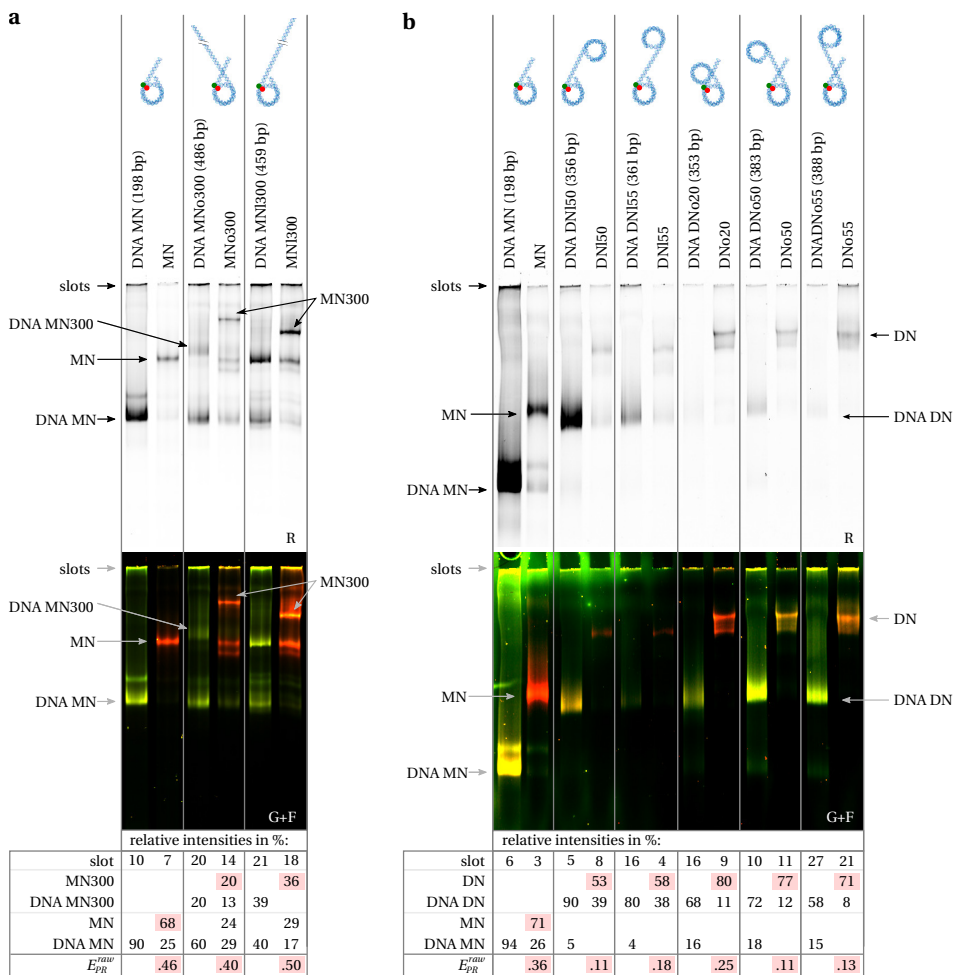


Figure 5.4 – Fluorescence images of 5% polyacrylamide gels with reconstituted mononucleosomes (**a**) and dinucleosomes (**b**). Tops (R): acceptor fluorescence upon direct acceptor excitation. Bottoms (G+F): false color overlay of donor and acceptor (FRET) fluorescence upon donor excitation. MN: mononucleosomes. DN: dinucleosomes. Reconstituted nucleosomes show FRET, in contrast to bare DNA. The relative intensities of the bands in each lane from the direct acceptor excitation image are displayed in the table at the bottom, providing a measure for the relative concentrations of the different components (bare DNA, nucleosomes, aggregates). Percentages are approximate within a few percent. Numbers corresponding to mononucleosome bands are highlighted, and the FRET efficiency calculated from the green and FRET intensities of the bands is indicated in the bottom row.

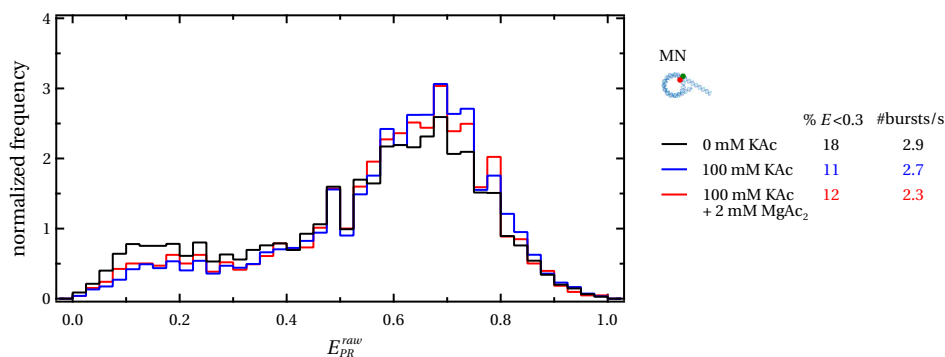


Figure 5.5 – FRET efficiency distributions of mononucleosomes in different salt conditions. The fraction open nucleosomes decreases from 17 to 11 % when increasing the monovalent salt concentration from 0 to 100 mM. Addition of 2 mM magnesium has no effect on the FRET efficiency distribution.

5.3.2 FRET distributions of mononucleosomes

Rather than an average FRET value, as determined from the gel, single-molecule experiments reveal the distribution of FRET values obtained from individual nucleosomes. We attribute bursts with an uncorrected proximity ratio lower than 0.3 to particles without FRET. This can be either bare DNA or nucleosomes that are partly unwrapped ('open').

18 % of the elementary mononucleosomes (MN), shows no FRET at 0 mM salt (figure 5.5). We observed that an increase of monovalent salt to 100 mM decreases the open population to 11 %.

5.3.3 Linker DNA increases DNA breathing

Although DNA breathing has been well established in mononucleosomes, it is unclear how extended DNA linkers affect nucleosome dynamics. Mechanical, hydrodynamic and electrostatic properties of DNA will determine the trajectory and dynamics of the linker DNA, which is linked to the nucleosomal DNA. FRET distributions of mononucleosomes with 300 bp linker DNA are compared with the distribution of mononucleosomes in figure 5.6. 300 bp of linker DNA attached to the label side cause an increase in the population without FRET from 18 % to 26 %. When attached to the opposite side, the population without FRET is more than doubled to 40 %. Increasing the monovalent salt concentration to 100 mM decreased this effect, indicating that electrostatic repulsion is mainly responsible for enhanced opening of the nucleosome.

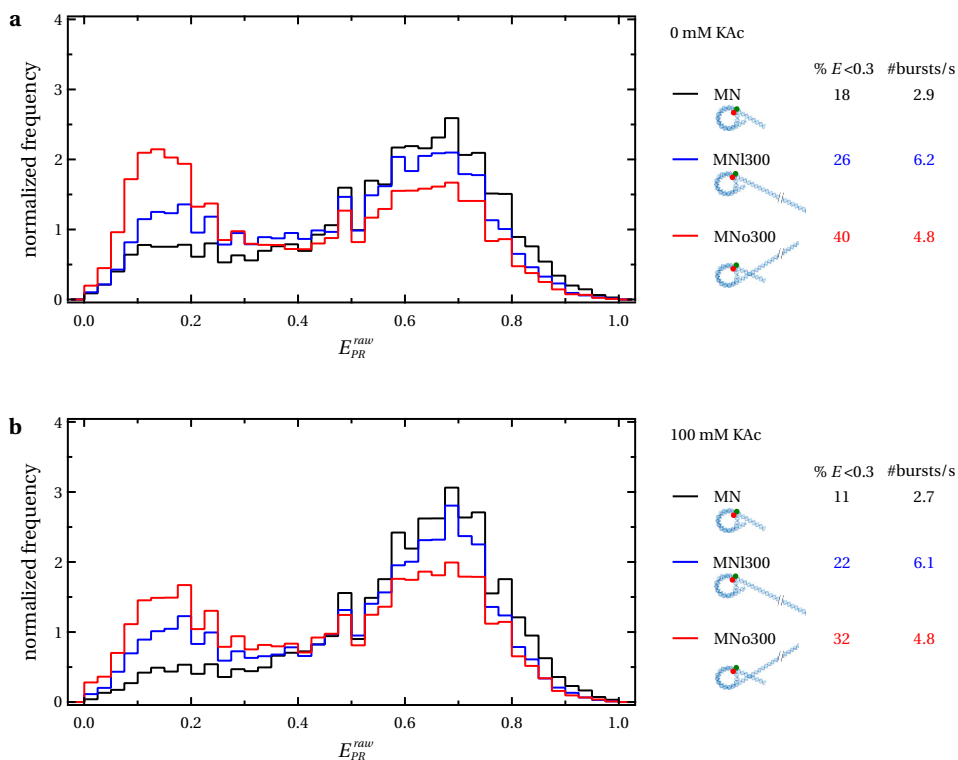


Figure 5.6 – FRET efficiency distributions of mononucleosomes with 300 bp linker DNA, without (a) and with (b) 100 mM monovalent salt. Nucleosomes with 300 bp linker DNA at the label side (MNI300) or the opposite side (MNo300) have a larger population of open nucleosomes than nucleosomes without the linker DNA. The linker DNA at the side opposite of the label positions has a surprisingly large effect on the population of open nucleosomes. Adding 100 mM monovalent salt decreases this effect about 25 %.

5.3.4 DNA breathing is affected by neighboring nucleosomes

While linker DNA has large effects on nucleosome dynamics, it can be expected that the presence of another nucleosome, connected by linker DNA, will further modulate this, as such a nucleosome is bulkier and carries a high charge density. All dinucleosomes were measured in 100 mM monovalent salt, for proper comparison with the mononucleosomes and in accordance with the conditions used for single-molecule force spectroscopy on chromatin fibers [134]. Moreover, we included 2 mM Mg^{2+} , which is required for folding of nucleosomal arrays into dense 30 nm fibers.

Dinucleosomes with linker DNA at the label side

The distance between non-interacting (straight linker DNA) neighboring nucleosomes with 50 or 55 bp linker DNA is too large for steric or electrostatic effects between the nucleosomes to play a role. Indeed, between the mononucleosomes and the dinucleosomes with 50 bp linker DNA, there are only minor changes in the FRET distribution (see figure 5.7). Dinucleosomes with 55 bp linker DNA, however, show a significantly larger population without FRET. This suggests that a difference in interactions between nucleosomes results in an increased unwrapping probability. We did however not observe an effect of 2 mM magnesium on the FRET distributions.

Dinucleosomes with linker DNA at the side opposite of the label

When the second nucleosome is attached to the side opposite of the labels, we similarly expect no steric or electrostatic effect between non-interacting nucleosomes. However, as can be seen in figure 5.8, dinucleosomes with 50 and with 55 bp linker DNA both show a FRET distribution that is different from that of the mononucleosome. In these constructs, both interactions between the two nucleosomes, between the linker DNAs, and between nucleosomes and linker DNA may play a role, giving rise to a more complex shape of the distribution, including more pronounced intermediate states.

For the dinucleosomes with the linker DNA attached to the side opposite of the fluorescent labels we could also build a construct with 20 bp linker DNA. This distance is too short for the nucleosomes to interact in a face-to-face orientation. The FRET distribution of dinucleosomes with 20 bp linker DNA has a slightly increased population with intermediate FRET values as compared to mononucleosomes, and a similar low FRET fraction. The close proximity of the nucleosomes (~7 nm linker DNA) could allow interactions between the DNA and/or histone octamers of neighboring nucleosomes which may affect nucleosome breathing.

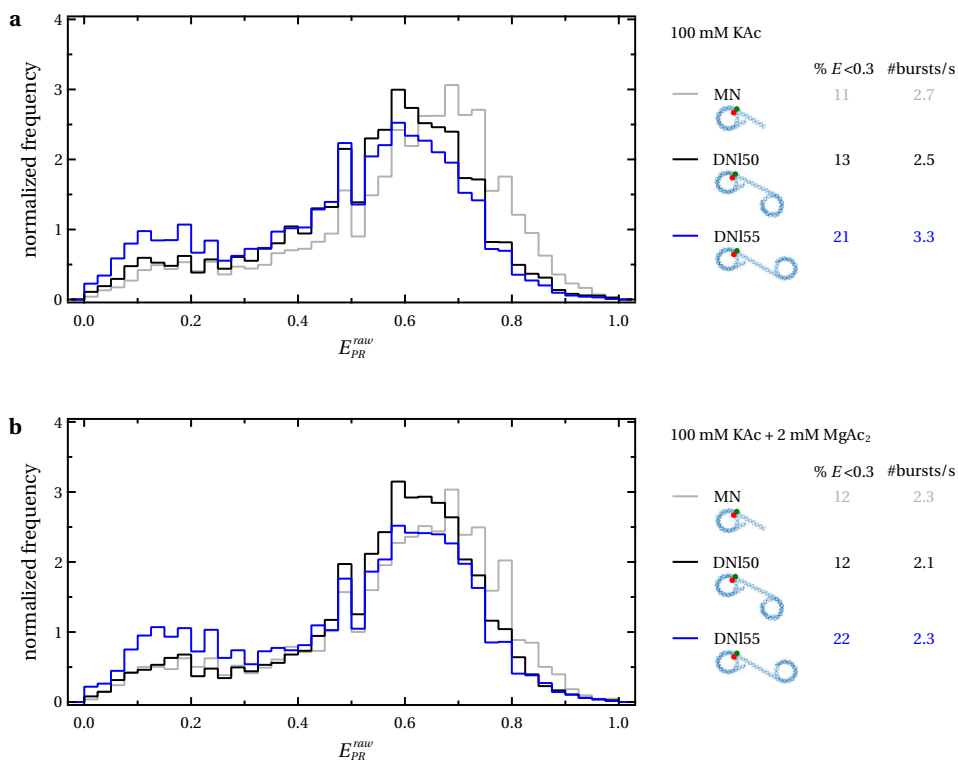


Figure 5.7 – FRET efficiency distributions of dinucleosomes linked via the fluorescent label side with either 50 bp (DNI50) or 55 bp (DNI55) linker DNA, without (a) and with (b) 2 mM magnesium. Dinucleosomes with 50 bp linker DNA show the same distribution as mononucleosomes. Dinucleosomes with 55 bp linker DNA on the other hand show a larger population of open nucleosomes. Addition of 2 mM Mg^{2+} has no visible effect on the FRET efficiency distributions.

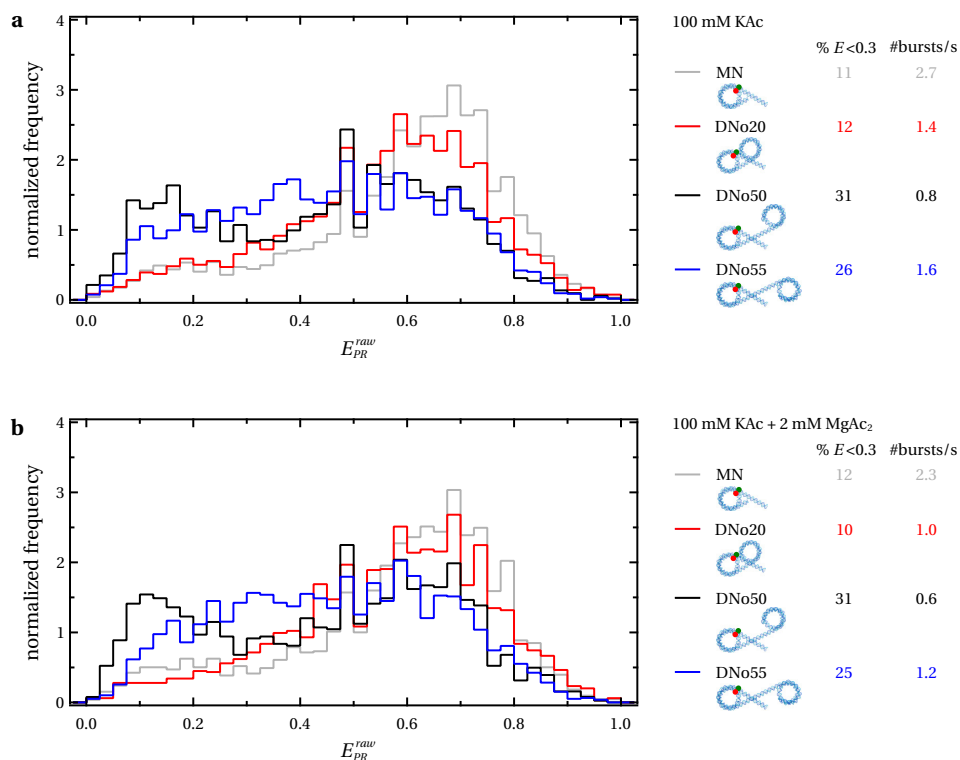


Figure 5.8 – FRET efficiency distributions of dinucleosomes linked via the side opposite of the fluorescent labels with either 20 bp (DNo20), 50 bp (DNo50) or 55 bp (DNo55) linker DNA, without (a) and with (b) 2 mM magnesium. Dinucleosomes with 20 bp linker DNA show a similar distribution to mononucleosomes. Dinucleosomes with 50 bp linker DNA show a much larger open population. Dinucleosomes with 55 bp linker DNA also show a much larger open population, and in addition a larger fraction with intermediate FRET efficiencies. Addition of 2 mM Mg^{2+} has no visible effect on the FRET efficiency distributions.

5.4 Discussion

Here, we showed that the presence of linker DNA and/or a neighboring nucleosome significantly influences nucleosomal DNA dynamics. Constructs of single nucleosomes flanked by long stretches of linker DNA or by neighboring nucleosomes differ in FRET efficiency distribution from mononucleosomes flanked by short stretches of linker DNA.

5.4.1 Sample handling

Nucleosomes are known to be very sensitive to concentration, buffer conditions and surface exposure [37, 41, 56, 141]. All FRET efficiency distributions that we report here are the result of multiple measurements, that are reproducible within 5 % (fraction $E_{PR}^{raw} < 0.3$). Under suboptimal measurement conditions, e.g. too high dilution and non-passivated surfaces (data not shown), the differences between samples showed the same trend, but generally had a larger fraction of bursts without FRET, indicating that nucleosomes dissociate under these conditions. It is interesting to note that dinucleosomes appeared to be less susceptible to dilution- and surface- driven dissociation than mononucleosomes. This is consistent with cooperative binding of nucleosomes [142].

5.4.2 Sample heterogeneity

Despite careful titration and the use of the strong 601 nucleosome positioning element, gel electrophoresis shows that the reconstitution yield is in many cases not perfect. For some constructs the percentage of nucleosomes in the sample was only about 30 %. Besides nucleosomes, the sample consists of one or more of following components: unreconstituted DNA, unligated DNA, nucleosomes on the unligated DNA and aggregates that remained in the slot. Although this heterogeneity in the sample makes quantification of the results difficult, the qualitative differences between the constructs still hold. The implications for the single-molecule data interpretation are described below.

Mononucleosomes

Quantification of the band intensities of the gel shown in figure 5.4 yields ~70 % of reconstituted nucleosomes and ~25 % of unreconstituted DNA. A significant amount of the material is left in the slots due to aggregation. In the single-molecule experiments however, the fraction without FRET is only 11 % (at 100 mM salt), which sets the maximum on the amount of unreconstituted DNA. The real amount is probably lower, because this population also consists of partly unwrapped nucleosomes. The amount of free DNA present in the gel, which is more than twice as high as the upper limit that

follows from single-molecule measurements, is therefore not representative for the reconstitution yield.

Gel electrophoresis can impose severe disruptions on a nucleosome sample. Conditions in the gel, such as low nucleosome concentration, drive nucleosome dissociation, resulting in a larger fraction of free DNA. Hence, we can not equate the reconstitution yield observed in the gel to the amount of unreconstituted DNA in the single-molecule experiments. The amount of free DNA is however the same in different single-molecule experiments of the same sample, i.e. mononucleosomes in different salt concentrations. The qualitative decrease of the fraction of open nucleosomes with increasing salt concentration can therefore not be explained by differences in reconstitution yield.

The material left in the slots after gel electrophoresis probably consists of aggregates, and can be as high as 20 % or more in some samples. Aggregates can be detected in the single-molecule experiments by bursts with increased duration and intensity. Hardly any such signatures of aggregates were found, indicating that the aggregates found in the slots are artifacts due to the gel electrophoresis, or that these aggregates precipitated before the single-molecule experiments.

Mononucleosomes with linker DNA

Due to incomplete ligation of the DNA construct, a mixture of mononucleosomes with and without 300 bp linker DNA can be present in these samples. Figure 5.4 shows that indeed about half of the nucleosomes lacks the linker. The increase in the fraction of nucleosomes without FRET when 300 bp linker is added is therefore underestimated and the effect of linker DNA on DNA breathing may be larger than measured here.

Dinucleosomes

Unreconstituted DNA is present in the polyacrylamide gels of the dinucleosome reconstitutions in various amounts. For the dinucleosomes with the second nucleosome attached to the label side (DNI50 and DNI55), the amount of unreconstituted DNA is as high as ~40 %, while for the dinucleosomes with the second nucleosome attached to the side opposite of the labels (DNo20, DNo50 and DNo55), it is only ~10 %. The difference between these sets of constructs could be explained by the concentration difference of the nucleosomes loaded into the gel. Comparison with the no-FRET fraction from single-molecule experiments shows that the real fraction of unreconstituted DNA is at most 10 % for both sets of constructs, which is comparable to the amount of unreconstituted DNA in the elementary mononucleosome. Differences should therefore be attributed to (dynamic) changes in nucleosome conformation.

5.4.3 Linker DNA increases breathing in mononucleosomes

The presence of 300 bp linker DNA enhances unwrapping of nucleosomal DNA on both sides of the nucleosome. This could be explained by electrostatic repulsion between the entering and exiting DNA, increasing the unwrapping probability of the nucleosomal DNA. Addition of salt decreases this effect by screening of charges on the DNA. This salt effect was smaller but still measurable in the elementary mononucleosome with 39 and 12 bp of linker DNA.

The increase of FRET between 0 and 100 mM KAc is somewhat counterintuitive, regarding that high salt destabilizes nucleosomes: DNA and histone octamers completely dissociate from each other at 2 M [143, 144]. In a recent paper, Gansen et al. [63] investigated FRET in mononucleosomes over a wide range of nucleosome and salt concentrations. They observed an increase in FRET at moderate salt concentrations as well, but around 400-600 mM. They attribute this to the formation of an intermediate nucleosome conformation towards full dissociation, probably missing one or two dimers. The possibility to observe this intermediate depends on the label positions. With our choice of label positions, at the second bp from the nucleosome exit, dimer loss would result in a complete loss of FRET. We attribute the increase in FRET at 100 mM salt, which is dependent on the length of the linker DNA, to diminished electrostatic repulsion between the linker DNAs. The destabilizing effect of salt on DNA-histone interactions and the electrostatic screening of linker DNAs counteract each other. At modest salt concentrations, the diminished repulsion between linker DNAs apparently dominates over the decreased stability of DNA-histone contacts, resulting in a net increase of the high-FRET population.

5.4.4 Dinucleosomes

Increased unwrapping due to electrostatic repulsion of the linker DNAs is also observed for dinucleosomes with 50 bp linker DNA (DN_o50), where the no-FRET fraction is increased compared to mononucleosomes. Dinucleosomes separated by 55 bp linker DNA, however, have a ~10% larger no-FRET population than with 50 bp linker DNA. Apparently, the neighboring nucleosome increases the unwrapping probability. Interactions between linker DNAs would be the same for both 50 and 55 bp linker DNA. The observed difference in FRET distribution must therefore be attributed to a difference in nucleosome-nucleosome interactions.

Surprisingly, we observe no effect of magnesium in nucleosome-nucleosome interactions. Magnesium is required to induce compaction in nucleosomal arrays with 50 bp linker DNA in [23, 134]. In our dinucleosomes, we do not observe any change in DNA breathing after addition of magnesium, suggesting that the nucleosome is not constrained differently with or without Mg²⁺. Perhaps a dinucleosome is a too small

unit for mimicking chromatin fiber folding. Magnesium could for example help to bring non-neighboring nucleosomes together, stabilizing two gyres of the 'super helix' in the fiber.

To rationalize the FRET distribution of dinucleosomes with 55 bp linker DNA at the side opposite of the fluorescent labels (DNo55), we need to consider several effects. First, electrostatic repulsion between the linker DNAs favors unwrapping, as for the 50 bp linker DNA construct (DNo50). Second, nucleosome-nucleosome interactions further enhance unwrapping at the side of the linker DNA, similar to the dinucleosomes with 55 bp linker DNA at the label side (DNI55). If such steric constraints are responsible for increased unwrapping, unwrapping at the side of the linker DNA would be anti-correlated to unwrapping at the opposite side, which is observed as a smaller no-FRET population for dinucleosomes with 55 bp rather than 50 bp of linker DNA. Third, if nucleosome-nucleosome interactions occur, the electrostatic interactions between the entering and exiting DNA change due to an altered linker DNA trajectory. The interplay between these effects determines the distribution of FRET efficiencies.

An increase in nucleosomes with intermediate FRET was observed for the dinucleosomes with 55 bp linker DNA attached to the side opposite of the fluorescent labels (DNo55). An intermediate FRET efficiency can result from the average of two conformations when the concentration of labeled nucleosomes in the sample is too high, such that multiple nucleosomes are in the excitation focus at the same time (see [63]). Here, the concentration of labeled nucleosomes is low enough to measure the FRET efficiency in each individual nucleosome separately, as verified by the number of bursts per second. Thus, there must be a fraction of nucleosomes that have a conformation in between open and fully wrapped.

Linker DNA of 20 bp is too short to allow neighboring nucleosomes to interact in a face-to-face manner. The linker DNA and the two nucleosomes are however so close that they are able to interact directly, for example via electrostatic interactions between the DNA and the histone tails. The FRET distribution for dinucleosomes with 20 bp linker DNA (DNo20) is indeed slightly altered compared to mononucleosomes. A small increase in the population with intermediate FRET efficiencies points to a partly unwrapped configuration that is favored, possibly due to interactions between the linker DNA and the neighboring nucleosome.

To probe nucleosome-nucleosome interactions and their dynamics directly, it will be worthwhile to investigate dinucleosomes with various linker lengths, where one FRET label is located at each of the two nucleosomes at well-chosen positions. High FRET will then correspond to nucleosome-nucleosome interactions. However, this requires detailed insight into the structure of dinucleosomes, as the small Förster radius imposes strict constraints on the positions of the pair of labels. Only for 20 bp linker DNA has it been possible to do this [54] with the help of the crystal structure [131].

Such higher order folding remains enigmatic for larger linker lengths.

5.5 Conclusions

We performed spFRET experiments on DNA breathing in nucleosomes flanked by linker DNA and/or a neighboring nucleosome. We observed that the presence of linker DNA and a neighboring nucleosome both influence breathing of nucleosomal DNA. Electrostatic repulsion between the entering and exiting DNA favors unwrapping. An increase of the salt concentration reduces the unwrapping probability by screening electrostatic interactions between the linker DNAs.

Like in previous studies, we observed that interactions between neighboring nucleosomes depend on linker length. Here we showed that not only the linker length but also the phasing relative to the pitch of the DNA affects the interaction between neighboring nucleosomes. A linker length of 50 bp does not seem to favor nucleosome-nucleosome interactions, whereas an increase in linker length with only 5 bp to 55 bp results in increased unwrapping of nucleosomal DNA, probably due to nucleosome-nucleosome interactions in such a dinucleosome.

The conformation and dynamics of nucleosomal DNA has important implications for the structure and dynamics of chromatin fibers. On one hand, the accessibility of nucleosomal DNA, which has mainly been investigated in isolated nucleosomes before, depends strongly on chromatin structure. On the other hand, DNA linker length modulates chromatin structure by allowing interactions between direct neighbors only for specific linker lengths. In this study we contributed to the understanding of these phenomena by carefully monitoring the effects that addition of linker DNA and nucleosome neighbors have on DNA breathing.

Acknowledgements

We thank Guilherme Santos and Prof. Dr. Daniela Rhodes from the MRC Laboratory of Molecular Biology, Cambridge, UK, for providing the chicken erythrocyte histone octamers and Ineke de Boer-Tuyn for technical support.

This work is part of the research program of the Foundation for Fundamental Research on Matter (FOM), which is part of the Netherlands Organization for Scientific Research (NWO).

Supplementary material

The elementary mononucleosome DNA construct was PCR amplified with fluorescently labeled primers (5'→3'):

AGTTCATCCCTTAACCGAGAGACCCTATACGCGGCCGCCCT(Cy3B)GGAGAATCCCGGTGCCGAGGCCGCTCAATTGGTCGTAGA and

TTC AATCCCAGCACAGGATGTATATATCTGACACGTGCCTGGAGACTAGGGAGTAATCCCCTTGCCGGTTAAAACGC(ATTO647N)GGGGGACA,

with non-palindromic restriction sites (underlined) BsaI (NNNNNGAGACC) and BseYI (CCAGC), respectively. Modified bases are indicated in bold.

The 300 bp linker DNA segments and unlabeled nucleosome segments were PCR amplified with primers (5'→3'):

MNI300: A(biotin)CGCTCAGTGAACGAAAAC and
GATAAATCTGGAGCCGGTGA

MNo300: CTCCAAGCTGGGCTGTGT and
A(biotin)AACCACCGCTACCAGCG

DNI50: CTGGAGAATCCCGGTGCCGAGGCCGCT and
TATCCGGTCTCCCGGTGCAAGGTCGCTGTTC

DNI55: CTGGAGAATCCCGGTGCCGAGGCCGCT and
AACACGGTCTCACGGTCACCGGCAAGGTCG

DNo20: TGTGATGCTGGGTATACGCGG and
ACAGGATGTATATATCTGACACGTG

DNo50: CATGATGCTGGGCACCGAGTT and
ACAGGATGTATATATCTGACACGTG

DNo55: GAAAGCGCTGGGCTTCACACC and
ACAGGATGTATATATCTGACACGTG

Template for all PCR reactions was the pgem3z plasmid containing a single 601 element [33]. All segments were digested with BsaI (MNI and DNI) or BseYI (MNo and DNo). The elementary nucleosome was digested with either BsaI or BseYI and ligated to one of the segments in the list above to form the corresponding construct.

References

- [1] H. Schiessel, "The physics of chromatin," *Journal of Physics: Condensed Matter*, vol. 15, pp. R699–R774, May 2003.
- [2] W. Flemming, *Zellsubstanz, Kern und Zelltheilung*. F.C.W. Vogel, 1882.
- [3] D. E. Olins and A. L. Olins, "Chromatin history: our view from the bridge," *Nature Reviews Molecular Cell Biology*, vol. 4, no. 10, pp. 809–814, 2003.
- [4] A. L. Olins and D. E. Olins, "Spheroid chromatin units (nu bodies)," *Science*, vol. 183, no. 4122, pp. 330–332, 1974.
- [5] C. L. Woodcock, J. Safer, and J. Stanchfield, "Structural repeating units in chromatin. Evidence for their general occurrence," *Experimental Cell Research*, vol. 97, no. 1, pp. 101–110, 1976.
- [6] T. J. Richmond, J. Finch, B. Rushton, D. Rhodes, and A. Klug, "Structure of the nucleosome core particle at 7 Å resolution," *Nature*, vol. 311, no. 5986, pp. 532–537, 1984.
- [7] K. Luger, A. W. Mäder, R. K. Richmond, D. F. Sargent, and T. J. Richmond, "Crystal structure of the nucleosome core particle at 2.8 Å resolution," *Nature*, vol. 389, no. 6648, pp. 251–260, 1997.
- [8] D. Lleres, J. James, S. Swift, D. G. Norman, and A. I. Lamond, "Quantitative analysis of chromatin compaction in living cells using FLIM-FRET," *Journal Of Cell Biology*, vol. 187, no. 4, pp. 481–496, 2009.
- [9] A. L. Olins, "Nu-bodies are close-packed in chromatin," *Cold Spring Harbor Symposium on Quantitative Biology XLII*, pp. 325–329, 1978.
- [10] D. E. Olins and A. L. Olins, "Nucleosomes: The structural quantum in chromosomes," *American Scientist*, vol. 66, no. 6, pp. 704–711, 1978.
- [11] A. L. Olins, J. P. Breillatt, R. D. Carlson, M. B. Senior, E. B. Wright, and D. E. Olins, "On nu models for chromatin structure," in *The Molecular Biology of the Mammalian Genetic Apparatus, Part A* (P. O. P. Tso, ed.), pp. 211–237, Elsevier/North Holland Biomedical Press, 1977.
- [12] C. A. Davey, D. F. Sargent, K. Luger, A. W. Maeder, and T. J. Richmond, "Solvent mediated interactions in the structure of the nucleosome core particle at 1.9 Å resolution," *Journal Of Molecular Biology*, vol. 319, no. 5, pp. 1097–1113, 2002.
- [13] K. Luger and T. J. Richmond, "DNA binding within the nucleosome core," *Current opinion in structural biology*, vol. 8, no. 1, pp. 33–40, 1998.
- [14] H. Schiessel, "The nucleosome: a transparent, slippery, sticky and yet stable DNA-protein complex," *The European physical journal E, Soft matter*, vol. 19, no. 3, pp. 251–262, 2006.
- [15] P. Prinsen and H. Schiessel, "Nucleosome stability and accessibility of its DNA to proteins," *Biochimie*, vol. 92, no. 12, pp. 1722–1728, 2010.

References

- [16] K. Luger, "Dynamic nucleosomes," *Chromosome Research*, vol. 14, no. 1, pp. 5–16, 2006.
- [17] A. Flaus and T. Owen-Hughes, "Mechanisms for nucleosome mobilization," *Biopolymers*, vol. 68, no. 4, pp. 563–578, 2003.
- [18] T. Fletcher and J. Hansen, "Core histone tail domains mediate oligonucleosome folding and nucleosomal DNA organization through distinct molecular mechanisms," *The Journal of biological chemistry*, vol. 270, no. 43, pp. 25359–25362, 1995.
- [19] W. Krajewski and J. Ausio, "Modulation of the higher-order folding of chromatin by deletion of histone H3 and H4 terminal domains," *Biochemical Journal*, vol. 316, pp. 395–400, 1996.
- [20] V. Allfrey, R. Faulkner, and A. Mirsky, "Acetylation and methylation of histones and their possible role in regulation of RNA synthesis," *Proceedings Of The National Academy Of Sciences Of The United States Of America*, vol. 51, no. 5, pp. 786–794, 1964.
- [21] M. S. Cosgrove, "Histone proteomics and the epigenetic regulation of nucleosome mobility.," *Expert review of proteomics*, vol. 4, no. 4, pp. 465–478, 2007.
- [22] M. Shogren-Knaak, H. Ishii, J. Sun, M. Pazin, J. Davie, and C. Peterson, "Histone H4-K16 acetylation controls chromatin structure and protein interactions," *Science*, vol. 311, no. 5762, pp. 844–847, 2006.
- [23] P. J. J. Robinson, W. An, A. Routh, F. Martino, L. Chapman, R. G. Roeder, and D. Rhodes, "30 nm chromatin fibre decompaction requires both H4-K16 acetylation and linker histone eviction.," *Journal Of Molecular Biology*, vol. 381, no. 4, pp. 816–825, 2008.
- [24] T. Jenuwein and C. Allis, "Translating the histone code," *Science*, vol. 293, no. 5532, pp. 1074–1080, 2001.
- [25] K. Polach and J. Widom, "Mechanism of Protein Access to Specific DNA Sequences in Chromatin: A Dynamic Equilibrium Model for Gene Regulation," *Journal Of Molecular Biology*, vol. 254, no. 2, pp. 130–149, 1995.
- [26] F.-T. Chien and J. van Noort, "10 Years of Tension on Chromatin: Results from Single Molecule Force Spectroscopy," *Current Pharmaceutical Biotechnology*, vol. 10, no. 5, pp. 474–485, 2009.
- [27] L. Stryer and R. Haugland, "Energy transfer - a spectroscopic ruler," *Proceedings Of The National Academy Of Sciences Of The United States Of America*, vol. 58, no. 2, pp. 719–726, 1967.
- [28] R. M. Clegg, "Fluorescence resonance energy transfer and nucleic acids," *Methods in enzymology*, vol. 211, pp. 353–388, 1992.
- [29] T. Ha, "Single-molecule fluorescence resonance energy transfer," *Methods (San Diego, Calif)*, vol. 25, no. 1, pp. 78–86, 2001.
- [30] R. Roy, S. Hohng, and T. Ha, "A practical guide to single-molecule FRET," *Nature Methods*, vol. 5, no. 6, pp. 507–516, 2008.
- [31] N. K. Lee, A. N. Kapanidis, Y. Wang, X. Michalet, J. Mukhopadhyay, R. H. Ebright, and S. Weiss, "Accurate FRET measurements within single diffusing biomolecules using alternating-laser excitation.," *Biophysical Journal*, vol. 88, no. 4, pp. 2939–2953, 2005.
- [32] A. Gansen, K. Tóth, N. Schwarz, and J. Langowski, "Structural variability of nucleosomes detected by single-pair Förster resonance energy transfer: histone acetylation, sequence variation, and salt effects.," *The Journal of Physical Chemistry B*, vol. 113, no. 9, pp. 2604–2613, 2009.
- [33] P. T. Lowary and J. Widom, "New DNA sequence rules for high affinity binding to histone octamer and sequence-directed nucleosome positioning," *Journal Of Molecular Biology*, vol. 276, no. 1, pp. 19–42, 1998.
- [34] W. J. A. Koopmans, R. Buning, and J. van Noort, "Engineering mononucleosomes for single-pair FRET experiments.," in *Methods in Molecular Biology: Protocols in DNA Nanotechnology* (G. Zuccheri and B. Samori, eds.), pp. 291–303, Humana Press, 2011.

- [35] G. Li and J. Widom, "Nucleosomes facilitate their own invasion," *Nature Structural & Molecular Biology*, vol. 11, no. 8, pp. 763–769, 2004.
- [36] G. Li, M. Levitus, C. Bustamante, and J. Widom, "Rapid spontaneous accessibility of nucleosomal DNA.," *Nature Structural & Molecular Biology*, vol. 12, no. 1, pp. 46–53, 2005.
- [37] A. Gansen, F. Hauger, K. Tóth, and J. Langowski, "Single-pair fluorescence resonance energy transfer of nucleosomes in free diffusion: optimizing stability and resolution of subpopulations," *Analytical biochemistry*, vol. 368, no. 2, pp. 193–204, 2007.
- [38] A. Gansen, A. Valeri, F. Hauger, S. Felekyan, S. Kalinin, K. Tóth, J. Langowski, and C. A. M. Seidel, "Nucleosome disassembly intermediates characterized by single-molecule FRET," *Proceedings Of The National Academy Of Sciences Of The United States Of America*, vol. 106, no. 36, pp. 15308–15313, 2009.
- [39] M. Tomschik, H. Zheng, K. van Holde, J. Zlatanova, and S. H. Leuba, "Fast, long-range, reversible conformational fluctuations in nucleosomes revealed by single-pair fluorescence resonance energy transfer," *Proceedings Of The National Academy Of Sciences Of The United States Of America*, vol. 102, no. 9, pp. 3278–3283, 2005.
- [40] W. J. A. Koopmans, A. Brehm, C. Logie, T. Schmidt, and J. van Noort, "Single-pair FRET microscopy reveals mononucleosome dynamics," *Journal of Fluorescence*, vol. 17, no. 6, pp. 785–795, 2007.
- [41] W. J. A. Koopmans, T. Schmidt, and J. van Noort, "Nucleosome Immobilization Strategies for Single-Pair FRET Microscopy," *Chemphyschem: a European journal of chemical physics and physical chemistry*, vol. 9, no. 14, pp. 2002–2009, 2008.
- [42] W. J. A. Koopmans, R. Buning, T. Schmidt, and J. van Noort, "spFRET using alternating excitation and FCS reveals progressive DNA unwrapping in nucleosomes," *Biophysical Journal*, vol. 97, no. 1, pp. 195–204, 2009.
- [43] A. N. Kapanidis, N. K. Lee, T. A. Laurence, S. Doose, E. Margeat, and S. Weiss, "Fluorescence-aided molecule sorting: analysis of structure and interactions by alternating-laser excitation of single molecules.," *Proceedings Of The National Academy Of Sciences Of The United States Of America*, vol. 101, no. 24, pp. 8936–8941, 2004.
- [44] J. Widengren, V. Kudryavtsev, M. Antonik, S. Berger, M. Gerken, and C. A. M. Seidel, "Single-molecule detection and identification of multiple species by multiparameter fluorescence detection," *Analytical Chemistry*, vol. 78, no. 6, pp. 2039–2050, 2006.
- [45] T. Torres and M. Levitus, "Measuring conformational dynamics: a new FCS-FRET approach.," *The Journal of Physical Chemistry B*, vol. 111, no. 25, pp. 7392–7400, 2007.
- [46] M. Tomschik, K. van Holde, and J. Zlatanova, "Nucleosome dynamics as studied by single-pair fluorescence resonance energy transfer: a reevaluation," *Journal of Fluorescence*, vol. 19, no. 1, pp. 53–62, 2009.
- [47] I. Rasnik, S. A. McKinney, and T. Ha, "Nonblinking and long-lasting single-molecule fluorescence imaging," *Nature Methods*, vol. 3, no. 11, pp. 891–893, 2006.
- [48] L. Kelbauskas, N. Chan, R. Bash, P. DeBartolo, J. Sun, N. Woodbury, and D. Lohr, "Sequence-dependent variations associated with H(2)A/H2B depletion of nucleosomes," *Biophysical Journal*, vol. 94, no. 1, pp. 147–158, 2008.
- [49] L. Kelbauskas, N. Woodbury, and D. Lohr, "DNA sequence-dependent variation in nucleosome structure, stability, and dynamics detected by a FRET-based analysis," *Biochemistry And Cell Biology-Biochimie Et Biologie Cellulaire*, vol. 87, no. 1, pp. 323–335, 2009.
- [50] H. Neumann, S. M. Hancock, R. Buning, A. Routh, L. Chapman, J. Somers, T. Owen-Hughes, J. van Noort, D. Rhodes, and J. W. Chin, "A method for genetically installing site-specific acetylation in recombinant histones defines the effects of H3 K56 acetylation," *Molecular Cell*, vol. 36, no. 1, pp. 153–163, 2009.

- [51] T. R. Blosser, J. G. Yang, M. D. Stone, G. J. Narlikar, and X. Zhuang, "Dynamics of nucleosome remodeling by individual ACF complexes.," *Nature*, vol. 462, no. 7276, pp. 1022–1027, 2009.
- [52] J. G. Yang and G. J. Narlikar, "FRET-based methods to study ATP-dependent changes in chromatin structure.," *Methods (San Diego, Calif)*, vol. 41, no. 3, pp. 291–295, 2007.
- [53] M. G. Poirier, M. Bussiek, J. Langowski, and J. Widom, "Spontaneous access to DNA target sites in folded chromatin fibers.," *Journal Of Molecular Biology*, vol. 379, no. 4, pp. 772–786, 2008.
- [54] M. G. Poirier, E. Oh, H. S. Tims, and J. Widom, "Dynamics and function of compact nucleosome arrays.," *Nature Structural & Molecular Biology*, vol. 16, no. 9, pp. 938–944, 2009.
- [55] A. Thåström, J. M. Gottesfeld, K. Luger, and J. Widom, "Histone-DNA binding free energy cannot be measured in dilution-driven dissociation experiments," *Biochemistry*, vol. 43, no. 3, pp. 736–741, 2004.
- [56] C. Claudet, D. Angelov, P. Bouvet, S. Dimitrov, and J. Bednar, "Histone octamer instability under single molecule experiment conditions," *The Journal of biological chemistry*, vol. 280, no. 20, pp. 19958–19965, 2005.
- [57] B. Treutlein, J. Exler, G. Ängst, and J. Michaelis, "Single-pair Fluorescence Resonance Energy Transfer study of mononucleosomes dynamics," in *Biophysical Journal*, p. 292, 2009.
- [58] H. S. Tims, K. Gurunathan, M. Levitus, and J. Widom, "Dynamics of nucleosome invasion by DNA binding proteins.," *Journal Of Molecular Biology*, vol. 411, no. 2, pp. 430–448, 2011.
- [59] V. Böhm, A. R. Hieb, A. J. Andrews, A. Gansen, A. Rocker, K. Tóth, K. Luger, and J. Langowski, "Nucleosome accessibility governed by the dimer/tetramer interface.," *Nucleic Acids Research*, vol. 39, no. 8, pp. 3093–3102, 2011.
- [60] P. Becker, "Chromatin Protocols," pp. 1–17, 2003.
- [61] I. Duband-Goulet, K. Ouararhni, and A. Hamiche, "Methods for chromatin assembly and remodeling," *Methods (San Diego, Calif)*, vol. 33, no. 1, pp. 12–17, 2004.
- [62] Y. Santoso and A. N. Kapanidis, "Probing biomolecular structures and dynamics of single molecules using in-gel alternating-laser excitation.," *Analytical Chemistry*, vol. 81, no. 23, pp. 9561–9570, 2009.
- [63] A. Gansen, A. R. Hieb, V. Böhm, K. Tóth, and J. Langowski, "Closing the Gap between Single Molecule and Bulk FRET Analysis of Nucleosomes," *Plos One*, vol. 8, no. 4, p. e57018, 2013.
- [64] E. V. Amirgoulova, J. Groll, C. D. Heyes, T. Ameringer, C. Röcker, M. Möller, and G. U. Nienhaus, "Biofunctionalized polymer surfaces exhibiting minimal interaction towards immobilized proteins.," *Chemphyschem: a European journal of chemical physics and physical chemistry*, vol. 5, no. 4, pp. 552–555, 2004.
- [65] J. Groll, T. Ameringer, J. P. Spatz, and M. Moeller, "Ultrathin coatings from isocyanate-terminated star PEG prepolymers: layer formation and characterization.," *Langmuir : the ACS journal of surfaces and colloids*, vol. 21, no. 5, pp. 1991–1999, 2005.
- [66] C. Eggeling, S. Berger, L. Brand, J. Fries, J. Schaffer, A. Volkmer, and C. A. M. Seidel, "Data registration and selective single-molecule analysis using multi-parameter fluorescence detection," *Journal of Biotechnology*, vol. 86, no. 3, pp. 163–180, 2001.
- [67] A. Hoffmann, D. Nettels, J. Clark, A. Borgia, S. E. Radford, J. Clarke, and B. Schuler, "Quantifying heterogeneity and conformational dynamics from single molecule FRET of diffusing molecules: recurrence analysis of single particles (RASP)," *Physical Chemistry Chemical Physics*, vol. 13, no. 5, p. 1857, 2011.
- [68] T. E. Tomov, R. Tsukanov, R. Masoud, M. Liber, N. Plavner, and E. Nir, "Disentangling Subpopulations in Single-Molecule FRET and ALEX Experiments with Photon Distribution Analysis," *Biophysical Journal*, vol. 102, no. 5, pp. 1163–1173, 2012.

- [69] M. Dahan, A. A. Deniz, T. Ha, D. S. Chemla, P. G. Schultz, and S. Weiss, "Ratiometric measurement and identification of single diffusing molecules," *Chemical Physics*, vol. 247, no. 1, pp. 85–106, 1999.
- [70] A. A. Deniz, M. Dahan, J. R. Grunwell, T. Ha, A. E. Faulhaber, D. S. Chemla, S. Weiss, and P. G. Schultz, "Single-pair fluorescence resonance energy transfer on freely diffusing molecules: observation of Förster distance dependence and subpopulations," *Proceedings Of The National Academy Of Sciences Of The United States Of America*, vol. 96, no. 7, pp. 3670–3675, 1999.
- [71] M. Grunstein, "Histone acetylation in chromatin structure and transcription.," *Nature*, vol. 389, no. 6649, pp. 349–352, 1997.
- [72] T. Kouzarides, "Chromatin modifications and their function.," *Cell*, vol. 128, no. 4, pp. 693–705, 2007.
- [73] C. L. Peterson and M.-A. Laniel, "Histones and histone modifications.," *Current biology : CB*, vol. 14, no. 14, pp. R546–51, 2004.
- [74] M. D. Shahbazian and M. Grunstein, "Functions of site-specific histone acetylation and deacetylation.," *Annual Review Of Biochemistry*, vol. 76, pp. 75–100, 2007.
- [75] D. E. Sterner and S. L. Berger, "Acetylation of histones and transcription-related factors.," *Microbiology and molecular biology reviews : MMBR*, vol. 64, no. 2, pp. 435–459, 2000.
- [76] X.-J. Yang, "Lysine acetylation and the bromodomain: a new partnership for signaling.," *BioEssays : news and reviews in molecular, cellular and developmental biology*, vol. 26, no. 10, pp. 1076–1087, 2004.
- [77] Q. Li, H. Zhou, H. Wurtele, B. Davies, B. Horazdovsky, A. Verreault, and Z. Zhang, "Acetylation of histone H3 lysine 56 regulates replication-coupled nucleosome assembly.," *Cell*, vol. 134, no. 2, pp. 244–255, 2008.
- [78] M. S. Cosgrove, J. D. Boeke, and C. Wolberger, "Regulated nucleosome mobility and the histone code.," *Nature Structural & Molecular Biology*, vol. 11, no. 11, pp. 1037–1043, 2004.
- [79] H. Masumoto, D. Hawke, R. Kobayashi, and A. Verreault, "A role for cell-cycle-regulated histone H3 lysine 56 acetylation in the DNA damage response.," *Nature*, vol. 436, no. 7048, pp. 294–298, 2005.
- [80] A. Ozdemir, S. Spicuglia, E. Lasonder, M. Vermeulen, C. Campsteijn, H. G. Stunnenberg, and C. Logie, "Characterization of lysine 56 of histone H3 as an acetylation site in *Saccharomyces cerevisiae*.," *The Journal of biological chemistry*, vol. 280, no. 28, pp. 25949–25952, 2005.
- [81] F. Xu, K. Zhang, and M. Grunstein, "Acetylation in histone H3 globular domain regulates gene expression in yeast.," *Cell*, vol. 121, no. 3, pp. 375–385, 2005.
- [82] B. A. Garcia, S. B. Hake, R. L. Diaz, M. Kauer, S. A. Morris, J. Recht, J. Shabanowitz, N. Mishra, B. D. Strahl, C. D. Allis, and D. F. Hunt, "Organismal differences in post-translational modifications in histones H3 and H4.," *The Journal of biological chemistry*, vol. 282, no. 10, pp. 7641–7655, 2007.
- [83] I. Celic, H. Masumoto, W. P. Griffith, P. Meluh, R. J. Cotter, J. D. Boeke, and A. Verreault, "The sirtuins hst3 and Hst4p preserve genome integrity by controlling histone h3 lysine 56 deacetylation.," *Current biology : CB*, vol. 16, no. 13, pp. 1280–1289, 2006.
- [84] I. Celic, A. Verreault, and J. D. Boeke, "Histone H3 K56 hyperacetylation perturbs replisomes and causes DNA damage.," *Genetics*, vol. 179, no. 4, pp. 1769–1784, 2008.
- [85] C.-C. Chen, J. J. Carson, J. Feser, B. Tamburini, S. Zabarone, J. Linger, and J. K. Tyler, "Acetylated lysine 56 on histone H3 drives chromatin assembly after repair and signals for the completion of repair.," *Cell*, vol. 134, no. 2, pp. 231–243, 2008.
- [86] C. Das, M. S. Lucia, K. C. Hansen, and J. K. Tyler, "CBP/p300-mediated acetylation of histone H3 on lysine 56," *Nature*, vol. 459, no. 7243, pp. 113–117, 2009.

References

- [87] R. Driscoll, A. Hudson, and S. P. Jackson, "Yeast Rtt109 promotes genome stability by acetylating histone H3 on lysine 56.," *Science*, vol. 315, no. 5812, pp. 649–652, 2007.
- [88] J. Han, H. Zhou, B. Horazdovsky, K. Zhang, R.-M. Xu, and Z. Zhang, "Rtt109 acetylates histone H3 lysine 56 and functions in DNA replication.," *Science*, vol. 315, no. 5812, pp. 653–655, 2007.
- [89] E. M. Hyland, M. S. Cosgrove, H. Molina, D. Wang, A. Pandey, R. J. Cottee, and J. D. Boeke, "Insights into the role of histone H3 and histone H4 core modifiable residues in *Saccharomyces cerevisiae*.," *Molecular and cellular biology*, vol. 25, no. 22, pp. 10060–10070, 2005.
- [90] A. Rufiange, P.-E. Jacques, W. Bhat, F. Robert, and A. Nourani, "Genome-wide replication-independent histone H3 exchange occurs predominantly at promoters and implicates H3 K56 acetylation and Asf1.," *Molecular Cell*, vol. 27, no. 3, pp. 393–405, 2007.
- [91] S. K. Williams, D. Truong, and J. K. Tyler, "Acetylation in the globular core of histone H3 on lysine-56 promotes chromatin disassembly during transcriptional activation.," *Proceedings of the National Academy of Sciences*, vol. 105, no. 26, pp. 9000–9005, 2008.
- [92] W. Xie, C. Song, N. L. Young, A. S. Sperling, F. Xu, R. Sridharan, A. E. Conway, B. A. Garcia, K. Plath, A. T. Clark, and M. Grunstein, "Histone h3 lysine 56 acetylation is linked to the core transcriptional network in human embryonic stem cells.," *Molecular Cell*, vol. 33, no. 4, pp. 417–427, 2009.
- [93] F. Xu, Q. Zhang, K. Zhang, W. Xie, and M. Grunstein, "Sir2 deacetylates histone H3 lysine 56 to regulate telomeric heterochromatin structure in yeast.," *Molecular Cell*, vol. 27, no. 6, pp. 890–900, 2007.
- [94] B. Yang, A. Miller, and A. L. Kirchmaier, "HST3/HST4-dependent deacetylation of lysine 56 of histone H3 in silent chromatin.," *Molecular biology of the cell*, vol. 19, no. 11, pp. 4993–5005, 2008.
- [95] R. K. McGinty, J. Kim, C. Chatterjee, R. G. Roeder, and T. W. Muir, "Chemically ubiquitylated histone H2B stimulates hDot1L-mediated intranucleosomal methylation.," *Nature*, vol. 453, no. 7196, pp. 812–816, 2008.
- [96] H. Neumann, S. Y. Peak-Chew, and J. W. Chin, "Genetically encoding N^ε-acetyllysine in recombinant proteins.," *Nature chemical biology*, vol. 4, no. 4, pp. 232–234, 2008.
- [97] K. Luger, T. J. Rechsteiner, and T. J. Richmond, "Preparation of nucleosome core particle from recombinant histones.," *Methods in enzymology*, vol. 304, pp. 3–19, 1999.
- [98] V. A. T. Huynh, P. J. J. Robinson, and D. Rhodes, "A method for the in vitro reconstitution of a defined "30 nm" chromatin fibre containing stoichiometric amounts of the linker histone.," *Journal Of Molecular Biology*, vol. 345, no. 5, pp. 957–968, 2005.
- [99] A. Routh, S. Sandin, and D. Rhodes, "Nucleosome repeat length and linker histone stoichiometry determine chromatin fiber structure," *Proceedings Of The National Academy Of Sciences Of The United States Of America*, vol. 105, no. 26, pp. 8872–8877, 2008.
- [100] J. Somers and T. Owen-Hughes, "Mutations to the histone H3 alpha N region selectively alter the outcome of ATP-dependent nucleosome-remodelling reactions.," *Nucleic Acids Research*, vol. 37, no. 8, pp. 2504–2513, 2009.
- [101] R. Bash, H. Wang, C. Anderson, J. Yodh, G. Hager, S. M. Lindsay, and D. Lohr, "AFM imaging of protein movements: histone H2A-H2B release during nucleosome remodeling.," *FEBS letters*, vol. 580, no. 19, pp. 4757–4761, 2006.
- [102] M. Bruno, A. Flaus, C. Stockdale, C. Rencurel, H. Ferreira, and T. Owen-Hughes, "Histone H2A/H2B dimer exchange by ATP-dependent chromatin remodeling activities.," *Molecular Cell*, vol. 12, no. 6, pp. 1599–1606, 2003.
- [103] A. J. Ruthenburg, H. Li, D. J. Patel, and C. D. Allis, "Multivalent engagement of chromatin modifications by linked binding modules.," *Nature Reviews Molecular Cell Biology*, vol. 8, no. 12, pp. 983–994, 2007.

- [104] S. D. Taverna, H. Li, A. J. Ruthenburg, C. D. Allis, and D. J. Patel, "How chromatin-binding modules interpret histone modifications: lessons from professional pocket pickers," *Nature Structural & Molecular Biology*, vol. 14, no. 11, pp. 1025–1040, 2007.
- [105] A. J. Bannister, P. Zegerman, J. F. Partridge, E. A. Miska, J. O. Thomas, R. C. Allshire, and T. Kouzarides, "Selective recognition of methylated lysine 9 on histone H3 by the HP1 chromo domain.," *Nature*, vol. 410, no. 6824, pp. 120–124, 2001.
- [106] C. Dhalluin, J. E. Carlson, L. Zeng, C. He, A. K. Aggarwal, and M. M. Zhou, "Structure and ligand of a histone acetyltransferase bromodomain.," *Nature*, vol. 399, no. 6735, pp. 491–496, 1999.
- [107] R. H. Jacobson, A. G. Ladurner, D. S. King, and R. Tjian, "Structure and function of a human TAFII250 double bromodomain module.," *Science*, vol. 288, no. 5470, pp. 1422–1425, 2000.
- [108] M. Kasten, H. Szerlong, H. Erdjument-Bromage, P. Tempst, M. Werner, and B. R. Cairns, "Tandem bromodomains in the chromatin remodeler RSC recognize acetylated histone H3 Lys14.," *The EMBO journal*, vol. 23, no. 6, pp. 1348–1359, 2004.
- [109] M. Lachner, D. O'Carroll, S. Rea, K. Mechtler, and T. Jenuwein, "Methylation of histone H3 lysine 9 creates a binding site for HP1 proteins.," *Nature*, vol. 410, no. 6824, pp. 116–120, 2001.
- [110] H. Li, S. Ilin, W. Wang, E. M. Duncan, J. Wysocka, C. D. Allis, and D. J. Patel, "Molecular basis for site-specific read-out of histone H3K4me3 by the BPTF PHD finger of NURF," *Nature*, vol. 442, no. 7098, pp. 91–95, 2006.
- [111] J. Wysocka, T. Swigut, H. Xiao, T. A. Milne, S. Y. Kwon, J. Landry, M. Kauer, A. J. Tackett, B. T. Chait, P. Badenhorst, C. Wu, and C. D. Allis, "A PHD finger of NURF couples histone H3 lysine 4 trimethylation with chromatin remodelling.," *Nature*, vol. 442, no. 7098, pp. 86–90, 2006.
- [112] K. Wang, H. Neumann, S. Y. Peak-Chew, and J. W. Chin, "Evolved orthogonal ribosomes enhance the efficiency of synthetic genetic code expansion.," *Nature Biotechnology*, vol. 25, no. 7, pp. 770–777, 2007.
- [113] P. E. Dawson, T. W. Muir, I. Clark-Lewis, and S. B. Kent, "Synthesis of proteins by native chemical ligation.," *Science*, vol. 266, no. 5186, pp. 776–779, 1994.
- [114] H. Ferreira, A. Flaus, and T. Owen-Hughes, "Histone modifications influence the action of Snf2 family remodelling enzymes by different mechanisms.," *Journal Of Molecular Biology*, vol. 374, no. 3, pp. 563–579, 2007.
- [115] M. D. Simon, F. Chu, L. R. Racki, C. C. de la Cruz, A. L. Burlingame, B. Panning, G. J. Narlikar, and K. M. Shokat, "The site-specific installation of methyl-lysine analogs into recombinant histones.," *Cell*, vol. 128, no. 5, pp. 1003–1012, 2007.
- [116] S. D. Taverna, B. M. Ueberheide, Y. Liu, A. J. Tackett, R. L. Diaz, J. Shabanowitz, B. T. Chait, D. F. Hunt, and C. D. Allis, "Long-distance combinatorial linkage between methylation and acetylation on histone H3 N termini.," *Proceedings Of The National Academy Of Sciences Of The United States Of America*, vol. 104, no. 7, pp. 2086–2091, 2007.
- [117] J. Zlatanova and A. Thakar, "H2A.Z: View from the Top," *Structure*, vol. 16, no. 2, pp. 166–179, 2008.
- [118] A. A. Thambirajah, D. Dryhurst, T. Ishibashi, A. Li, A. H. Maffey, and J. Ausió, "H2A.Z stabilizes chromatin in a way that is dependent on core histone acetylation.," *The Journal of biological chemistry*, vol. 281, no. 29, pp. 20036–20044, 2006.
- [119] Y.-J. Park, P. N. Dyer, D. J. Tremethick, and K. Luger, "A new fluorescence resonance energy transfer approach demonstrates that the histone variant H2AZ stabilizes the histone octamer within the nucleosome," *The Journal of biological chemistry*, vol. 279, no. 23, pp. 24274–24282, 2004.
- [120] H. Zhang, D. N. Roberts, and B. R. Cairns, "Genome-wide dynamics of Htz1, a histone H2A variant that poises repressed/basal promoters for activation through histone loss.," *Cell*, vol. 123, no. 2, pp. 219–231, 2005.

References

- [121] D. W. Abbott, V. S. Ivanova, X. Wang, W. M. Bonner, and J. Ausio, "Characterization of the stability and folding of H2A.Z chromatin particles: implications for transcriptional activation.," *The Journal of biological chemistry*, vol. 276, no. 45, pp. 41945–41949, 2001.
- [122] R. K. Suto, M. J. Clarkson, D. J. Tremethick, and K. Luger, "Crystal structure of a nucleosome core particle containing the variant histone H2A.Z.," *Nature structural biology*, vol. 7, no. 12, pp. 1121–1124, 2000.
- [123] C. M. Weber, J. G. Henikoff, and S. Henikoff, "H2A.Z nucleosomes enriched over active genes are homotypic," *Nature Structural & Molecular Biology*, vol. 17, no. 12, pp. 1500–1507, 2010.
- [124] S. V. Kumar and P. A. Wigge, "H2A.Z-Containing Nucleosomes Mediate the Thermosensory Response in Arabidopsis," *Cell*, vol. 140, no. 1, pp. 136–147, 2010.
- [125] National Human Genome Research Institute - Histone Database. <http://research.nhgri.nih.gov/histones/index.cgi>, checked may 2014.
- [126] Protein Calculator v3.4. <http://protcalc.sourceforge.net/>, checked may 2014.
- [127] R. Buning and J. van Noort, "Single-pair FRET experiments on nucleosome conformational dynamics.," *Biochimie*, vol. 92, no. 12, pp. 1729–1740, 2010.
- [128] T. T. M. Ngo, R. Zhou, J. Yodh, and T. Ha, "Asymmetric Unwrapping of Nucleosome Revealed by Single Molecule Fluorescence-Force Spectroscopy," *Biophysical Journal*, vol. 104, no. S1, p. 210a, 2013.
- [129] A. Prunell and R. D. Kornberg, "Variable center to center distance of nucleosomes in chromatin," *Journal Of Molecular Biology*, vol. 154, no. 3, pp. 515–523, 1982.
- [130] P. J. J. Robinson, L. Fairall, V. Huynh, and D. Rhodes, "EM measurements define the dimensions of the "30-nm" chromatin fiber: Evidence for a compact, interdigitated structure," *Proceedings Of The National Academy Of Sciences Of The United States Of America*, vol. 103, no. 17, pp. 6506–6511, 2006.
- [131] T. Schalch, S. Duda, D. F. Sargent, and T. J. Richmond, "X-ray structure of a tetranucleosome and its implications for the chromatin fibre.," *Nature*, vol. 436, no. 7047, pp. 138–141, 2005.
- [132] F. Song, P. Chen, D. Sun, M. Wang, L. Dong, D. Liang, R.-M. Xu, P. Zhu, and G. Li, "Cryo-EM study of the chromatin fiber reveals a double helix twisted by tetranucleosomal units.," *Science*, vol. 344, no. 6182, pp. 376–380, 2014.
- [133] S. C. Howell, K. Andresen, I. Jimenez-Useche, C. Yuan, and X. Qiu, "Elucidating Internucleosome Interactions and the Roles of Histone Tails," *Biophysical Journal*, vol. 105, no. 1, pp. 194–199, 2013.
- [134] M. Kruithof, F.-T. Chien, A. Routh, C. Logie, D. Rhodes, and J. van Noort, "Single-molecule force spectroscopy reveals a highly compliant helical folding for the 30-nm chromatin fiber," *Nature Structural & Molecular Biology*, vol. 16, no. 5, pp. 534–540, 2009.
- [135] T. Ha, T. Enderle, D. F. Ogletree, D. S. Chemla, P. R. Selvin, and S. Weiss, "Probing the interaction between two single molecules: fluorescence resonance energy transfer between a single donor and a single acceptor," *Proceedings Of The National Academy Of Sciences Of The United States Of America*, vol. 93, no. 13, pp. 6264–6268, 1996.
- [136] J. Widom, "A relationship between the helical twist of DNA and the ordered positioning of nucleosomes in all eukaryotic cells.," *Proceedings of the National Academy of Sciences*, vol. 89, no. 3, pp. 1095–1099, 1992.
- [137] J.-P. Wang, Y. Fondufe-Mittendorf, L. Xi, G.-F. Tsai, E. Segal, and J. Widom, "Preferentially Quantized Linker DNA Lengths in *Saccharomyces cerevisiae*," *PLoS Computational Biology*, vol. 4, no. 9, p. e1000175, 2008.
- [138] K. Brogaard, L. Xi, J.-P. Wang, and J. Widom, "A map of nucleosome positions in yeast at base-pair resolution.," *Nature*, vol. 486, no. 7404, pp. 496–501, 2012.

- [139] G. Zheng, X.-J. Lu, and W. K. Olson, "Web 3DNA—a web server for the analysis, reconstruction, and visualization of three-dimensional nucleic-acid structures.," *Nucleic Acids Research*, vol. 37, no. Web Server issue, pp. W240–6, 2009.
- [140] K. Tóth, N. Brun, and J. Langowski, "Trajectory of nucleosomal linker DNA studied by fluorescence resonance energy transfer," *Biochemistry*, vol. 40, no. 23, pp. 6921–6928, 2001.
- [141] A. J. Andrews and K. Luger, "Nucleosome Structure(s) and Stability: Variations on a Theme," *Annual Review Of Biophysics, Vol 40*, vol. 40, pp. 99–117, 2011.
- [142] J. G. Yodh, Y. L. Lyubchenko, L. S. Shlyakhtenko, N. Woodbury, and D. Lohr, "Evidence for Nonrandom Behavior in 208-12 Subsaturated Nucleosomal Array Populations Analyzed by AFM," *Biochemistry*, vol. 38, no. 48, pp. 15756–15763, 1999.
- [143] T. H. Eickbush and E. N. Moudrianakis, "The histone core complex: an octamer assembled by two sets of protein-protein interactions.," *Biochemistry*, vol. 17, no. 23, pp. 4955–4964, 1978.
- [144] K. Rippe, J. Mazurkiewicz, and N. Kepper, "Interactions of Histones with DNA: Nucleosome Assembly, Stability, Dynamics, and Higher Order Structure," *DNA Interactions with Polymers and Surfactants*, p. 135, 2008.

Summary

In this thesis, I describe the results of single-pair Fluorescence Resonance Energy Transfer (spFRET) studies on the dynamics of individual nucleosomes, modulated by histone modifications, histone variants, and by neighboring nucleosomes.

At the basis of the regulation of the genetic code (DNA) in eukaryotes is its organization into nucleosomes: 10 nm wide structures, in which ~ 150 basepairs (bp) of DNA are wrapped around a disk of proteins, the histone octamer. Arrays of nucleosomes are organized in fiber-like structures called chromatin. Nucleosomes modulate DNA accessibility through conformational dynamics like DNA breathing - the transient unwrapping of DNA from the nucleosome -, repositioning of nucleosomes along the DNA, or partial dissociation. Thus, nucleosomes play a crucial role in regulating all processes involving DNA, including transcription, replication and repair. Single-molecule techniques, in particular single-pair Fluorescence Resonance Energy Transfer (spFRET), have the ability to resolve such conformational dynamics in individual nucleosomes and may help to understand these processes at a fundamental level.

Chapter 1 reviews the results of experiments that have used spFRET to elucidate single-nucleosome dynamics, including fluorescence correlation spectroscopy (FCS), confocal single-molecule microscopy on freely diffusing nucleosomes and widefield total internal reflection fluorescence (TIRF) microscopy on immobilized nucleosomes. The combined spFRET studies on single nucleosomes reveal a very dynamic organization of the nucleosome, that has been shown to be modulated by post-translational modifications of the histones and by DNA sequence.

Performing spFRET experiments on nucleosomes and interpreting their results is far from trivial. Nucleosomes are susceptible to dissociation when diluted to sub-nM concentrations - typical for single-molecule experiments - and in the presence of surfaces, depending on the specific histone composition and buffer conditions. Nucleosome instability during storage and sample preparation, sample heterogeneity, and simplifications in the analysis of single-molecule fluorescence data can introduce artifacts or obscure the underlying conformational behavior of nucleosomes. **Chapter 2** describes the challenges we encountered during the preparation of nucleosome sam-

ples, the detection of spFRET with confocal fluorescence spectroscopy and the analysis of FRET efficiencies, and how we have dealt with them.

Post-translational modifications to the histone proteins play an essential role in the regulation of various processes involving DNA. Lysine acetylation of histones, for example, defines the epigenetic status of human embryonic stem cells, and orchestrates DNA replication, chromosome condensation, transcription, telomeric silencing, and DNA repair. A detailed mechanistic explanation of these phenomena is impeded by the limited availability of homogeneously acetylated histones for *in vitro* studies. **Chapter 3** reports a new method for the production of homogeneously and site-specifically acetylated recombinant histones by genetically encoding acetyl-lysine. Using such histones it is possible to reconstitute nucleosomes bearing defined acetylated lysine residues. With these designer nucleosomes it is demonstrated that, in contrast to the prevailing dogma, acetylation of H3 K56 does not directly affect the compaction of chromatin, and has modest effects on remodeling by SWI/SNF and RSC. However, our single-molecule FRET experiments reveal that H3 K56 acetylation increases DNA breathing 7-fold. These results provide a molecular and mechanistic insight in the cellular phenomena that have been linked to H3 K56 acetylation.

The incorporation of histone variants is another way in which eukaryotic cells regulate their DNA activity. H2A.Z is a highly conserved histone variant involved in many transcription-related functions. In *Arabidopsis Thaliana*, H2A.Z plays an essential role in ambient temperature sensing. The mechanism by which H2A.Z does so remains however unresolved. Both enhanced and reduced nucleosome stability have been reported. **Chapter 4** focuses on the effect of H2A.Z incorporation on nucleosome stability and dynamics. Here I show that H2A.Z-containing nucleosomes are more stable than H2A-containing nucleosomes. In single-pair FRET experiments on individual nucleosomes we found that H2A.Z-containing nucleosomes have a lower unwrapping probability and are less susceptible to dissociation during gel electrophoresis, at low concentrations, or in the presence of surfaces. Ambient temperature changes between 7 and 37 °C have no detectable effect on the dynamics of H2A.Z-containing nucleosomes. Our results suggest that H2A.Z containing nucleosomes do not directly respond to temperature changes, but that H2A.Z incorporation may act as a nucleosomal stability switch.

Finally, in **Chapter 5**, we investigate how DNA breathing is affected by extension of the linker DNA and by the presence of a neighboring nucleosome. We found that both electrostatic interactions between the entering and exiting linker DNA and nucleosome-nucleosome interactions increase unwrapping. Interactions between neighboring nucleosomes are more likely in dinucleosomes spaced by 55 bp of linker DNA than in dinucleosomes spaced by 50 bp of linker DNA. Such increased unwrapping may not only increase the accessibility of nucleosomal DNA in chromatin fibers, it may also be key to folding of nucleosomes into higher order structures.

Taken together, our data shed new light on the molecular mechanisms underlying DNA accessibility in chromatin, which in turn may play a role in the regulation of processes like transcription, replication and DNA repair. spFRET was shown to be able to reveal subtle changes in nucleosome conformation due to histone modifications, variations, or constraints imposed by linker DNA and nucleosome neighbors. The spFRET experiments described here can be extended to investigate conformational changes when embedding the nucleosome in a chromatin fiber. Moreover, single-molecule fluorescence techniques may be extended with more colors, allowing the detection of other factors that interact with nucleosomal DNA, yielding even more detailed insight in the molecular mechanisms that control our genome.

Samenvatting

spFRET studies naar de invloed van histonmodificaties, histonvarianten en buur-nucleosomen op nucleosoomdynamica.

Elk levend organisme gebruikt DNA (deoxyribonucleïnezuur) als drager van genetische informatie. DNA is een molecuul dat bestaat uit lange ketens van baseparen (bp) - A, T, C en G genoemd - in een volgorde uniek voor elk individu. Iedere cel in een levend organisme bevat de gehele DNA code van dat organisme, verdeeld over een of meer DNA moleculen. Bij mensen zijn dat 46 DNA moleculen (chromosomen genoemd) bestaande uit in totaal zes miljard ($6 \cdot 10^9$) bp en met een gezamenlijke lengte van 2 meter. DNA vormt de blauwdruk voor het produceren van eiwitten, die essentieel zijn voor het uitvoeren van alle cellulaire functies. De DNA code is identiek voor alle cellen van een organisme. Toch bestaat er een grote variëteit aan cel-typen en -functies. Ook moet een cel zich voortdurend aanpassen aan veranderingen in de omgeving, wat inhoudt dat het productieniveau van allerlei eiwitten en daarmee de DNA-activiteit moet veranderen.

Het principe van het coderen van erfelijke informatie door middel van DNA moleculen opgebouwd uit slechts 4 verschillende bouwstenen is verbluffend eenvoudig. De vertaalslag van DNA sequentie naar een functionerend organisme is daarentegen uitermate complex en nog verre van doorgrond. Dit proefschrift focust op de kleinste onderdelen van chromatine, de nucleosomen, en hoe de fysische eigenschappen van deze nucleosomen het DNA toegankelijk maken voor de processen in de cel.

Nucleosomen

Aan de basis van de regulatie van de genetische code in eukaryoten¹ ligt de organisatie van DNA in structuren die nucleosomen genoemd worden. Een nucleosoom is een

¹Hiertoe behoren alle mensen, dieren, planten en schimmels.

complex van DNA en eiwitten, met een diameter van ongeveer 10 nm, waarin ~150 bp DNA gewikkeld zijn om een schijfje eiwitten, het histon octameer (figuur 1.1c op pagina 7). Lange kettingen van nucleosomen zijn op hun beurt weer georganiseerd in complexere, vezel-achtige structuren, chromatine genoemd (figuur 1.1b op pagina 7). Uiteindelijk vormt chromatine het bekende chromosoom, dat in zijn meest compacte toestand, tijdens de celdeling, goed zichtbaar is² in een normale lichtmicroscop.

Nucleosomen zorgen voor een enorme compactie van het DNA. Als 2 meter DNA (de hoeveelheid die aanwezig is in iedere menselijke cel) aan zichzelf wordt overgelaten, vormt het een kluwen van ~ 100 µm doorsnede, maar door het vormen van nucleosomen past het in de celkern van slechts ~ 5 µm doorsnede (figuur 1.1a op pagina 7). Naast compactie biedt de organisatie in de vorm van nucleosomen tegelijkertijd de essentiële mogelijkheid voor het reguleren van de beschikbaarheid van DNA. Nucleosomen vormen obstakels voor eiwitten die aan het DNA binden om het bijvoorbeeld af te lezen (transcriptie), te kopiëren (replicatie) of te repareren. Door thermische fluctuaties kan het nucleosomaal DNA tijdelijk vanaf de uiteinden van het nucleosoom loskomen van de histon kern. Deze dynamica maakt nucleosomaal DNA eventjes toegankelijk zodat een eiwit zou kunnen binden (figuur 1.2 op pagina 9). De waarschijnlijkheid waarmee het nucleosomaal DNA loskomt is vermoedelijk belangrijk voor het vervullen van de verschillende functies van het DNA zoals transcriptie en replicatie. Daarom willen we weten hoe het loskomen van nucleosomaal DNA beïnvloed kan worden.

Veranderingen in de bindingsenergie tussen DNA en de histonen kunnen in de cel worden gerealiseerd door modificaties aan de histon eiwitten of door het uitwisselen van histonvarianten. Ook interacties tussen nucleosomen beïnvloeden de mogelijkheden tot het loskomen van nucleosomaal DNA. In dit proefschrift beschrijf ik de resultaten van experimenten die subtiele vormveranderingen van één enkel nucleosoom zichtbaar kunnen maken. Ik heb onderzocht hoe het loskomen van nucleosomaal DNA wordt gemoduleerd door histonmodificaties, histonvarianten en de aanwezigheid van een buur-nucleosoom.

FRET

Met een standaard lichtmicroscop zijn structuren te zien van op z'n kleinst een paar honderd nanometer, gelimiteerd door de golflengte van zichtbaar licht. Een nucleosoom is enkele tientallen malen zo klein en dus niet met een lichtmicroscop waar te nemen, laat staan kleine vormveranderingen binnen het nucleosoom. Om toch een enkel nucleosoom zichtbaar te maken, maken we gebruik van fluorescentie: een klein fluorescent molecuul (een fluorofoor) van ongeveer 1 nm zit vast aan het nucleosomaal DNA en verraadt zijn aanwezigheid door licht uit te zenden als het met een laser

²Mits gekleurd.

van de juiste kleur wordt beschenen ('aangeslagen'). Door middel van twee fluoroforen met verschillende kleuren, in dit geval rood en groen, kunnen ook vormveranderingen worden waargenomen. Dit werkt als volgt: de groene fluorofoor (Cy3B) wordt door laserlicht met een golflengte van 515 nm aangeslagen en zendt vervolgens licht uit met een golflengte van 570 nm (groen/geel). In plaats van groen licht uit te zenden, kan deze fluorofoor, de donor, zijn energie ook overdragen aan een andere fluorofoor, de acceptor. De acceptor (ATTO647N) zendt deze overgedragen energie ook uit als licht, maar met een golflengte van 670 nm (rood). De energieoverdracht van donor- naar acceptor-fluorofoor heet Fluorescentie Resonantie Energie Overdracht (in het Engels: Fluorescence Resonance Energy Transfer³, kortweg FRET). De efficiëntie van FRET hangt sterk af van de afstand tussen de fluoroforen, en daalt van 100 % naar 0 % over een afstand van ongeveer 10 nm (figuur 1.3 op pagina 11). Dit maakt FRET een uitermate geschikt gereedschap om afstanden (of afstandsveranderingen) te detecteren binnen structuren met afmetingen rond de 10 nm, zoals nucleosomen. Door een donor en een acceptor fluorofoor op slimme posities aan nucleosomaal DNA en/of histonen te verbinden is een bepaalde vormverandering van het nucleosoom te volgen via de verhouding tussen groen en rood licht dat van het nucleosoom afkomt (figuur 1.4 op pagina 13). FRET is dan ook veelvuldig toegepast in het onderzoek naar nucleosoomdynamica.

Een typische vormverandering die onderzocht wordt is het loskomen van nucleosomaal DNA. Met behulp van FRET kan er onderscheid gemaakt worden tussen een gesloten nucleosoom (hoge FRET, rood licht) en een open nucleosoom (geen FRET, alleen groen licht). Zouden er veel nucleosomen tegelijkertijd gemeten worden, dan zou de gemiddelde FRET efficiëntie van alle nucleosomen samen gemeten worden. Omdat het loskomen van nucleosomaal DNA over het algemeen kort duurt, en dat voor elk nucleosoom op willekeurige tijdstippen gebeurt, zal de gemiddelde waarde niet veel informatie geven over de dynamica. Alleen door één enkel nucleosoom tegelijk te meten kunnen subtiele vormveranderingen aan het licht komen. Dit kan wanneer de concentratie gelabelde nucleosomen zo laag is dat slechts één nucleosoom tegelijkertijd zich in het laserfocus bevindt. We spreken dan van enkel-paar FRET (single-pair, spFRET). Door één nucleosoom te volgen in de tijd kan gezien worden hoe vaak en hoe lang dat nucleosoom open staat. Door van heel veel nucleosomen één voor één te meten of ze op een bepaald moment open of dicht zijn kan de verdeling tussen open en gesloten nucleosomen bepaald worden.

Hoofdstuk 1 geeft een overzicht van experimenten die spFRET hebben gebruikt om nucleosoomdynamica in kaart te brengen. Daartoe behoren verschillende experimentele technieken. De confocale fluorescentie microscoop en de daarbij behorende analysetechniek Fluorescentie Correlatie Spectroscopie (FCS) bekijkt nucleosomen die

³Of Förster Resonance Energy Transfer, naar de ontdekker van FRET, Theodor Förster (1946).

vrij door het laserfocus diffunderen. Op deze manier kunnen duizenden nucleosomen één voor één enkele milliseconden (ms) lang gemeten worden. Totale Interne Reflectie Fluorescentie (TIRF) microscopie bekijkt geïmmobiliseerde nucleosomen, die vast zitten aan het microscoop glaasje. Op deze manier kan één nucleosoom voor honderden seconden gevolgd worden. Een schematisch overzicht van de opstellingen die hiervoor gebruikt kunnen worden is te zien in figuur 1.5 (pagina 17). Deze experimenten hebben gezamenlijk een beeld geschetst van een zeer dynamisch nucleosoom, dat over het algemeen open is gedurende tientallen ms, voor ongeveer 10% van de tijd. Ook hebben ze laten zien dat nucleosoomdynamica wordt gemoduleerd door histonmodificaties en DNA sequentie.

Metten aan enkele nucleosomendynamica

Wij hebben spFRET aan nucleosomen gemeten met confocale fluorescentie microscopie. We maken onderscheid tussen open en gesloten nucleosomen door de donor- en de acceptor-fluoroforen zodanig op het nucleosomaal DNA te plaatsen dat er maximale FRET is als het nucleosoom gesloten is, en geen FRET als het nucleosoom open is (figuur 2.2 op pagina 34). Om te zorgen dat het nucleosoom zich exact op die locatie op het DNA vormt waar de fluoroforen zitten, gebruiken we een DNA sequentie met een zeer hoge affiniteit voor het histon octameer, de zogenoemde 601-sequentie. Door de fluoroforen op een andere locatie op het DNA in te bouwen, verder naar binnen of aan het andere uiteinde, kan onderzocht worden hoe ver het nucleosoom opent en of dat aan beide uiteinden gebeurt (figuur 4.2 op pagina 79 en 4.9 op pagina 93).

Als nucleosomen met FRET labels gevormd zijn, en hun concentratie laag genoeg is om er één tegelijk in het laserfocus te hebben, worden er afzonderlijke pieken van rode en groene fluorescentie gemeten zoals weergegeven in figuur 2.7b (pagina 43). Iedere piek correspondeert met één nucleosoom dat door het laserfocus beweegt. Voor ieder nucleosoom kunnen we uit de intensiteit van de groene en de rode piek de FRET efficiëntie bepalen. Dit leidt tot een histogram zoals in figuur 2.1 (pagina 33), dat weergeeft hoe vaak elke FRET efficiëntie voorkomt. Door de verdeling tussen lage en hoge FRET efficiënties te vergelijken onder verschillende omstandigheden kan de invloed van deze omstandigheden op de verdeling tussen open en gesloten nucleosomen onderzocht worden.

Het uitvoeren van de hierboven beschreven experimenten en het interpreteren van de meetgegevens brengt heel wat uitdagingen met zich mee. Nucleosomen blijken nogal instabiel te zijn bij lage concentraties - die juist nodig zijn voor spFRET experimenten - en in de aanwezigheid van oppervlaktes zoals microscoop glaasjes, pipetpuntjes en buisjes om ze in te bewaren. Dit alles hangt ook nog sterk af van de specifieke histoncompositie en buffercondities (concentratie van zouten e.d.). Het bewaren van nucleosomen, het prepareren van een monster voor op de microscoop en zelfs

het controleren of nucleosomen succesvol gevormd zijn door middel van gel electroforese kan ertoe leiden dat nucleosomen uit elkaar vallen in los DNA en histonen (te zien in figuren 2.3 (pagina 38), 2.4 (pagina 39), 2.5 (pagina 41) en 2.6 (pagina 41) aan de verhoogde piek met lage FRET efficiëntie). Ook is de analyse van spFRET data niet triviaal. Dit kan leiden tot artefacten of de onderliggende nucleosoomdynamica verdoezelen. De uitdagingen waar we mee te maken kregen tijdens onze spFRET experimenten aan nucleosomen beschrijf ik in **hoofdstuk 2**, samen met suggesties hoe deze aan te pakken.

H3 K56 Ac

De kern van het nucleosoom wordt gevormd door een combinatie van acht histonen, twee exemplaren van H2A, H2B, H3 en H4. Histonen zijn eiwitten en bestaan uit ketens van aminozuren. Deze aminozuren kunnen gemodificeerd worden, wat betekent dat er een bepaalde chemische groep aan wordt gekoppeld. Een voorbeeld hiervan is acetylactie⁴. Daarbij wordt er een acetylgroep aan een aminozuur gekoppeld, waardoor een positieve lading wordt geneutraliseerd. Modificaties van de histon-eiwitten komen op grote schaal voor in levende cellen en spelen een essentiële rol bij de regulatie van allerlei DNA-gerelateerde processen. Dat kunnen ze doen door de electrostatische interactie tussen histonen en DNA te veranderen, of door een signaal te vormen voor nucleosoom-bindende eiwitten.

Hoofdstuk 3 behandelt het effect op het gedrag van nucleosomen van een specifieke acetylactie, namelijk van een lysine in histon H3 (H3 K56). Dit aminozuur bevindt zich precies op een plek waar histon H3 contact maakt met het nucleosomaal DNA en wordt gecorreleerd met verhoogde transcriptie-activiteit. Het was eerder niet mogelijk om het effect van deze specifieke modificatie nauwkeurig vast te stellen door een gebrek aan homogeen geacetylerde histonen. In hoofdstuk 3 wordt een nieuwe methode beschreven voor de productie van homogeen, op een specifiek gedefinieerde locatie, geacetylerde histonen. De truc hierbij is om acetyl-lysine genetisch te coderen, iets wat normaliter niet gebeurt. Door gebruik te maken van nucleosomen met op deze manier geproduceerde histonen met een acetylactie op H3 K56 konden wij het effect bepalen van H3 K56 acetylactie op het loskomen van nucleosomaal DNA. Terwijl H3 K56 acetylactie weinig tot geen direct effect laat zien op de hogere orde structuur (chromatine-compactie en nucleosoom mobiliteit), tonen onze spFRET experimenten een 7-voudige toename in het loskomen van nucleosomaal DNA (figuur 3.4 op pagina 63).

⁴Andere voorbeelden zijn methylering, fosforylering en ubiquitilatie.

H2A.Z

Het vervangen van een van de histonen in een nucleosoom door een histonvariant is een andere manier waarmee eukaryote cellen hun DNA activiteit reguleren. Een histonvariant die van gist tot de mens (met kleine verschillen) betrokken is bij meerdere vitale processen in de cel is H2A.Z. Bij *Arabidopsis Thaliana* (AT, het plantje zandrukt) speelt H2A.Z een essentiële rol bij het waarnemen van de omgevingstemperatuur. Het groeien en bloeien van *Arabidopsis* hangt sterk af van temperatuursveranderingen tussen de 12 en 27 °C. Dit is gecorreleerd met de aanwezigheid van H2A.Z in nucleosomen. Planten zonder H2A.Z blijken zich niet op de juiste manier aan de omgevingstemperatuur te kunnen aanpassen. Het mechanisme waarmee H2A.Z zijn rol vervult bij de perceptie van temperatuur is tot nog toe echter onduidelijk gebleven. Zowel verhoogde als verminderde nucleosoom stabiliteit zijn gerapporteerd.

Hoofdstuk 4 focust op het effect van het vervangen van H2A voor H2A.Z op nucleosoomstabiliteit en -dynamica. Ik laat zien dat H2A.Z-nucleosomen stabielere zijn dan H2A-nucleosomen. In spFRET experimenten zagen wij dat H2A.Z-nucleosomen een lagere waarschijnlijkheid hebben voor het loskomen van nucleosomaal DNA en minder vatbaar zijn voor dissociatie tijdens gel-electroforese, bij lage concentraties, of in de nabijheid van oppervlaktes. Variaties in de omgevingstemperatuur tussen 7 en 37 °C hebben geen waarneembaar effect op de dynamica van H2A.Z-nucleosomen. Onze resultaten suggereren dat H2A.Z-nucleosomen niet direct op temperatuurswisselingen reageren, maar dat het uitwisselen van H2A en H2A.Z wel gebruikt zou kunnen worden als mechanisme om de stabiliteit en daarmee de toegankelijkheid van nucleosomaal DNA te reguleren.

Dinucleosomen

Nucleosomen komen *in vivo* nooit alleen voor, ze maken altijd onderdeel uit van chromatine. Chromatine bestaat uit lange kettingen van nucleosomen, verbonden door 10-90 bp linker DNA. Interacties tussen nucleosomen bepalen de hogere orde structuur. Deze interacties en de aanwezigheid van linker DNA beperken de bewegingsmogelijkheden van nucleosomaal DNA en we verwachten dan ook een effect op het loskomen van nucleosomaal DNA.

Hoofdstuk 5 behandelt nucleosomen die verbonden zijn aan een lang stuk linker DNA of aan een buur-nucleosoom. Daartoe hebben wij ons nucleosoom-construct uitgebreid met een stuk DNA van 300 bp of met een tweede nucleosoom, waarbij de twee nucleosomen verbonden zijn met 20, 50 of 55 bp linker DNA (figuur 5.2 op pagina 105). We hebben gevonden dat zowel electrostatische interacties tussen het flankerend DNA aan beide zijden van het nucleosoom, als de aanwezigheid van een buur-nucleosoom het loskomen van nucleosomaal DNA bevordert.

Interacties tussen buur-nucleosomen kunnen alleen plaatsvinden als het linker DNA sterk gebogen wordt. Ter compensatie voor de energie die nodig is om het linker DNA te buigen, zouden nucleosoom-nucleosoom interacties samen kunnen gaan met het loskomen van nucleosomaal DNA, wat te zien zou zijn als een verminderde FRET. Dat is inderdaad wat we zien bij dinucleosomen met 55 bp linker DNA. Bij dinucleosomen met 50 bp linker DNA zien we daarentegen geen verschil in FRET met enkele nucleosomen. Het lengteverschil van 5 bp is klein, maar door de helix vorm van het DNA molecuul met een periodiciteit van 10 bp leidt deze 5 bp tot een oriëntatieverandering tussen de buur-nucleosomen van 180°. Interacties tussen buur-nucleosomen blijken meer waarschijnlijk bij dinucleosomen met 55 bp linker DNA dan bij dinucleosomen met 50 bp linker DNA.

De toegankelijkheid van nucleosomaal DNA in chromatine vezels kan zelfs *groter* zijn dan in 'losse' nucleosomen, door een verhoging in het loskomen van nucleosomaal DNA onder invloed van buur-nucleosomen. Daarnaast bepaalt de lengte van linker DNA de structuur van chromatine door interacties tussen buur-nucleosomen alleen toe te staan voor specifieke linker lengtes. Deze resultaten laten zien dat de toegankelijkheid van nucleosomaal DNA afhangt van de structuur van chromatine.

Conclusie

De resultaten van de experimenten gepresenteerd in dit proefschrift belichten de moleculaire mechanismen die ten grondslag liggen aan de toegankelijkheid van DNA in chromatine, wat op zijn beurt een rol speelt bij de regulatie van processen als transcriptie, replicatie en reparatie van DNA. We hebben laten zien dat spFRET in staat is om subtiele vormveranderingen van nucleosomen te onthullen, die het gevolg zijn van histonmodificaties, histonvariaties, of beperkingen opgelegd door linker DNA en buur-nucleosomen. De spFRET experimenten die hier beschreven zijn kunnen worden uitgebreid om nucleosoomdynamica te onderzoeken in een chromatine vezel. Ook zou direct de interactie tussen buur-nucleosomen onderzocht kunnen worden door op beide nucleosomen één van de FRET fluoroforen te plaatsen. Bovendien zouden spFRET experimenten kunnen worden uitgebreid met meerdere kleuren, zodat naast vormveranderingen van het nucleosoom ook interacties tussen nucleosomen en andere eiwitten kunnen worden gedetecteerd. Zo groeit het inzicht in de moleculaire mechanismen die ons genoom reguleren.

List of publications

Publications related to the work presented in this thesis:

1. R. Buning, A. Brestovitsky, C. Ravarani, P. A. Wigge, and J. van Noort:
Single pair FRET reveals increased stability of H2A.Z nucleosomes.
Manuscript in preparation - **Chapter 4.**
2. R. Buning, W. Kropff, K. Martens, and J. van Noort:
spFRET reveals changes in nucleosome breathing by neighboring nucleosomes.
Accepted for publication in Journal of Physics: Condensed Matter - **Chapter 5.**
3. R. Buning and J. van Noort:
Single-pair FRET experiments on nucleosome conformational dynamics.
Biochimie, vol. 92, no. 12, pp. 1729–1740, 2010 - **Chapter 1.**
4. H. Neumann, S. M. Hancock, R. Buning, A. Routh, L. Chapman, J. Somers, T. Owen-Hughes, J. van Noort, D. Rhodes, and J. W. Chin:
A method for genetically installing site-specific acetylation in recombinant histones defines the effects of H3 K56 acetylation.
Molecular Cell, vol. 36, no. 1, pp. 153– 163, 2009 - **Chapter 3.**
5. W. J. A. Koopmans, R. Buning, and J. van Noort:
Engineering mononucleosomes for single-pair FRET experiments.
in Methods in Molecular Biology: Protocols in DNA Nanotechnology (G. Zuccheri and B. Samori, eds.), pp. 291–303, Humana Press, 2011.
6. W. J. A. Koopmans, R. Buning, T. Schmidt, and J. van Noort:
spFRET using alternating excitation and FCS reveals progressive DNA unwrapping in nucleosomes.
Biophysical Journal, vol. 97, no. 1, pp. 195–204, 2009.

Other publications to which the author contributed:

1. W. Ubachs, J. Bagdonaite, M. T. Murphy, R. Buning, and L. Kaper:
Search for Cosmological μ - Variation from High-Redshift H_2 Absorption; A Status Report.
in From Varying Couplings to Fundamental Physics (Astrophysics and Space Science Proceedings) (C. Martins and P. Molaro, eds.), pp. 125–137, Springer, 2011.
2. J. Tumlinson, A. L. Malec, R. F. Carswell, M. T. Murphy, R. Buning, N. Milutinovic, S. L. Ellison, J. X. Prochaska, R. A. Jorgenson, W. Ubachs, and A. M. Wolfe:
Cosmological concordance or chemical coincidence? Deuterated molecular hydrogen abundances at high redshift.
The Astrophysical Journal, vol. 718, no. 2, pp. L156–L160, 2010.
3. A. L. Malec, R. Buning, M. T. Murphy, N. Milutinovic, S. L. Ellison, J. X. Prochaska, L. Kaper, J. Tumlinson, R. F. Carswell, and W. Ubachs:
Keck telescope constraint on cosmological variation of the proton-to-electron mass ratio.
Monthly Notices of The Royal Astronomical Society, vol. 403, no. 3, pp. 1541–1555, 2010.
4. W. Ubachs, R. Buning, K. S. E. Eikema, and E. Reinhold:
On a possible variation of the proton-to-electron mass ratio: H_2 spectra in the line of sight of high-redshift quasars and in the laboratory.
Journal of Molecular Spectroscopy, vol. 241, no. 2, pp. 155–179, 2007.
5. E. Reinhold, R. Buning, U. Hollenstein, A. Ivanchik, P. Petitjean, and W. Ubachs:
Indication of a cosmological variation of the proton-electron mass ratio based on laboratory measurement and reanalysis of H_2 spectra.
Physical Review Letters, vol. 96, no. 15, p. 151101, 2006.
6. W. Ubachs, R. Buning, and E. Reinhold:
Is er toch variatie van natuurconstanten?
Nederlands Tijdschrift voor Natuurkunde, vol. 72, pp. 184–185, 2006.

Curriculum Vitae

Ruth Buning was born on November 10, 1981 in Amsterdam. After graduating from the St. Ignatius Gymnasium in 1999, she started to study biology at the Vrije Universiteit Amsterdam. After two years she switched to physics at the same university, where she got her bachelor's degree in 2004 and her master's degree in 2007, both cum laude. During her third and fourth year, Ruth was appointed as a supervisor for first year physics students and taught exercise classes in classical mechanics.

Ruth conducted her bachelor's research in the group of prof. dr. Wim Ubachs, on the interface between molecular physics and astrophysics, titled "Cosmological variation of the proton-electron mass ratio". She did her master's research in the same group, under supervision of dr. Rick Bethlem, titled "Building and testing a Stark decelerator for ammonia molecules". After finishing her undergraduate studies, she was employed for a year as researcher to continue her bachelor's work. This included international collaborations with astrophysicists and astronomical observations at the Very Large Telescope in Chili.

In May 2008, Ruth joined the chromatin research group of dr. John van Noort at the Physics of Life Processes group at Leiden University as a PhD student, employed by stichting FOM. There, she worked on single-molecule FRET investigations of mono- and dinucleosome dynamics, the results of which are presented in this thesis. She visited and presented her work at several conferences and summerschools in the Netherlands, France, Germany and the USA. Ruth assisted in several bachelor courses and supervised bachelor and master students. In 2009 and 2010 she was a member and secretary of the FOM central works council.

In February 2014, Ruth started a job as physics lecturer at The Hague University of Applied Science (De Haagse Hogeschool) in Delft.

Dankwoord

Ik ben veel mensen dankbaar voor de waardevolle hulp die zij mij hebben gegeven bij het succesvol volbrengen van mijn promotietraject.

John, bedankt voor je aanstekelijke enthousiasme over chromatine, je dagelijkse begeleiding, je betrokkenheid en het vertrouwen dat je in mij stelt. Bedankt Thomas voor de adequate begeleiding die je me daar waar nodig hebt gegeven. Wiepke, bedankt dat je aan het eind van je eigen promotie zo veel tijd en aandacht hebt besteed om mij op weg te helpen. Mede-promovendi en post-docs in de Physics of Life Processes groep Fan-Tso, Maarten, Thijn, Joke, Meng, Wietske, Sara, Laurent, Freek, Stefan, Anna, Paige, Jante, Hedde, Rolf, Susanne, Dominique, Michaela, Lena en Veer: bedankt voor de goede wetenschappelijke en sociale atmosfeer. Studenten Lucia, Wim, Alan en Kirsten: bedankt voor jullie bijdrage aan mijn onderzoek en voor wat ik van jullie heb geleerd.

Ineke, bedankt voor je enorme inzet bij het realiseren van diverse DNA- en nucleosoom-constructen, je medeleven en interesse. Sylvie, bedankt voor je hulp op biochemisch gebied. John van Egmond, Fred Schenkel, en de overige leden van de fijn mechanische werkplaats, bedankt voor het op maat fabriceren van allerlei componenten voor de setups. Fred Kranenburg, bedankt voor het telkens weer snel en op een vrolijke manier oplossen van software en hardware problemen. Yvonne, bedankt voor de prettige ondersteuning op administratief gebied.

Anna Brestovitsky, thanks for the fruitful and agreeable collaboration on H2A.Z-nucleosomes.

Ik bedank Niels, Ineke, Egge, Dick, Ron, Mark, Johan, Maaïke, Barend, Henk, Harm, Hajnal, Joke, Yuk Man, Miranda, Alex en ook Wim en Renée-Andrée voor vele leerzame ervaringen tijdens het werk bij de centrale ondernemingsraad van FOM.

Jaap en Judith, bedankt voor jullie onvoorwaardelijke steun en medeleven. Jullie hebben mij geleerd om tegelijkertijd kritisch en trots op mezelf te zijn. Jaap, bedankt voor je adequate coaching, en ook voor de inhoudelijke gedachtenwisselingen over mijn samenvatting.

Bram, ik ben je heel dankbaar voor je enorme niet aflatende steun. Door jou gedra-

gen heb ik het op kunnen brengen dit proefschrift af te maken tijdens de eerste levensjaren van onze kinderen. Ik bedank je ook voor de inhoudelijke discussies over biofysica en nucleosomen en je feedback op diverse onderdelen van mijn proefschrift.

Casimir PhD series 2014-34

ISBN: 978-90-8593-206-2

